# HYDRODYNAMIC COEFFICIENTS
# OF LARGE VERTICAL CYLINDERS

by

## THOMAS MATHAI

B. Sc., University of Kerala, 1982

M. Tech., Indian Institute of Technology, Madras, 1984


A THESIS SUBMITTED IN PARTIAL FULFILMENT OF

THE REQUIREMENTS FOR THE DEGREE OF

DOCTOR OF PHILOSOPHY

in

THE FACULTY OF GRADUATE STUDIES

Department of Civil Engineering


We accept this thesis as conforming

to the required standard


THE UNIVERSITY OF BRITISH COLUMBIA

April 1992

In presenting this thesis in partial fulfilment of the requirements for an advanced degree at the University of British Columbia, I agree that the library shall make it freely available for reference and study. I further agree that permission for extensive copying of this thesis for scholarly purposes may be granted by the head of my department or by his or her representatives. It is understood that copying or publication of this thesis for financial gain shall not be allowed without my written permission.

Department of Civil Engineering

The University of British Columbia

Vancouver, Canada

April 7, 1992

# ABSTRACT

The evaluation of hydrodynamic loads on a large surface-piercing vertical cylinder of arbitrary section oscillating in water is addressed. By exploiting the restriction to the structure's geometry, the problem is formulated in the frequency domain as a series of two-dimensional linear radiation problems. Analytical solutions are first obtained for the special cases of circular and elliptic cylinders. A numerical solution based on the method of integral equations is then developed. This is initially applied to circular and elliptic cylinders, so that results may be compared with the corresponding closed-form solutions. Two extrapolation schemes to accelerate the convergence of the numerical results are evaluated. The occurrence of irregular frequencies in the method of integral equations is studied and available methods to eliminate them are summarized.

To circumvent numerical difficulties in the integral equation method at high frequencies, alternative approaches to calculating the hydrodynamic coefficients are investigated. Two schemes for calculating damping coefficients are outlined: a short-wave approximation to the propagating mode potential, and a method based on geometrical optics. Of these, the former is found to be particularly suitable. Two different methods for calculating high frequency added masses are also proposed. One involves discarding the propagating mode and using only the evanescent modes, which are free of irregular frequencies. The other is based on an application of the Kramers-Kronig relations and is valid over the entire frequency range.

The extension of the various methods to very high frequencies at which compressibility effects become significant is also examined. Of the four high frequency methods, damping coefficients may be obtained by the short-wave approximation, and added masses may be obtained by the evanescent mode approximation.

As examples of the application of the various methods, results are presented for a square cylinder and a typical ocean engineering application is illustrated.

# TABLE OF CONTENTS

# LIST OF TABLES

# LIST OF FIGURES

# LIST OF SYMBOLS

| | |
|---|---|
| a | cylinder characteristic dimension; radius of circular cylinder; semi-major axis of elliptic cylinder; side length of square |
| C | horizontal length along body surface |
| $C_b$ | body contour in the horizontal plane |
| c | speed of sound in water |
| $ce_r, se_r$ | even and odd periodic Mathieu functions |
| $c_g$ | group velocity of the incident wave |
| d | still water depth |
| $F_j, F_{jk}$ | overall forces and moments |
| $F'_j, F'_{jk}$ | sectional forces and moments |
| $\mathsf{F}_j$ | complex amplitude of the force $F_j$ |
| $f^k_m$ | source strength distribution function |
| $f^{(3)}_0$ | $\dfrac{\sinh^2(k_0 d)}{k_0 N_0^2}$ |
| $f^{(3)}_m$ | $\dfrac{\sin^2(k_m d)}{k_m N_m^2}$ |
| $f^{(4)}_0$ | $\dfrac{1}{k_0 N_0^2} \sinh(k_0 d) [\, k_0 d \sinh(k_0 d) - \cosh(k_0 d) + 1\,]$ |
| $f^{(4)}_m$ | $\dfrac{1}{k_m N_m^2} \sin(k_m d) [\, k_m d \sin(k_m d) + \cos(k_m d) - 1\,]$ |
| $f^{(5)}_0$ | $\dfrac{1}{k_0 N_0^2} [\, k_0 d \sinh(k_0 d) - \cosh(k_0 d) + 1\,]^2$ |
| $f^{(5)}_m$ | $\dfrac{1}{k_m N_m^2} [\, k_m d \sin(k_m d) + \cos(k_m d) - 1\,]^2$ |
| $G_m$ | Green's function |

| | |
|---|---|
| g | gravitational constant |
| H | incident wave height |
| $H_n^{(1)}$ | Hankel function of the first kind and order n |
| i | $\sqrt{-1}$ |
| $K_n$ | modified Bessel function of the second kind and order n |
| $k_m$ | wave number of the m-th evanescent mode |
| $k_0$ | wave number of the propagating mode |
| $Mc_r^{(i)}$, $Ms_r^{(i)}$ | radial Mathieu functions of the i-th kind |
| $N_m$ | $[\,\frac{d}{2}\,(\,1+\frac{1}{2k_m d}\,\sin(2k_m d)\,)\,]^{\frac{1}{2}}$ |
| $N_0$ | $[\,\frac{d}{2}\,(\,1+\frac{1}{2k_0 d}\,\sinh(2k_0 d)\,)\,]^{\frac{1}{2}}$ |
| n | distance in the direction of **n** |
| **n** | unit vector normal to $C_b$ and directed into the fluid |
| $n_x$, $n_y$ | direction cosines of **n** with respect to the x and y directions |
| p | hydrodynamic pressure |
| r, θ, z | cylindrical polar coordinates (see Fig. 1) |
| T | period of oscillation |
| t | time |
| x, y, z | Cartesian coordinates (see Fig. 1) |
| $Z_m$ | $\frac{1}{N_m}\cos(k_m z)$ |
| $Z_0$ | $\frac{1}{N_0}\cosh(k_0 z)$ |

| | |
|---|---|
| $\delta_{jk}$ | Kronecker delta function |
| $\zeta_k$ | amplitude of motion in the k-th mode |
| $\eta(r,\theta)$ | water surface elevation above still water level |
| $\lambda_{jk}$ | damping coefficient |
| $\lambda'_{jk}$ | sectional damping coefficient |
| $\mu_{jk}$ | added mass |
| $\mu'_{jk}$ | sectional added mass |
| $\xi, \eta, z$ | cylindrical elliptic coordinates |
| $\rho$ | fluid density |
| $\Phi$ | velocity potential |
| $\omega$ | angular frequency |

# ACKNOWLEDGEMENT

# Chapter 1

# INTRODUCTION

## 1.1 General

A variety of offshore structures have been used in the exploration or production of hydrocarbon reserves from offshore oil fields. These include fixed structures that extend to the seabed, such as jacket platforms, gravity platforms, and caisson-retained artificial islands, compliant structures such as guyed towers and tension-leg platforms, and floating structures such as semi-submersibles and drill ships. Representative examples are shown in Fig. 1.

An important requirement in the design of any offshore structure is an assessment of the environmental loads acting on the structure. These include hydrodynamic forces associated with waves, currents, earthquakes, ice impacts, etc. These forces are often estimated by mathematical models, which may be just as reliable as physical models and almost always more economical. Fluid-structure interaction problems generally encompass two distinct flow regimes, one associated with slender member structures for which flow separation is significant, and the other with large structures, for which it is not. In the case of slender structures, hydrodynamic force calculations are generally based on the Morison equation (Morison *et al.*, 1950) which expresses the total hydrodynamic force as the sum of inertia and drag components involving empirical coefficients. On the other hand, if the characteristic dimension of a structure is large compared to the distance travelled by fluid particles relative to the body, appreciable flow separation should not occur. It is then appropriate to neglect the effects of viscosity and treat the flow as irrotational. An attempt can then be made to describe the flow on the basis of potential theory. An exception occurs if the body contains sharp corners, in which case flow separation inevitably occurs, but then the effects of flow separation and vortex shedding are generally localized near the corners and the overall effects, such as the total force exerted on the structure, will not be greatly affected. Even with the neglect of viscosity, the resulting potential flow problem is nonlinear and generally difficult to solve.

More commonly, the problem is linearized by making an assumption of small amplitude waves or motions, and a simple harmonic excitation is considered so that a solution is obtained in the frequency domain.

The hydrodynamic problem is generally classified as belonging to one of two categories. One is the scattering problem which corresponds to a stationary body subjected to an incident wave field. The other is the radiation problem which corresponds to a body oscillating in otherwise still water. In the latter case, the forces are usually expressed in terms of added masses and damping coefficients corresponding to force components in phase with the acceleration and velocity of the structure respectively. The scattering problem applies to fixed offshore structures subjected to ocean waves. The radiation problem applies to an offshore structure undergoing motions which may be due to ice impact, earthquake excitation, etc. The latter category of problem also applies to the problem of earthquake excitation of bridge piers, intake towers etc. which are surrounded by water. The more general case of a floating body subjected to incident waves can be considered as an appropriate combination of both the scattering and radiation problems.

Both the scattering and radiation boundary value problems are well defined and are closely related. In either case, the flow field is described by a velocity potential which satisfies the Laplace equation within the fluid region and which is subject to boundary conditions on the seabed, the still water level, the equilibrium body surface and the far field. For more fundamental body shapes, these elliptic boundary value problems may be solved analytically. However for structures of arbitrary geometry, numerical methods must be used. The use of computer programs to calculate forces on large offshore structures of arbitrary shape based on the finite element method or the method of integral equations is now an established procedure in offshore design. In the integral equation method most commonly used, the application of the body surface boundary condition gives rise to a surface integral equation taken over the submerged structure surface, which is then solved on a computer. However, such programs are quite costly and alternative methods, which are much more economical, may be sought for more restricted configurations.

2

Particular configurations for which simplified numerical treatments are possible are sketched in Fig. 2 and include:

(a)    vertical axisymmetric bodies

(b)    horizontal cylinders of arbitrary section (vertical plane problem)

(c)    vertical cylinders of arbitrary section (horizontal plane problem)

The case of a vertical axisymmetric body (Fig. 2a) has been treated by Black (1975), Fenton (1978), Eatock Taylor and Dolla (1978), and Isaacson (1982) using an integral equation method, and by Bai (1977) using the finite element method. Black (1975) and Fenton (1978) addressed the corresponding scattering problem, whereas Eatock Taylor and Dolla (1978), Bai (1977), and Isaacson (1982) calculated also the added masses and damping coefficients of the radiation problem. In the integral equation method, various functions are expressed as Fourier series in the angle about the body's vertical axis, and the governing surface integral equation is thereby reduced to a series of line integral equations. Of these, only two need be solved in order to determine the forces and moments on the body.

For infinitely long horizontal cylinders of arbitrary section (Fig. 2b), several treatments of the corresponding two-dimensional problem are available in the literature. The flow is studied in the cross-sectional plane and forces are calculated per unit axial length of the cylinder. Studies relating to wave force calculations for this vertical plane problem include those by Black, Mei and Bray (1971), Maeda (1974), Bai (1975), and Naftzger and Chakrabarti (1979). Published computations of added masses and damping coefficients arising for the corresponding radiation problem include those by Yu and Ursell (1961), Vugts (1968), Kim (1965), and Kim (1969).

For a surface-piercing vertical cylinder of arbitrary section extending to the seabed (Fig. 2c), Isaacson (1978) has described an integral equation method for treating the scattering problem. However, a corresponding simplified treatment of the radiation problem of a surface-piercing vertical cylinder of arbitrary section extending to the seabed has been notably absent in the published literature. The problem is of practical importance in the determination of fluid loading on

3

large structures which may be approximated as vertical cylinders of arbitrary section, and which may undergo oscillatory motions due to earthquakes, ice impact, and so on. This problem is the focus of the present thesis.

One difficulty with the integral equation methods arises at relatively high frequencies, since the methods break down at certain 'irregular' frequencies (John, 1950). The difficulty is not too serious in the scattering problem associated with ocean waves, because the relatively short wave lengths corresponding to the irregular frequencies are not usually critical in design. On the other hand, irregular frequencies do pose a serious limitation in applications of the radiation problem, since excitation frequencies may then be relatively high. It is therefore of interest to examine such issues as the numerical accuracy of the integral equation methods, the prediction of irregular frequencies, methods of avoiding their occurrence, and the use of alternative methods which are valid in the high frequency range and which are free from such irregularities. The present study is intended to address these issues. Only the particular case of vertical cylinders of arbitrary section is treated. Solutions for this restricted geometry are not only of practical importance in their own right, but are also indicative of the more general case of structures of arbitrary three-dimensional shapes, while being easier to obtain numerically.

When the oscillation frequency is sufficiently high, a modification to the hydrodynamic loading arises from the effects of compressibility of the water. Although simplified solutions taking account of compressibility exist for two-dimensional dam-reservoir systems (for example, Humar and Jablonski, 1988) and vertical axisymmetric structures (Kokkinowrachos and Thanos, 1990; Sun and Nogami, 1991), a simplified treatment for a vertical cylinder of arbitrary section is generally not available.

A further modification which may arise at high frequencies is that elastic deformations of a structure are more likely to become significant. However the present study considers only the case of a rigid structure.

4

# 1.2 Scope of Present Investigation

As indicated above, the primary scope of the investigation described in this thesis has been to examine various aspects of the radiation problem of a vertical surface-piercing cylinder of arbitrary section extending to the seabed. In particular, vertical cylinders of the following cross-sections have been treated:

(a)  circular section

(b)  elliptic section

(c)  arbitrary section (e.g. square section)

Analytical solutions for circular and elliptic sections are initially described. The corresponding closed-form results are attractive both in their own right as exact solutions and as possible means of testing numerical methods applicable to more general geometries. Numerical methods for arbitrary sections are then developed and initially applied to circular and elliptic cylinders such that the results may be compared with the corresponding analytical results. As an example of the application of the methods, they are then used to obtain results for a square cylinder for which an analytical solution is not available. Only rigid body oscillations have been treated, although no particular difficulty is foreseen in possible extensions to include elastic modes of structure motion.

By fully exploiting the restriction to geometry, the three-dimensional boundary value problem for the radiated potential is initially reduced to a series of two-dimensional problems in the horizontal plane by the use of appropriate eigenfunctions that represent the variation of the velocity potential in the vertical direction. This reformulation of the three-dimensional problem as a series of two-dimensional problems in the horizontal plane is given in Chapter 2. In Chapter 3, analytical solutions to the radiation problem for circular and elliptic cylinders are indicated. The development for the former is similar to those of Yeung (1981), and Sabuncu and Calisal (1981). The development for the latter is similar to that of Williams and Darwiche (1990), but here is based on the more familiar notations of Ince (1932a,b) and Blanch (1946) for the periodic and radial Mathieu functions. Solutions described by Yeung, Sabuncu and Calisal, and Williams and Darwiche, however, apply to a cylinder raised above the seabed, and are more complicated than the solutions

5

for a cylinder extending to the seabed because of the need to account for the fluid region directly beneath the cylinder. In Chapter 4, the method of integral equations applicable to cylinders of arbitrary section is described and developed. Numerical difficulties which are encountered in the method due to the presence of irregular frequencies are illustrated and available methods to eliminate them are summarized. In Chapter 5, alternative approaches are described which may be used to circumvent the effects of irregular frequencies. Two schemes for damping coefficients are outlined: a short-wave solution to the propagating mode potential and a method based on geometrical optics. The two methods cannot be used to obtain the added masses. Instead two alternative methods are proposed. One is based on discarding the propagating mode and using the evanescent modes alone which are free of irregular frequencies. The other involves a somewhat more elaborate procedure based on an application of the Kramers-Kronig relations. When the oscillation frequency is sufficiently high, a modification to the hydrodynamic loading arises from the effects of compressibility of the water. Extensions to the methods already described to account for compressibility may readily be made and are indicated in Chapter 6. In Chapter 7, results obtained by the various methods for a number of fundamental configurations are presented, compared and discussed. Chapter 8 provides an illustration of the application of the methods described to a typical ocean engineering application. Finally, Chapter 9 summarizes the important conclusions of the study, and provides a set of recommendations for further study.

It is hoped that the methods described in this study will provide a contribution towards more efficient, accurate predictions of fluid loads due to earthquakes, ice impact and other high frequency excitation for large structures which may be approximated as vertical cylinders of arbitrary section surrounded by water. Examples of such structures include bridge piers, intake towers, offshore oil-storage tanks, caisson-retained islands, and so on.

# Chapter 2

# THEORETICAL FORMULATION

## 2.1 Governing Equations

As indicated in the previous chapter, the scattering and radiation problems are closely related. While the radiation problem of vertical cylinders is treated here, available solutions to the corresponding scattering problem are summarized in Appendix A.

A rigid vertical surface-piercing cylinder of arbitrary section extends to the seabed in water of constant depth d as indicated in Fig. 3. Fixed Cartesian and cylindrical coordinate systems, (x,y,z) and (r,θ,z) respectively, as indicated in the figure are used, with z measured upwards from the seabed. It is assumed that the prescribed body motions are of small amplitude, that the fluid is incompressible and inviscid, and that the fluid motion is irrotational. Consequently, the flow may be described by a velocity potential which satisfies the Laplace equation within the fluid region, linearized kinematic and dynamic boundary conditions at the free surface, a radiation condition in the far field, and suitable kinematic conditions at the seabed, as well as on the equilibrium body surface. Thus the linearized problem (see, for example, Sarpkaya and Isaacson, 1981) corresponds to a determination of the velocity potential $\Phi(x,y,z,t)$ such that:

$$\nabla^2\Phi = 0 \qquad \text{within the fluid region} \qquad (2.1)$$

subject to the boundary conditions:

$$\frac{\partial\Phi}{\partial z} + \frac{1}{g}\frac{\partial^2\Phi}{\partial t^2} = 0 \qquad \text{at } z = d \qquad (2.2)$$

$$\frac{\partial\Phi}{\partial n} = 0 \qquad \text{at } z = 0 \qquad (2.3)$$

7

$$\frac{\partial \Phi}{\partial n} = V \qquad\qquad \text{on } S_b \qquad\qquad\qquad (2.4)$$

$$\underset{r \to \infty}{\text{Limit}} \sqrt{r} \left( \frac{\partial \Phi}{\partial r} - i k_0 \Phi \right) = 0 \qquad\qquad\qquad (2.5)$$

Here $\Phi$ is the velocity potential, g is the gravitational constant, t denotes time, $i = \sqrt{-1}$, and n denotes distance in the direction of the unit vector **n** normal to the body surface and directed into the fluid (see Fig. 3). $k_0$ corresponds to the wave number of the radiated waves and satisfies the linear dispersion relation:

$$k_0 d \tanh(k_0 d) = \frac{\omega^2 d}{g} \qquad\qquad\qquad (2.6)$$

where $\omega$ is the angular frequency of the body oscillation. V is the velocity of a point on the equilibrium body surface normal to the surface due to the body motion.

Equation (2.2) derives from the linearized kinematic and dynamic free surface boundary conditions. The former describes the condition that the fluid particle velocity normal to the free surface is equal to the velocity of the free surface itself in that direction, while the latter states that the pressure at the free surface, expressed in terms of the Bernoulli equation, is constant. Equations (2.3) and (2.4) correspond to the kinematic boundary conditions at the seabed and at the equilibrium body surface $S_b$ respectively. The former imposes a zero normal component on the fluid particle velocity at the seabed, and the latter requires that the normal component of the fluid particle velocity at the equilibrium body surface is equal to the velocity of the body surface itself in the same normal direction. The radiation condition (2.5) ensures that at large distances from the structure, $\Phi$ represents an outgoing wave.

The structure may oscillate with six degrees of freedom as indicated in Fig. 3 (only rigid body modes are considered), with the translational motions in the x, y and z directions (surge, sway and heave respectively) and the rotational motions about the x, y and z axes (roll, pitch and yaw

respectively) denoted by the subscripts 1, ..., 6 in the above order. Each mode of motion is taken to be harmonic and thus may be expressed in the form:

$$\alpha_k = \zeta_k \exp(-i\omega t) \qquad\qquad \text{for } k = 1, 2, ..., 6 \qquad\qquad (2.7)$$

where $\alpha_k$ is a displacement for $k = 1, 2, 3$, and a rotation for $k = 4, 5, 6$, and $\zeta_k$ is the complex amplitude of each component motion.

The normal velocity V in (2.4) at any point $(x,y,z)$ on the body is made up of six components associated with each mode of motion and each proportional to the corresponding velocity. Thus V may be expressed in the form:

$$V = \sum_{k=1}^{6} - i\omega \zeta_k n_k \exp(-i\omega t) \qquad\qquad (2.8)$$

where $n_k$, corresponding to the k-th mode, is given as:

$$n_k = \left\{ \begin{array}{ll} n_k' & k = 1, 2, 3, 6 \\ z\,n_k' & k = 4, 5 \end{array} \right. \qquad\qquad (2.9)$$

and:

$$\begin{array}{lll} n_1' = n_x \; ; & n_2' = n_y \; ; & n_3' = 0 \; ; \\ n_4' = -n_y \; ; & n_5' = n_x \; ; & n_6' = x\,n_y - y\,n_x \end{array} \qquad\qquad (2.10)$$

Here $n_x$ and $n_y$ are the components of $n$ in the x and y directions respectively, and x and y are the coordinates of the point on the body surface. Since the body has vertical sides, $n$ has no component in the z direction.

As with the velocity V, it is convenient to decompose the overall velocity potential of the flow into six components associated with each degree of freedom, with each component harmonic and proportional to the corresponding velocity. Thus $\Phi$ may be expressed in the form:

$$\Phi = \sum_{k=1}^{6} - i \omega \zeta_k \phi^k \exp(-i\omega t) \tag{2.11}$$

where $\phi^k(x,y,z)$ is independent of time and the body motions. Substituting (2.8) and (2.11) into (2.4), and separating out terms corresponding to the various modes of motion, the boundary value problem for each of the spatial potentials $\phi^k$, $k = 1, \dots 6$, may then be given as follows:

$$\frac{\partial^2 \phi^k}{\partial x^2} + \frac{\partial^2 \phi^k}{\partial y^2} + \frac{\partial^2 \phi^k}{\partial z^2} = 0 \qquad \text{within the fluid region} \tag{2.12}$$

$$\frac{\partial \phi^k}{\partial z} - \frac{\omega^2}{g} \phi^k = 0 \qquad \text{at } z = d \tag{2.13}$$

$$\frac{\partial \phi^k}{\partial z} = 0 \qquad \text{at } z = 0 \tag{2.14}$$

$$\frac{\partial \phi^k}{\partial n} = n_k \qquad \text{on } S_b \tag{2.15}$$

$$\underset{r \to \infty}{\text{Limit}} \sqrt{r} \left( \frac{\partial \phi^k}{\partial r} - i k_0 \phi^k \right) = 0 \tag{2.16}$$

It is noted that the six boundary value problems corresponding to $k = 1, 2, \dots, 6$ differ only by the right-hand side of the boundary condition (2.15).

## 2.2 Reduction to the Horizontal Plane

Since the structure has vertical sides, $\phi^k$ may be expressed in the form of an eigenfunction expansion which satisfies the free surface and seabed boundary conditions, (2.13) and (2.14) respectively. Thus:

$$\phi^k(x,y,z) = \phi_0^k(x,y) Z_0(k_0 z) + \sum_{m=1}^{\infty} \phi_m^k(x,y) Z_m(k_m z) \tag{2.17}$$

where:

$$Z_0(k_0 z) = \frac{1}{N_0} \cosh(k_0 z) \qquad\qquad (2.18)$$

$$Z_m(k_m z) = \frac{1}{N_m} \cos(k_m z) \qquad\qquad (2.19)$$

$$N_0 = [\frac{d}{2}(1 + \frac{1}{2k_0 d} \sinh(2k_0 d))]^{\frac{1}{2}} \qquad\qquad (2.20)$$

$$N_m = [\frac{d}{2}(1 + \frac{1}{2k_m d} \sin(2k_m d))]^{\frac{1}{2}} \qquad\qquad (2.21)$$

and $\phi_m^k$, m = 0, 1, 2, ..., are two-dimensional potentials. The variables $Z_0$ and $Z_m$ are eigenfunctions in the vertical direction, and $k_0$ and $k_m$ are corresponding eigenvalues which are real and positive. The former satisfies the linear dispersion relation given in (2.6) and the latter satisfy instead:

$$k_m d \tan(k_m d) = -\frac{\omega^2 d}{g} \qquad m = 1, 2, ... \qquad\qquad (2.22)$$

The governing equations for $\phi_m^k$ within the fluid region can be developed by substituting (2.17) into (2.12). This leads to:

$$\frac{\partial^2 \phi_0^k}{\partial x^2} + \frac{\partial^2 \phi_0^k}{\partial y^2} + k_0^2 \phi_0^k = 0 \qquad\qquad (2.23)$$

$$\frac{\partial^2 \phi_m^k}{\partial x^2} + \frac{\partial^2 \phi_m^k}{\partial y^2} - k_m^2 \phi_m^k = 0 \qquad m = 1, 2, ... \qquad\qquad (2.24)$$

The orthogonality properties of the functions $Z_m$ can now be utilized to determine appropriate boundary conditions to be satisfied on the body surface contour $C_b$ (see Fig. 3). In order to do so, (2.17) is substituted into (2.15), both sides are multiplied by $Z_l(k_l z)$, $l$ = 0, 1, 2, ... in turn, and integrated with respect to z over (0,d). Thus:

$$\int_0^d \left\{ \frac{\partial \phi_0^k}{\partial n} Z_0(kz) + \sum_{m=1}^{\infty} \frac{\partial \phi_m^k}{\partial n} Z_m(k_m z) \right\} Z_l(k_l z) \, dz = \int_0^d n_k \, Z_l(k_l z) \, dz \qquad (2.25)$$

Thus:

$$\frac{\partial \phi_m^k}{\partial n} = n_k' \, b_m^k \qquad\qquad m = 0, 1, 2, \ldots \qquad\qquad (2.26)$$

where:

$$b_m^k = \begin{cases} \displaystyle\int_0^d Z_m(k_m z) \, dz & k = 1, 2, 3, 6 \\[2ex] \displaystyle\int_0^d z \, Z_m(k_m z) \, dz & k = 4, 5 \end{cases} \qquad (2.27)$$

The integrals in (2.27) may be evaluated by substituting for $Z_m$ from (2.18) and (2.19). Thus:

$$b_m^k = \begin{cases} \dfrac{\sinh(k_0 d)}{k_0 N_0} & m = 0; \ k = 1, 2, 3, 6 \\[2ex] \dfrac{\sin(k_m d)}{k_m N_m} & m \geq 1; \ k = 1, 2, 3, 6 \\[2ex] \dfrac{1}{k_0^2 N_0} [ \, k_0 d \sinh(k_0 d) - \cosh(k_0 d) + 1] & m = 0; \ k = 4, 5 \\[2ex] \dfrac{1}{k_m^2 N_m} [ \, k_m d \sin(k_m d) + \cos(k_m d) - 1] & m \geq 1; \ k = 4, 5 \end{cases} \qquad (2.28)$$

The three-dimensional problem for $\phi^k$ has now been reduced to a series of two-dimensional problems in the horizontal plane for the potentials $\phi_m^k$, $m = 0, 1, 2, \ldots$, with the governing equation for each mode of motion k given by (2.23) or (2.24) as appropriate, a boundary condition on $C_b$ given by (2.26), and a radiation condition similar to (2.16).

Solutions to the Helmholtz equation (2.23), which also satisfy a radiation condition similar to

(2.16), are generally complex and give rise to a wave-like propagating potential $\phi_0^k$. On the other hand, appropriate solutions to (2.24) are real, and satisfy the radiation condition trivially since they exhibit an exponential decay. Thus $\phi_0^k$ corresponds to a propagating mode and satisfies the radiation condition:

$$\lim_{r \to \infty} \sqrt{r} \; (\frac{\partial \phi_0^k}{\partial r} - i \, k_0 \, \phi_0^k) = 0 \tag{2.29}$$

On the other hand, the potentials $\phi_m^k$, $m \geq 1$, correspond to evanescent modes and satisfy:

$$\lim_{r \to \infty} \phi_m^k = 0 \qquad\qquad m \geq 1 \tag{2.30}$$

## 2.3 Hydrodynamic Coefficients

The solution to these two-dimensional problems for $\phi_m^k$ is considered in detail in subsequent chapters of this thesis. Once the potentials $\phi_m^k$ due to the body motion in the k-th mode are known, the resulting hydrodynamic pressure and subsequently the loads on the body may readily be determined. The hydrodynamic pressure p at any point in the fluid is given by a linearized form of the unsteady Bernoulli equation:

$$p = - \rho \frac{\partial \Phi}{\partial t} \tag{2.31}$$

in which $\rho$ is the fluid density. Applying (2.11) to (2.31), the pressure p may be expressed in terms of the body motion amplitudes $\zeta_k$ as:

$$p = \rho \omega^2 \sum_{k=1}^{6} \zeta_k \, \phi^k \, \exp(-i \omega t) \tag{2.32}$$

An integration of the hydrodynamic pressure around the body surface gives the sectional forces and sectional overturning moments $F_j'$ acting on the body as follows:

$$F_j' = - \int_{C_b} p \; n_j \; dC \qquad\qquad j = 1, ..., 6 \qquad\qquad (2.33)$$

where $F_1'$, $F_2'$, $F_3'$ denote the force components in the x, y, z directions, and $F_4'$, $F_5'$, $F_6'$ denote the moment components about the x, y, z axes respectively. By virtue of (2.32), each of these may be expressed as the sum of components associated with the six modes of motion. Thus:

$$F_j' = \sum_{k=1}^{6} F_{jk}' \qquad\qquad (2.34)$$

where:

$$F_{jk}' = - \rho \, \omega^2 \, \zeta_k \int_{C_b} \phi^k \, n_j \, dC \; \exp(-i\omega t) \qquad \text{for } k = 1, ..., 6 \qquad (2.35)$$

Here $F_{1k}'$, $F_{2k}'$, $F_{3k}'$ denote the force components in the x, y, z directions respectively, and $F_{4k}'$, $F_{5k}'$, $F_{6k}'$ denote the moment components about the x, y, z axes respectively, all these applying to each mode of motion indicated by k. These may in turn be described in terms of sectional added masses $\mu_{jk}'$ and sectional damping coefficients $\lambda_{jk}'$ which are real. In order to do so, $F_{jk}'$ is expressed as:

$$F_{jk}' = ( \omega^2 \, \mu_{jk}' + i \, \omega \, \lambda_{jk}' ) \, \zeta_k \exp(-i\omega t) \qquad\qquad (2.36)$$

Thus the added mass $\mu_{jk}'$ corresponds to the component of $F_{jk}'$ in phase with the acceleration of the k-th mode of motion, and the damping coefficient $\lambda_{jk}'$ corresponds to the component of $F_{jk}'$ in phase with the velocity of the k-th mode of motion. Equating the right-hand sides of (2.35) and (2.36), one obtains:

$$\mu_{jk}' = - \rho \, \text{Re}\{I_{jk}'\} \qquad\qquad (2.37)$$

$$\lambda_{jk}' = - \rho \, \omega \, \text{Im}\{I_{jk}'\} \qquad\qquad (2.38)$$

where Re{ } and Im{ } represent real and imaginary parts respectively and $I_{jk}'$ is given by:

14

$$I'_{jk} = \begin{cases} \displaystyle\sum_{m=0}^{\infty} \left[ \int_{C_b} \phi_m^k \, n_j' \, dC \right] Z_m(k_m z) & j = 1, 2, 3, 6 \\[20pt] z \displaystyle\sum_{m=0}^{\infty} \left[ \int_{C_b} \phi_m^k \, n_j' \, dC \right] Z_m(k_m z) & j = 4, 5 \end{cases} \tag{2.39}$$

It is noted that the potentials $\phi_m^k$, m = 1, 2, ..., which are solutions to (2.24), have been already indicated to be real, and hence do not contribute to the damping coefficients.

The corresponding overall forces and moments are obtained by integrating the sectional forces over depth:

$$F_j = \int_0^d F_j' \, dz = \sum_{k=1}^{6} F_{jk} \tag{2.40}$$

where:

$$F_{jk} = \int_0^d F_{jk}' \, dz \tag{2.41}$$

The overall force and moment components $F_{jk}$ are analogous to the corresponding sectional components $F_{jk}'$ and in a similar way may in turn be described in terms of added masses $\mu_{jk}$ and damping coefficients $\lambda_{jk}$ which are real. In order to do so, $F_{jk}$ is expressed as:

$$F_{jk} = ( \omega^2 \mu_{jk} + i \omega \lambda_{jk} ) \, \zeta_k \exp(-i\omega t) \tag{2.42}$$

Equating the right-hand sides of (2.41) and (2.42) and evaluating the integral with respect to z over (0,d), one obtains:

$$\mu_{jk} = - \rho \, \text{Re}\{I_{jk}\} \tag{2.43}$$

$$\lambda_{jk} = - \rho \, \omega \, \text{Im}\{I_{jk}\} \tag{2.44}$$

where $I_{jk}$ is given by:

$$I_{jk} = \sum_{m=0}^{\infty} b_m^j \int_{C_b} \phi_m^k \, n_j' \, dC \qquad (2.45)$$

A consequence of Green's theorem is that the added mass and damping coefficient matrices are in fact symmetric: $\mu_{jk} = \mu_{kj}$, $\lambda_{jk} = \lambda_{kj}$. Furthermore, for a vertical cylinder, $\mu_{jk}$, $\lambda_{jk}$ are always zero if $j = 3$ and/or $k = 3$, since heave motions of the body do not cause fluid motion.

Various methods may be adopted for the solution of the series of horizontal plane problems defined in section 2.2, and the subsequent evaluation of the added masses and damping coefficients. These will be described in the following chapters. In summary, the j-th component of hydrodynamic force due to a body motion in the k-th mode, denoted $F_{jk}$, is expressed in terms of the added mass $\mu_{jk}$ and the damping coefficient $\lambda_{jk}$ as in (2.42). The added mass and damping coefficient are expressed in terms of the potential functions $\phi_m^k$ as in (2.43) - (2.45). The potential functions $\phi_m^k$ are themselves defined by the boundary value problems posed by (2.23), (2.24), (2.26), (2.29) and (2.30). The sectional counterparts to the above are $F_{jk}'$, $\mu_{jk}'$ and $\lambda_{jk}'$ respectively.

## 2.4 Haskind Relations

The radiation problem described so far is closely related to the corresponding scattering problem of incident waves interacting with a stationary cylinder, summarized in Appendix A. In the scattering problem, the velocity potential $\Phi$ is first represented as the sum of incident wave and scattered wave potentials as follows:

$$\Phi = \Phi_i + \Phi_s \qquad (2.46)$$

where $\Phi_i$ corresponds to the incident wave field and is known, and $\Phi_s$ corresponds to the scattered wave field. The boundary value problem is then set up for the scattered potential $\Phi_s$, and is identical to that for the potential of the radiation problem, defined by (2.1) - (2.5), except that in (2.4) V is replaced by $-\partial \Phi_i/\partial n$. Once $\Phi_s$, and consequently $\Phi$, are determined, the pressure

throughout the fluid may be evaluated by the linearized Bernoulli equation (2.31). Appropriate integrations of the pressure acting on the body surface may then be carried out to obtain sectional forces, total forces and overturning moments as required.

Now the Haskind relations provide a connection between the scattering and radiation problems, whereby the diagonal terms in the damping matrix of the radiation problem are related to the corresponding force components of the scattering problem. For structures of arbitrary geometry, this relationship is given as (see, for example, Sarpkaya and Isaacson, 1981):

$$\lambda_{kk} = \frac{k_0}{2\pi\rho g c_g} \int_0^{2\pi} \mid \frac{F_k(\alpha)}{H} \mid^2 d\alpha \tag{2.47}$$

where, with respect to the scattering problem, $F_k$ is the complex amplitude of the k-th mode exciting force, H is the incident wave height, $c_g$ is the group velocity of the incident wave, and the incident wave direction makes an angle $\alpha$ with the x axis.

Thus (2.47) provides a means of deducing the damping coefficients of the radiation problem from the exciting forces of the corresponding scattering problem. Alternatively this relationship may be used to provide a check on numerical estimates that have been made.

17

# Chapter 3

# ANALYTICAL SOLUTIONS

The series of horizontal plane problems for $\phi_m^k$ described in the previous chapter may be solved analytically for the special cases of circular and elliptic cylinders. Such analytical solutions are attractive both in their own right in providing estimates of added masses and damping coefficients for suitable prototype structures, as well as in providing a means of testing numerical methods applicable to more general geometries developed in the next chapter.

## 3.1 Circular Cylinder

The radiation problem of a vertical circular cylinder has been treated analytically by McCormick (1989), but results were given only for slender cylinders. Other analytical or semi-analytical treatments of the radiation problem of floating and submerged circular cylinders include those by Yeung (1981), and Sabuncu and Calisal (1981) for a floating circular cylinder, Calisal and Sabuncu (1984) for a floating compound cylinder, and Tung (1979) for a submerged circular cylinder resting on the seabed. A variational method has been applied by Black, Mei and Bray (1971) to a floating circular cylinder and a submerged circular cylinder resting on the seabed, but only the exciting forces in the corresponding scattering problem were calculated using the Haskind relations.

In the related problem of water wave scattering by a vertical circular cylinder, a solution has existed for some time. An analytical solution to the scattering problem due to MacCamy and Fuchs (1954) is widely cited in the literature, and is summarized in Appendix A. The case of two or more vertical circular cylinders has been treated by Spring and Monkmeyer (1974, 1975) and by Chakrabarti (1978). Somewhat similar analytical or semi-analytical solutions for floating and submerged circular cylinders include those by Garrett (1971) and Isaacson (1979).

In this section, analytical expressions for the added masses and damping coefficients of a vertical circular cylinder are formulated, together with corresponding high frequency asymptotic forms, as well as their vertical distributions, all with a view to generating a complete set of results. The development is similar to those of Yeung (1981), and Sabuncu and Calisal (1981). Their solutions apply to a circular cylinder raised above the seabed, and are more complicated than that for a cylinder extending to the seabed because of the need to account for the fluid region directly beneath the cylinder.

Letting $C_b$ in Fig. 3 correspond to a circle, the potentials $\phi_m^k$, m = 0, 1, 2, ... may be obtained analytically by adopting the method of separation of variables in cylindrical coordinates. Writing (2.23) in cylindrical coordinates, substituting $\phi_0^k$ as $R_0(r)\Theta_0(\theta)$, and separating variables, the following equations are obtained for the propagating mode:

$$\bar{r}^2 \frac{d^2R_0}{d\bar{r}^2} + \bar{r}\frac{dR_0}{d\bar{r}} + (\bar{r}^2 - n^2)R_0 = 0 \tag{3.1}$$

$$\frac{d^2\Theta_0}{d\theta^2} + n^2\Theta_0 = 0 \tag{3.2}$$

where $\bar{r} = k_0 r$. Equation (3.1) is Bessel's equation. Its general solution corresponds to the Hankel functions of the first and second kinds, of which only the former satisfies the radiation condition in the far-field. Solutions to (3.2) are the circular sine and cosine functions. Thus the potential $\phi_0^k$ corresponding to the propagating mode may be expressed as:

$$\phi_0^k = \sum_{n=0}^{\infty} c_n^0 H_n^{(1)}(k_0 r) \cos(n\theta) + s_n^0 H_n^{(1)}(k_0 r) \sin(n\theta) \tag{3.3}$$

where $H_n^{(1)}$ is the Hankel function of the first kind and order n, and $c_n^0$ and $s_n^0$ are initially unknown complex coefficients.

Similarly, for the evanescent modes corresponding to m = 1, 2, ..., the method of separation of variables applied to (2.24) gives:

19

$$\bar{r}^2 \frac{d^2 R_m}{d\bar{r}^2} + \bar{r}\frac{dR_m}{d\bar{r}} - (\bar{r}^2 + n^2)R_m = 0 \tag{3.4}$$

$$\frac{d^2\Theta_0}{d\theta^2} + n^2\Theta_0 = 0 \tag{3.5}$$

Equation (3.4) is Bessel's modified equation. Its general solutions are the modified Bessel functions of the first and second kinds, of which the former increases exponentially at large distances and hence is discarded. Thus the potentials $\phi_m^k$ are given as:

$$\phi_m^k = \sum_{n=0}^{\infty} c_n^m\, K_n(k_m r)\, \cos(n\theta) + s_n^m\, K_n(k_m r)\, \sin(n\theta) \qquad m = 1, 2, \dots \tag{3.6}$$

where $K_n$ is the modified Bessel function of the second kind and order n, and $c_n^m$ and $s_n^m$ are initially unknown complex coefficients.

The boundary condition to be satisfied on $C_b$ is given by (2.26) and in cylindrical coordinates becomes:

$$\frac{\partial \phi_m^k}{\partial r} = n_k{}'\, b_m^k \qquad m = 0, 1, 2, \dots \tag{3.7}$$

where:

$$n_1{}' = n_5{}' = n_x = \cos\theta \tag{3.8}$$

In (3.7), $b_m^k$ is given by (2.28). Substituting (3.3) and (3.6) in (3.7), multiplying both sides by $\cos(n\theta)$ and $\sin(n\theta)$ in turn, integrating with respect to $\theta$ from 0 to $2\pi$, and using orthogonality of the sine and cosine functions, one obtains for surge and pitch motions:

$$\phi_0^k = \frac{b_0^k}{k_0\, H_1^{(1)'}(k_0 a)}\, H_1^{(1)}(k_0 r)\, \cos\theta \qquad k = 1, 5 \tag{3.9}$$

$$\phi_m^k = \frac{b_m^k}{k_m\, K_1{}'(k_m a)}\, K_1(k_m r)\, \cos\theta \qquad m = 0, 1, 2, \dots \qquad k = 1, 5 \tag{3.10}$$

20

where the prime denotes a derivative with respect to the argument. $\phi_m^3$ is zero because the cylinder extends from the seabed to the free surface and the sides are vertical, $\phi_m^6$ is zero due to axisymmetry, and $\phi_m^2$ and $\phi_m^4$ are identical to $\phi_m^1$ and $- \phi_m^5$ respectively with the angular variation described by $\sin\theta$ instead of $\cos\theta$.

## 3.1.1 Hydrodynamic Coefficients

In order to obtain the hydrodynamic coefficients, the expressions (3.9) and (3.10) for the potentials are substituted into (2.45). Using (2.43) and (2.44), the following expression is obtained:

$$\frac{\mu_{jk} + i\,\lambda_{jk}/\omega}{\rho a^l} = -\frac{\pi}{(k_0 a)^{l-1}} \frac{H_1^{(1)}(k_0 a)}{H_1^{(1)'}(k_0 a)} f_0^{(l)}(k_0 d)$$

$$-\sum_{m=1}^{\infty} \frac{\pi}{(k_m a)^{l-1}} \frac{K_1(k_m a)}{K_1'(k_m a)} f_m^{(l)}(k_m d) \qquad j, k = 1, 5 \qquad (3.11)$$

where:

$$l = \begin{cases} 3 & j, k = 1 \\ 5 & j, k = 5 \\ 4 & j = 1, k = 5 \end{cases} \qquad (3.12)$$

Also:

$$f_0^{(3)}(k_0 d) = \frac{\sinh^2(k_0 d)}{k_0 N_0^2} \qquad (3.13)$$

$$f_m^{(3)}(k_m d) = \frac{\sin^2(k_m d)}{k_m N_m^2} \qquad m = 1, 2, \dots \qquad (3.14)$$

$$f_0^{(4)}(k_0 d) = \frac{1}{k_0 N_0^2}\sinh(k_0 d)\,[\,k_0 d\,\sinh(k_0 d) - \cosh(k_0 d) + 1\,] \qquad (3.15)$$

$$f_m^{(4)}(k_m d) = \frac{1}{k_m N_m^2}\sin(k_m d)\,[\,k_m d\,\sin(k_m d) + \cos(k_m d) - 1\,] \qquad m = 1, 2, \dots \qquad (3.16)$$

$$f_0^{(5)}(k_0 d) = \frac{1}{k_0 N_0^2} [\, k_0 d \, \sinh(k_0 d) - \cosh(k_0 d) + 1\,]^2 \tag{3.17}$$

$$f_m^{(5)}(k_m d) = \frac{1}{k_m N_m^2} [\, k_m d \, \sin(k_m d) + \cos(k_m d) - 1\,]^2 \qquad m = 1, 2, \ldots \tag{3.18}$$

The added masses and damping coefficients are obtained from (3.11) by using the real and imaginary parts respectively of the right-hand side of (3.11). Bearing in mind the symmetry of the added mass and damping coefficient matrices in general and the symmetry of the structure in particular, the complete set of hydrodynamic coefficients are then given as:

$$
[\mu_{jk}] = \begin{bmatrix}
\mu_{11} & 0 & 0 & 0 & \mu_{15} & 0 \\
0 & \mu_{11} & 0 & -\mu_{15} & 0 & 0 \\
0 & 0 & 0 & 0 & 0 & 0 \\
0 & -\mu_{15} & 0 & \mu_{55} & 0 & 0 \\
\mu_{15} & 0 & 0 & 0 & \mu_{55} & 0 \\
0 & 0 & 0 & 0 & 0 & 0
\end{bmatrix} ; \qquad
[\lambda_{jk}] = \begin{bmatrix}
\lambda_{11} & 0 & 0 & 0 & \lambda_{15} & 0 \\
0 & \lambda_{11} & 0 & -\lambda_{15} & 0 & 0 \\
0 & 0 & 0 & 0 & 0 & 0 \\
0 & -\lambda_{15} & 0 & \lambda_{55} & 0 & 0 \\
\lambda_{15} & 0 & 0 & 0 & \lambda_{55} & 0 \\
0 & 0 & 0 & 0 & 0 & 0
\end{bmatrix} \tag{3.19}
$$

The diagonal terms in the damping matrix may also be obtained from the exciting forces, which are given in Appendix A, by use of (2.47) deriving from the Haskind relations. Using (A.9) and (A.10) in (2.47), an alternative expression for the damping coefficients may thereby be obtained:

$$\frac{\lambda_{kk}}{\rho a^l \omega} = 2 \frac{f_0^{(l)}(k_0 d)}{(k_0 a)^l} \frac{1}{|H_1'(k_0 a)|^2} \qquad k = 1, 5 \tag{3.20}$$

where:

$$l = \begin{cases} 3 & \qquad k = 1 \\ 5 & \qquad k = 5 \end{cases} \tag{3.21}$$

## 3.1.2 High Frequency Approximations

At high frequencies, $\omega$ is large and hence $k_0 a$ and $k_0 d$ become large. Simplified expressions for the hydrodynamic coefficients may then be developed by using suitable approximations to the Bessel

and hyperbolic functions (see Abramowitz and Stegun, 1972). For example, when $k_0a \to \infty$:

$$\frac{H_1^{(1)}(k_0a)}{H_1^{(1)'}(k_0a)} = -i \qquad (3.22)$$

When $k_0d \to \infty$:

$$f_0^{(3)}(k_0d) = 2 \qquad (3.23)$$

$$f_0^{(5)}(k_0d) = 2 (k_0d)^2 - 4 k_0d + 2 \qquad (3.24)$$

$$f_0^{(4)}(k_0d) = 2 k_0d - 2 \qquad (3.25)$$

Substituting these into (3.11), high frequency approximations to the damping coefficients can readily be obtained as:

$$\frac{\lambda_{11}}{\rho a^3 \omega} = \frac{2\pi}{(k_0a)^2} \qquad (3.26)$$

$$\frac{\lambda_{55}}{\rho a^5 \omega} = \frac{2\pi}{(k_0a)^2} \left(\frac{d}{a}\right)^2 - \frac{4\pi}{(k_0a)^3} \left(\frac{d}{a}\right) + \frac{2\pi}{(k_0a)^4} \qquad (3.27)$$

$$\frac{\lambda_{15}}{\rho a^4 \omega} = \frac{2\pi}{(k_0a)^2} \left(\frac{d}{a}\right) - \frac{2\pi}{(k_0a)^3} \qquad (3.28)$$

The terms involving the modified Bessel function in (3.11) are real and hence do not contribute to the damping coefficients.

It remains to find corresponding expressions for the added masses. When $\omega$ is infinitely large, the solutions for $k_md$ in (2.22) are:

$$k_md = \frac{\pi}{2}(2m-1) \qquad\qquad m = 1, 2, \dots \qquad (3.29)$$

Consequently, expressions for $f_m^{(l)}(k_md)$ which appear in (3.11) are simplified:

23

$$f_m^{(3)}(k_md) = \frac{4}{(2m-1)\pi} \qquad\qquad m = 1, 2, \ldots \qquad\qquad (3.30)$$

$$f_m^{(5)}(k_md) = (2m-1)\pi + \frac{4}{(2m-1)\pi} + 4(-1)^m \qquad\qquad m = 1, 2, \ldots \qquad\qquad (3.31)$$

$$f_m^{(4)}(k_md) = 2 + \frac{4(-1)^m}{(2m-1)\pi} \qquad\qquad m = 1, 2, \ldots \qquad\qquad (3.32)$$

The limiting values of the added masses then become:

$$\frac{\mu_{11}}{\rho a^3} = -\frac{16}{\pi^2}\left(\frac{d}{a}\right)^2 \sum_{m=1}^{\infty} \frac{1}{(2m-1)^3} \frac{K_1(k_ma)}{K_1'(k_ma)} \qquad\qquad (3.33)$$

$$\frac{\mu_{55}}{\rho a^5} = -\frac{16}{\pi^3}\left(\frac{d}{a}\right)^4 \sum_{m=1}^{\infty} \left[ \frac{\pi}{(2m-1)^3} + \frac{4}{(2m-1)^5\pi} + \frac{4(-1)^m}{(2m-1)^4} \right] \frac{K_1(k_ma)}{K_1'(k_ma)} \qquad\qquad (3.34)$$

$$\frac{\mu_{15}}{\rho a^4} = -\frac{8}{\pi^2}\left(\frac{d}{a}\right)^3 \sum_{m=1}^{\infty} \left[ \frac{2}{(2m-1)^3} + \frac{4(-1)^m}{(2m-1)^4\pi} \right] \frac{K_1(k_ma)}{K_1'(k_ma)} \qquad\qquad (3.35)$$

where $k_ma$ is now given by:

$$k_ma = (2m-1)\frac{\pi}{2}\frac{a}{d} \qquad\qquad m = 1, 2, \ldots \qquad\qquad (3.36)$$

Equation (3.33) agrees with the corresponding result given some time ago by Jacobsen (1949) when the corrections indicated by Garrison and Berklite (1973) are taken into account. In addition, when a/d is also large, $k_ma$ will be sufficiently large for all m for the large argument asymptotic form of the modified Bessel function to be used. This gives:

$$\frac{K_1(k_ma)}{K_1'(k_ma)} = -1 \qquad\qquad (3.37)$$

Thus for large a/d ratios, the limiting values of the added masses are simply:

$$\frac{\mu_{11}}{\rho a^3} = \frac{16}{\pi^2}\left(\frac{d}{a}\right)^2 \sum_{m=1}^{\infty} \frac{1}{(2m-1)^3} \qquad\qquad (3.38)$$

24

$$\frac{\mu_{55}}{\rho a^5} = \frac{16}{\pi^3} \left(\frac{d}{a}\right)^4 \sum_{m=1}^{\infty} \left[ \frac{\pi}{(2m-1)^3} + \frac{4}{(2m-1)^5\pi} + \frac{4(-1)^m}{(2m-1)^4} \right]$$ (3.39)

$$\frac{\mu_{15}}{\rho a^4} = \frac{8}{\pi^2} \left(\frac{d}{a}\right)^3 \sum_{m=1}^{\infty} \left[ \frac{2}{(2m-1)^3} + \frac{4(-1)^m}{(2m-1)^4\pi} \right]$$ (3.40)

In principle, the approximations for the damping coefficients and the added masses in (3.26) - (3.28) and (3.38) - (3.40) may be further improved by retaining additional terms in the asymptotic expansions for the Bessel functions in (3.22) and (3.37) respectively, but this is not attempted.

## 3.1.3 Vertical Distributions

In order to obtain the sectional added masses and damping coefficients at different elevations, the expressions (3.9) and (3.10) for the potentials are substituted instead into (2.39). Using (2.37) and (2.38), the following expressions are obtained for the sectional added masses $\mu'_{jk}$ and damping coefficients $\lambda'_{jk}$:

$$\frac{\mu'_{1k} + i\,\lambda'_{1k}/\omega}{\rho a^l} = -\frac{\pi}{(k_0 a)^{l-1}} \frac{H_1^{(1)}(k_0 a)}{H_1^{(1)'}(k_0 a)} \frac{\cosh(k_0 z)}{\sinh(k_0 d)} f_0^{(l+1)}(k_0 d)$$

$$- \sum_{m=1}^{\infty} \frac{\pi}{(k_m a)^{l-1}} \frac{K_1(k_m a)}{K_1'(k_m a)} \frac{\cos(k_m z)}{\sin(k_m d)} f_m^{(l+1)}(k_m d) \qquad k = 1, 5 \qquad (3.41)$$

$$\frac{\mu'_{5k} + i\,\lambda'_{5k}/\omega}{\rho a^l} = -\frac{\pi}{(k_0 a)^{l-2}} \frac{H_1^{(1)}(k_0 a)}{H_1^{(1)'}(k_0 a)} \frac{\cosh(k_0 z)}{\sinh(k_0 d)} f_0^{(l)}(k_0 d) \frac{z}{a}$$

$$- \sum_{m=1}^{\infty} \frac{\pi}{(k_m a)^{l-2}} \frac{K_1(k_m a)}{K_1'(k_m a)} \frac{\cos(k_m z)}{\sin(k_m d)} f_m^{(l)}(k_m d) \frac{z}{a} \qquad k = 1, 5 \qquad (3.42)$$

where:

$$l = \begin{cases} 2 & j, k = 1 \\ 4 & j, k = 5 \\ 3 & j = 1, k = 5; \text{ or } j = 5, k = 1 \end{cases} \qquad (3.43)$$

As may be seen from the expansions for $(\mu'_{15}+i\lambda'_{15}/\omega)$ and $(\mu'_{51}+i\lambda'_{51}/\omega)$ in (3.41) and (3.42), the sectional added mass and damping coefficient matrices are not symmetric. However, bearing in mind the symmetry of the structure, the complete set of sectional hydrodynamic coefficients may be given as follows:

$$[\mu'_{jk}] = \begin{bmatrix} \mu'_{11} & 0 & 0 & 0 & \mu'_{15} & 0 \\ 0 & \mu'_{11} & 0 & -\mu'_{15} & 0 & 0 \\ 0 & 0 & 0 & 0 & 0 & 0 \\ 0 & -\mu'_{51} & 0 & \mu'_{55} & 0 & 0 \\ \mu'_{51} & 0 & 0 & 0 & \mu'_{55} & 0 \\ 0 & 0 & 0 & 0 & 0 & 0 \end{bmatrix}; \quad [\lambda'_{jk}] = \begin{bmatrix} \lambda'_{11} & 0 & 0 & 0 & \lambda'_{15} & 0 \\ 0 & \lambda'_{11} & 0 & -\lambda'_{15} & 0 & 0 \\ 0 & 0 & 0 & 0 & 0 & 0 \\ 0 & -\lambda'_{51} & 0 & \lambda'_{55} & 0 & 0 \\ \lambda'_{51} & 0 & 0 & 0 & \lambda'_{55} & 0 \\ 0 & 0 & 0 & 0 & 0 & 0 \end{bmatrix} \qquad (3.44)$$

## 3.2 Elliptic Cylinder

The radiation problem for a vertical elliptic cylinder has been treated by Chen and Mei (1971). However, only the damping coefficients were derived. More recently, Williams and Darwiche (1990) calculated the added masses and damping coefficients of a floating elliptic cylinder and a submerged elliptic cylinder resting on the seabed.

In the corresponding scattering problem, the form of the analytical solution has been known for some time in the field of electromagnetic and acoustic scattering in terms of Mathieu functions (see Bowman et al., 1969), but corresponding results in the context of water wave scattering were only calculated more recently by Chen and Mei (1971) using the program of Clemm (1969) to evaluate the Mathieu functions. The solution is summarized in Appendix A. Williams (1985a) simplified the exact solution of Chen and Mei (1971), on the basis of an expansion for small values of the eccentricity of the ellipse. Somewhat similar analytical solutions for floating and submerged

26

elliptic cylinders include those by Chen and Mei (1973) for a floating cylinder in shallow water, Williams (1985b) for a floating cylinder and a submerged cylinder resting on the seabed in shallow water, and Williams and Darwiche (1988) without the shallow water restriction.

In this section, the hydrodynamic coefficients of a vertical surface-piercing elliptic cylinder extending to the seabed are derived. The development is similar to that of Williams and Darwiche (1990), but is now based on the more familiar notation of Ince (1932a,b) and Blanch (1946) for the periodic and radial Mathieu functions. Williams and Darwiche's solution applies to a cylinder raised above the seabed, and is more complicated than that for a cylinder extending to the seabed because of the need to account for the fluid region directly beneath the cylinder.

Letting $C_b$ in Fig. 3 correspond to an ellipse, the potentials $\phi_m^k$, $m = 0, 1, 2, \ldots$ may be obtained analytically by adopting the method of separation of variables in elliptic coordinates. Elliptic coordinates $(\xi, \eta)$ are introduced as:

$$x = h \cosh\xi \cos\eta; \qquad\qquad y = h \sinh\xi \sin\eta \qquad\qquad (3.45)$$

such that $\xi = \xi_0$ conforms to the horizontal contour of the cylinder $C_b$ and $\xi = 0$ coincides with the major axis. The semi-focal distance h of the ellipse is given as $(a^2 - b^2)^{1/2}$, where a and b are respectively the semi-major and semi-minor axes of the ellipse. A concise summary of the features of the coordinate system is given in Appendix A of Chen and Mei (1971).

Writing (2.23) in elliptic coordinates, substituting $\phi_0^k$ as $\Xi_0(\xi)H_0(\eta)$, and separating variables, the following equations are obtained for the propagating mode:

$$\frac{d^2 H_0}{d\eta^2} + [\lambda - 2q_0 \cos(2\eta)] H_0 = 0 \qquad\qquad (3.46)$$

$$\frac{d^2 \Xi_0}{d\xi^2} - [\lambda - 2q_0 \cosh(2\xi)] \Xi_0 = 0 \qquad\qquad (3.47)$$

Equations (3.46) and (3.47) are the canonical form of Mathieu's differential equation and

Mathieu's modified differential equation respectively. $\lambda$ is a separation constant and $q_0$ is a parameter defined as:

$$q_0 = \frac{k_0^2 h^2}{4} \tag{3.48}$$

The solutions to (3.46) and (3.47) are the Mathieu functions, and the corresponding solution for $\phi_0^k$ is then:

$$\phi_0^k = \sum_{n=0}^{\infty} [\ c_{2n}^o\ Mc_{2n}^{(3)}(\xi,q_0)\ ce_{2n}(\eta,q_0)\ +\ c_{2n+1}^o\ Mc_{2n+1}^{(3)}(\xi,q_0)\ ce_{2n+1}(\eta,q_0)$$

$$+\ s_{2n+2}^o\ Ms_{2n+2}^{(3)}(\xi,q_0)\ se_{2n+2}(\eta,q_0)\ +\ s_{2n+1}^o\ Ms_{2n+1}^{(3)}(\xi,q_0)\ se_{2n+1}(\eta,q_0)] \tag{3.49}$$

$ce_r(\eta,q_0)$ and $se_r(\eta,q_0)$ are respectively the even and odd periodic Mathieu functions based on the notation of Ince (1932a, b): the order r is of the form 2n+p, where n is an integer and p is a parameter equal to 0 or 1 indicating that the period of the Mathieu function is $\pi$ or $2\pi$ respectively. $Mc_r^{(i)}(\xi,q_0)$ and $Ms_r^{(i)}(\xi,q_0)$ are the corresponding radial Mathieu functions of the i-th kind based on Blanch's (1962) notation. $c_r^o$, $s_r^o$ are initially unknown complex coefficients.

The evanescent mode potentials $\phi_m^k$ may be obtained in a similar way. Writing (2.24) in elliptic coordinates, substituting $\phi_m^k$ as $\Xi_m(\xi)H_m(\eta)$, and separating variables, the following equations are obtained for the evanescent modes corresponding to m = 1, 2, ...:

$$\frac{d^2 H_m}{d\eta^2} + [\ \lambda + 2q_m \cos(2\eta)\ ] H_m = 0 \tag{3.50}$$

$$\frac{d^2 \Xi_m}{d\xi^2} - [\ \lambda + 2q_m \cosh(2\xi)\ ] \Xi_m = 0 \tag{3.51}$$

where:

$$q_m = \frac{k_m^2 h^2}{4} \qquad\qquad m = 1, 2, ... \tag{3.52}$$

28

Solutions to (3.50) and (3.51) are the periodic and radial Mathieu functions with negative parameters. The corresponding solutions for the evanescent potentials are then:

$$\phi_m^k = \sum_{n=0}^{\infty} [\ c_{2n}^m\ Mc_{2n}^{(3)}(\xi,-q_m)\ ce_{2n}(\eta,-q_m)$$

$$+\ c_{2n+1}^m\ Mc_{2n+1}^{(3)}(\xi,-q_m)\ ce_{2n+1}(\eta,-q_m)$$

$$+s_{2n+2}^m\ Ms_{2n+2}^{(3)}(\xi,-q_m)\ se_{2n+2}(\eta,-q_m)$$

$$+\ s_{2n+1}^m\ Ms_{2n+1}^{(3)}(\xi,-q_m)\ se_{2n+1}(\eta,-q_m)\ ] \qquad m = 1, 2, ... \qquad (3.53)$$

where $c_r^m$, $s_r^m$ are unknown coefficients to be determined from the boundary condition on $C_b$.

The boundary condition on $C_b$ is given by (2.26) and is needed to obtain the unknown coefficients $c_r^m$, $s_r^m$. In elliptic coordinates this becomes:

$$\frac{\partial \phi_m^k}{l_1 \partial \xi} = n_k'\ b_m^k \qquad \text{at } \xi = \xi_0 \qquad m = 0, 1, 2, ... \qquad (3.54)$$

where:

$$n_1' = n_x = \frac{h}{l_1}\sinh\xi_0\cos\eta; \qquad n_4' = -n_y = -\frac{h}{l_1}\cosh\xi_0\sin\eta;$$

$$n_2' = n_y = \frac{h}{l_1}\cosh\xi_0\sin\eta; \qquad n_5' = n_x = \frac{h}{l_1}\sinh\xi_0\cos\eta; \qquad (3.55)$$

$$n_3' = 0; \qquad n_6' = x\,n_y - y\,n_x = \frac{h^2}{2l_1}\sin2\eta$$

In (3.54), $b_m^k$ is given by (2.28), the coordinate $\xi = \xi_0$ conforms to the horizontal contour of the cylinder such that $\tanh\xi_0 = b/a$, and $l_1$ denotes:

$$l_1 = h\ (\sinh^2\xi_0 + \sin^2\eta)^{1/2} = h\ (\cosh^2\xi_0 - \cos^2\eta)^{1/2} \qquad (3.56)$$

By applying the boundary condition (3.54) to the expressions obtained for $\phi_m^k$, the unknown coefficients may be determined. Thus substituting (3.49) and (3.53) into (3.54), multiplying both

sides by $ce_{2n}$, $ce_{2n+1}$, $se_{2n+2}$ and $se_{2n+1}$ in turn, integrating with respect to $\eta$ from 0 to $2\pi$, and using the orthogonality of the periodic Mathieu functions, one obtains for the various modes of motion:

$$\phi_0^k = b_0^k \, h \, \sinh\xi_0 \sum_{n=0}^{\infty} \frac{A_1^{(2n+1)}(q_0)}{Mc_{2n+1}^{(3)'}(\xi_0,q_0)} Mc_{2n+1}^{(3)}(\xi,q_0) \, ce_{2n+1}(\eta,q_0) \qquad k = 1,5 \qquad (3.57)$$

$$\phi_m^k = b_m^k \, h \, \sinh\xi_0 \sum_{n=0}^{\infty} \frac{A_1^{(2n+1)}(-q_m)}{Mc_{2n+1}^{(3)'}(\xi_0,-q_m)} Mc_{2n+1}^{(3)}(\xi,-q_m) \, ce_{2n+1}(\eta,-q_m) \qquad k = 1,5; \ m \geq 1 \quad (3.58)$$

$$\phi_0^k = -i^k \, b_0^k \, h \, \cosh\xi_0 \sum_{n=0}^{\infty} \frac{B_1^{(2n+1)}(q_0)}{Ms_{2n+1}^{(3)'}(\xi_0,q_0)} Ms_{2n+1}^{(3)}(\xi,q_0) \, se_{2n+1}(\eta,q_0) \qquad k = 2,4 \qquad (3.59)$$

$$\phi_m^k = -i^k \, b_m^k \, h \, \cosh\xi_0 \sum_{n=0}^{\infty} \frac{B_1^{(2n+1)}(-q_m)}{Ms_{2n+1}^{(3)'}(\xi_0,-q_m)} Ms_{2n+1}^{(3)}(\xi,-q_m) \, se_{2n+1}(\eta,-q_m) \quad k = 2,4; \ m \geq 1 \quad (3.60)$$

$$\phi_0^6 = b_0^6 \frac{h^2}{2} \sum_{n=0}^{\infty} \frac{B_2^{(2n+2)}(q_0)}{Ms_{2n+2}^{(3)'}(\xi_0,q_0)} Ms_{2n+2}^{(3)}(\xi,q_0) \, se_{2n+2}(\eta,q_0) \qquad (3.61)$$

$$\phi_m^6 = b_m^6 \frac{h^2}{2} \sum_{n=0}^{\infty} \frac{B_2^{(2n+2)}(-q_m)}{Ms_{2n+2}^{(3)'}(\xi_0,-q_m)} Ms_{2n+2}^{(3)}(\xi,-q_m) \, se_{2n+2}(\eta,-q_m) \qquad m \geq 1 \qquad (3.62)$$

The prime denotes a derivative with respect to $\xi$, and $A_{2l+p}^{(2n+p)}$ and $B_{2l+p}^{(2n+p)}$ are Fourier coefficients obtained from:

$$ce_{2n+p}(\eta,q_m) = \sum_{l=0}^{\infty} A_{2l+p}^{(2n+p)}(q_m) \cos[\ (2l+p)\eta\ ] \qquad (3.63)$$

$$se_{2n+p}(\eta,q_m) = \sum_{l=0}^{\infty} B_{2l+p}^{(2n+p)}(q_m) \sin[\ (2l+p)\eta\ ] \qquad (3.64)$$

with:

$$\int_0^{2\pi} [ce_r(\eta,q_m)]^2 \, d\eta = \int_0^{2\pi} [se_r(\eta,q_m)]^2 \, d\eta = \pi \qquad (3.65)$$

30

and $A_0$, $A_1$, $B_2$ and $B_1$ positive, according to Ince (1932a,b).

## 3.2.1 Hydrodynamic Coefficients

Substituting the above expressions for the potentials into (2.45), and using (2.43) and (2.44), the hydrodynamic coefficients for the various modes may be expressed as:

$$\frac{\mu_{jk} + i\lambda_{jk}/\omega}{\rho a^l} = -\frac{\pi}{(k_0 a)^{l-2}}\frac{b^2}{a^2}\sum_{n=0}^{\infty}\frac{A_1^{(2n+1)}(q_0)^2}{Mc_{2n+1}^{(3)'}(\xi_0,q_0)}Mc_{2n+1}^{(3)}(\xi_0,q_0)\,f_0^{(l)}(k_0 d)$$

$$-\sum_{m=1}^{\infty}\frac{\pi}{(k_m a)^{l-2}}\frac{b^2}{a^2}\sum_{n=0}^{\infty}\frac{A_1^{(2n+1)}(-q_m)^2}{Mc_{2n+1}^{(3)'}(\xi_0,-q_m)}Mc_{2n+1}^{(3)}(\xi_0,-q_m)\,f_m^{(l)}(k_m d) \qquad j,k=1,5 \qquad (3.66)$$

$$\frac{\mu_{jk} + i\lambda_{jk}/\omega}{\rho a^l} = (-1)^l\frac{\pi}{(k_0 a)^{l-2}}\sum_{n=0}^{\infty}\frac{B_1^{(2n+1)}(q_0)^2}{Ms_{2n+1}^{(3)'}(\xi_0,q_0)}Ms_{2n+1}^{(3)}(\xi_0,q_0)\,f_0^{(l)}(k_0 d)$$

$$+\sum_{m=1}^{\infty}(-1)^l\frac{\pi}{(k_m a)^{l-2}}\sum_{n=0}^{\infty}\frac{B_1^{(2n+1)}(-q_m)^2}{Ms_{2n+1}^{(3)'}(\xi_0,-q_m)}Ms_{2n+1}^{(3)}(\xi_0,-q_m)\,f_m^{(l)}(k_m d) \qquad j,k=2,4 \qquad (3.67)$$

$$\frac{\mu_{66} + i\lambda_{66}/\omega}{\rho a^5} = -\frac{\pi}{4}\frac{1}{(k_0 a)}\frac{1}{\cosh^4\xi_0}\sum_{n=0}^{\infty}\frac{B_2^{(2n+2)}(q_0)^2}{Ms_{2n+2}^{(3)'}(\xi_0,q_0)}Ms_{2n+2}^{(3)}(\xi_0,q_0)\,f_0^{(3)}(k_0 d)$$

$$-\sum_{m=1}^{\infty}\frac{1}{4}\frac{1}{(k_m a)}\frac{1}{\cosh^4\xi_0}\sum_{n=0}^{\infty}\frac{B_2^{(2n+2)}(-q_m)^2}{Ms_{2n+2}^{(3)'}(\xi_0,-q_m)}Ms_{2n+2}^{(3)}(\xi_0,-q_m)\,f_m^{(3)}(k_m d) \qquad (3.68)$$

where:

$$l = \begin{cases} 3 & \text{for } j, k = 1; \text{ or } j, k = 2 \\ 5 & \text{for } j, k = 5; \text{ or } j, k = 4 \\ 4 & \text{for } j = 1, k = 5; \text{ or } j = 2, k = 4 \end{cases} \qquad (3.69)$$

Bearing in mind the symmetry of the added mass and damping coefficient matrices in general and the symmetry of the structure in particular, the complete set of hydrodynamic coefficients are then given as:

$$[\mu_{jk}] = \begin{bmatrix} \mu_{11} & 0 & 0 & 0 & \mu_{15} & 0 \\ 0 & \mu_{22} & 0 & \mu_{24} & 0 & 0 \\ 0 & 0 & 0 & 0 & 0 & 0 \\ 0 & \mu_{24} & 0 & \mu_{44} & 0 & 0 \\ \mu_{15} & 0 & 0 & 0 & \mu_{55} & 0 \\ 0 & 0 & 0 & 0 & 0 & \mu_{66} \end{bmatrix} ; \quad [\lambda_{jk}] = \begin{bmatrix} \lambda_{11} & 0 & 0 & 0 & \lambda_{15} & 0 \\ 0 & \lambda_{22} & 0 & \lambda_{24} & 0 & 0 \\ 0 & 0 & 0 & 0 & 0 & 0 \\ 0 & \lambda_{24} & 0 & \lambda_{44} & 0 & 0 \\ \lambda_{15} & 0 & 0 & 0 & \lambda_{55} & 0 \\ 0 & 0 & 0 & 0 & 0 & \lambda_{66} \end{bmatrix} \qquad (3.70)$$

The diagonal terms in the damping matrix may also be obtained from the corresponding exciting forces, given in Appendix A, by use of (2.47). Noting that the periodic Mathieu functions are normalized according to (3.65):

$$\int_0^{2\pi} | C_x |^2 \, d\alpha = 4\pi \frac{b^2}{a^2} \sum_{n=0}^{\infty} \left[ \frac{A_1^{(2n+1)}(q)}{|Mc_{2n+1}^{(3)'}(\xi_0,q_0)|} \right]^2 \qquad (3.71)$$

$$\int_0^{2\pi} | C_y |^2 \, d\alpha = 4\pi \sum_{n=0}^{\infty} \left[ \frac{B_1^{(2n+1)}(q)}{|Ms_{2n+1}^{(3)'}(\xi_0,q_0)|} \right]^2 \qquad (3.72)$$

$$\int_0^{2\pi} | C_{xy} |^2 \, d\alpha = \frac{\pi}{\cosh^4(\xi_0)} \sum_{n=0}^{\infty} \left[ \frac{B_2^{(2n+2)}(q)}{|Ms_{2n+2}^{(3)'}(\xi_0,q_0)|} \right]^2 \qquad (3.73)$$

where $C_x$, $C_y$ and $C_{xy}$ are given in (A.20) - (A.22). Applying (2.47) to (A.15) - (A.19) and making use of (3.71) - (3.73), alternative expressions for the damping coefficients are obtained:

$$\frac{\lambda_{kk}}{\rho a^l \omega} = 2 \frac{f_0^{(l)}(k_0 d)}{(k_0 a)^{l-2}} \frac{b^2}{a^2} \sum_{n=0}^{\infty} \left[ \frac{A_1^{(2n+1)}(q_0)}{|Mc_{2n+1}^{(3)'}(\xi_0,q_0)|} \right]^2 \qquad k = 1, 5 \qquad (3.74)$$

$$\frac{\lambda_{kk}}{\rho a^l \omega} = 2 \frac{f_0^{(l)}(k_0 d)}{(k_0 a)^{l-2}} \sum_{n=0}^{\infty} \left[ \frac{B_1^{(2n+1)}(q_0)}{|Ms_{2n+1}^{(3)'}(\xi_0,q_0)|} \right]^2 \qquad k = 2, 4 \qquad (3.75)$$

$$\frac{\lambda_{66}}{\rho a^5 \omega} = \frac{1}{2\cosh^4(\xi_0)} \frac{f_0^{(3)}(k_0 d)}{k_0 a} \sum_{n=0}^{\infty} \left[ \frac{B_2^{(2n+2)}(q_0)}{|Ms_{2n+2}^{(3)'}(\xi_0,q_0)|} \right]^2 \qquad (3.76)$$

where:

$$l = \begin{cases} 3 & k = 1,\ 2 \\ 5 & k = 5,\ 4 \end{cases} \tag{3.77}$$

It is to be noted that high frequency approximations for the damping coefficients similar to those developed for the circular cylinder in section 3.1.2 are extremely difficult, if not impossible, to obtain, due to the absence of suitable asymptotic expansions for the Mathieu functions in (3.66) - (3.68). Nevertheless, limiting values of the added masses may still be calculated by discarding the propagating mode and using (3.30) - (3.32) in (3.66) - (3.68), provided that the vertical eigenvalues in (3.52) are now obtained from (3.29) instead of (2.22).

This completes an outline of the analytical solutions for circular and elliptic cylinders. For the more general case of cylinders of arbitrary section, the boundary value problems in Chapter 2 will need to be solved numerically and appropriate numerical methods are taken up in the next chapter.

# Chapter 4

# NUMERICAL SOLUTIONS

Numerical solutions for the horizontal plane problems for $\phi_m^k$ described in Chapter 2 are based on the finite element method or the method of integral equations. The two methods are described in texts by Zienkiewicz *et al.* (1978), Sarpkaya and Isaacson (1981), Mei (1983), Chakrabarti (1987), Brebbia and Dominguez (1989), and Faltinsen (1990). A comparison of the two methods has been given by Bettess (1987), and some guidelines for the choice of one over the other are given in a review by Yeung (1982). The method of integral equations has been more widely used in design practice, and is considered here in the context of the radiation problem under consideration.

## 4.1 Method of Integral Equations

Three closely related versions of integral equation methods exist in the literature of body-wave hydrodynamics. In the present context, the two-dimensional potential functions $\phi_m^k$ described in Chapter 2 are to satisfy the governing equation (2.23) or (2.24) subject to the radiation condition (2.29) or (2.30), and the body surface condition (2.26). For this potential $\phi_m^k$ described everywhere outside the body contour $C_b$ (Fig. 4), these alternative versions are related to an assumption made about the behaviour of a potential $\bar{\phi}_m^k$ for a related, fictitious problem for the interior of $C_b$.

Green's integral equation, which is a direct consequence of Green's second identity, expresses the potential at any point $x = (x,y)$ within a fluid domain S in the form of an integral over the boundary of S, which is taken to comprise of the body boundary $C_b$ and a radiation boundary $C_r$ located at a large distance from the body, as indicated in Fig. 4. Green's second identity may be applied to the region S outside $C_b$, bounded by $C_r$, and which excludes the neighbourhood of a field point $x = (x,y)$ which may be located entirely within the fluid (Fig. 4a) or on the boundary $C_b$

(Fig. 4b):

$$\iint_S [\ \nabla^2 G_m(x,\xi)\ \phi_m^k(\xi) - G_m(x,\xi)\ \nabla^2\phi_m^k(\xi)\ ]\ dS\ =$$

$$\int_{C_b+C_r+C_\epsilon} [\ \phi_m^k(\xi)\ \frac{\partial G_m}{\partial n'}(x,\xi) - \frac{\partial \phi_m^k}{\partial n'}(\xi)\ G_m(x,\xi)\ ]\ dC \qquad (4.1)$$

Here, $n'$ denotes distance measured normal to $C_b$ at $\xi = (\xi,\eta)$ and directed into S (see Fig. 4), and the integrals are with respect to $\xi$. $G_m$ is a Green's function which is chosen to satisfy the same field equation (2.23) or (2.24), and the same radiation condition (2.29) or (2.30) as $\phi_m^k$. Adopting the method of separation of variables in cylindrical coordinates, (2.23) and (2.24) yield Bessel's equation and Bessel's modified equation respectively. The general solution of the former involves the Hankel functions of the first and second kinds. Of these, only the Hankel function of the first kind satisfies the far field condition. The general solution of the latter involves the modified Bessel functions of the first and second kinds. Of these, the modified Bessel function of the second kind vanishes for large values of the argument, whereas the modified Bessel function of the first kind increases exponentially with distance and so is discarded. Accordingly, appropriate Green's functions may be chosen as:

$$G_m(x,\xi) = \begin{cases} \dfrac{i}{2}\ H_0^{(1)}(k_0 R) & m = 0 \\[2ex] \dfrac{1}{\pi}\ K_0(k_m R) & m \geq 1 \end{cases} \qquad (4.2)$$

where $R = |\ x - \xi\ |$. Since both $\phi_m^k$ and $G_m$ satisfy the field equation, and the point x is excluded from S, the left-hand side of (4.1) vanishes, and since $\phi_m^k$ and $G_m$ also satisfy the radiation condition on $C_r$, (2.29) or (2.30), the integral over the radiation boundary $C_r$ vanishes as well. The right-hand side of (4.1) can thus be separated into integrals over $C_b$ and $C_\epsilon$. Of these the integral over $C_\epsilon$ in the limit $\epsilon \to 0$ takes alternate forms depending on whether x is entirely within S (Fig. 4a) or lies on $C_b$ (Fig. 4b). In the first case we have:

35

$$\underset{\epsilon \to 0}{\text{Limit}} \int_{C_\epsilon} [\ \phi_m^k \frac{\partial G_m}{\partial n'} - \frac{\partial \phi_m^k}{\partial n'} G_m\ ]\ dC\ =\ \underset{\epsilon \to 0}{\text{Limit}} \int_0^{2\pi} [\ \phi_m^k\ (-\frac{1}{\pi\epsilon}) - \frac{\partial \phi_m^k}{\partial n'} (\ -\frac{1}{\pi}\ \ln(k_m\epsilon))]\ \epsilon\ d\theta$$

$$=\ -2\phi_m^k \qquad\qquad (4.3)$$

where the limiting forms for small arguments of the Green's functions have been used.

In the case where x lies on $C_b$, and assuming that $C_b$ is smooth in the neighbourhood of x (Fig. 4b), the integral may be re-evaluated as follows:

$$\underset{\epsilon \to 0}{\text{Limit}} \int_{C_\epsilon} [\ \phi_m^k \frac{\partial G_m}{\partial n'} - \frac{\partial \phi_m^k}{\partial n'} G_m\ ]\ dC\ =\ \underset{\epsilon \to 0}{\text{Limit}} \int_0^{\pi} [\ \phi_m^k\ (-\frac{1}{\pi\epsilon}) - \frac{\partial \phi_m^k}{\partial n'} (\ -\frac{1}{\pi}\ \ln(k_m\epsilon))]\ \epsilon\ d\theta$$

$$=\ -\phi_m^k \qquad\qquad (4.4)$$

Finally, when x lies outside S (i.e. within $\overline{S}$) the integral over $C_\epsilon$ is absent. Using (4.1), (4.3) and (4.4), Green's integral equation for $\phi_m^k$ may thus be given as follows:

$$\int_{C_b} [\ \phi_m^k(\xi)\ \frac{\partial G_m}{\partial n'}(x,\xi) - \frac{\partial \phi_m^k}{\partial n'}(\xi)\ G_m(x,\xi)\ ]\ dC\ =\ \kappa\ \phi_m^k(x) \qquad\qquad (4.5)$$

where:

$$\kappa\ =\ \begin{cases} 2 & x \text{ in } S \\ 1 & x \text{ on } C_{b+} \\ 0 & x \text{ in } \overline{S} \end{cases} \qquad\qquad (4.6)$$

In (4.5), for x on $C_b$, the Cauchy principal value of the integral is implied and x lies on $C_b$ approached from within S.

Turning now to the interior potential $\overline{\phi}_m^k$ which applies to a (fictitious) potential flow problem for the region $\overline{S}$ within $C_b$, $\overline{\phi}_m^k$ is governed by the same equation, (2.23) or (2.24), as $\phi_m^k$ and

36

consequently must satisfy an integral equation similar to (4.5). Thus:

$$\int_{C_b} [ \ \bar{\phi}_m^k(\xi) \ \frac{\partial G_m}{\partial n'}(x,\xi) - \frac{\partial \bar{\phi}_m^k}{\partial n'}(\xi) \ G_m(x,\xi) \ ] \ dC \ = \ \bar{\kappa} \ \bar{\phi}_m^k(x) \tag{4.7}$$

where:

$$\bar{\kappa} = \begin{cases} 0 & x \text{ in } S \\ -1 & x \text{ on } C_{b-} \\ -2 & x \text{ in } \bar{S} \end{cases} \tag{4.8}$$

In (4.7), for $x$ on $C_b$, the Cauchy principal value of the integral is implied and $x$ lies on $C_b$ approached from within $\bar{S}$. Subtraction of (4.7) from (4.5) for the case $x$ in $S$ (i.e. $\kappa = 2$, $\bar{\kappa} = 0$) yields:

$$2 \ \phi_m^k(x) \ = \ \int_{C_b} [ \ ( \ \phi_m^k(\xi) - \bar{\phi}_m^k(\xi) \ ) \ \frac{\partial G_m}{\partial n'}(x,\xi) - ( \ \frac{\partial \phi_m^k}{\partial n'}(\xi) - \frac{\partial \bar{\phi}_m^k}{\partial n'}(\xi) \ ) \ G_m(x,\xi) \ ] \ dC$$

$$\text{for } x \text{ in } S \tag{4.9}$$

Now, depending on the boundary condition imposed on $C_b$ in defining the interior problem for $\bar{\phi}_m^k$, (4.9) gives rise to various forms of expressions for the exterior potential.

*(a)     Source Distribution*

First, the selected boundary condition on $C_b$ is taken as:

$$\bar{\phi}_m^k = \phi_m^k \qquad\qquad \text{on } C_b \tag{4.10}$$

Substituting $f_m^k = (\partial \bar{\phi}_m^k/\partial n' - \partial \phi_m^k/\partial n')/2$ in (4.9), the exterior potential $\phi_m^k$ is given as:

$$\phi_m^k(x) \ = \ \int_{C_b} f_m^k(\xi) \ G_m(x,\xi) \ dC \qquad \text{for } x \text{ in } S \tag{4.11}$$

37

This corresponds to a continuous distribution of sources of strength $f_m^k$ along $C_b$. The body surface boundary condition has not yet been applied, and the source strength function $f_m^k$ will have to be chosen so as to ensure that this is satisfied. This condition is given by (2.26), and by applying the representation for $\phi_m^k$ given by (4.11), this gives rise to the following integral equation for the unknown function $f_m^k$:

$$-f_m^k(x) + \int_{C_b} f_m^k(\xi) \frac{\partial G_m}{\partial n}(x,\xi)\, dC = n_k'(x)\, b_m^k \qquad (4.12)$$

Here, $x$ lies on $C_b$ and $n$ is distance in the direction of the normal vector at $x$ directed into S.

*(b)    Dipole Distribution*

As an alternative to (4.10), the boundary condition for $\overline{\phi}_m^k$ is taken as:

$$\frac{\partial \phi_m^k}{\partial n'} = \frac{\partial \overline{\phi}_m^k}{\partial n'} \qquad\qquad \text{on } C_b \qquad (4.13)$$

In this case, substituting $\mu_m^k = (\phi_m^k - \overline{\phi}_m^k)/2$ into (4.9), the exterior potential $\phi_m^k$ is now given as:

$$\phi_m^k(x) = \int_{C_b} \mu_m^k(\xi) \frac{\partial G_m}{\partial n'}(x,\xi)\, dC \qquad (4.14)$$

This corresponds to a continuous distribution of dipoles of strength $\mu_m^k$ along $C_b$. The body boundary condition given by (2.26) now takes the form:

$$\int_{C_b} \mu_m^k(\xi) \frac{\partial^2 G_m}{\partial n \partial n'}(x,\xi)\, dC = n_k'(x)\, b_m^k \qquad (4.15)$$

*(c)    Mixed Distribution*

Thirdly, the boundary condition on $C_b$ may be taken as:

$$\overline{\phi}_m^k = 0 \qquad\qquad \text{on } C_b \qquad (4.16)$$

Such a homogeneous Dirichlet condition for $\overline{\phi}_m^k$ on $C_b$ makes $\overline{\phi}_m^k$ vanish uniformly in $\overline{S}$, except at a set of irregular frequencies. Except at these values, (4.5) is recovered and may be alternately thought of as due to a distribution of sources and doublets over $C_b$. The integral equation to be solved is obtained from (4.5) with x on $C_b$, and applying the boundary condition (2.26) this may be recast as:

$$-\phi_m^k(x) + \int_{C_b} \phi_m^k(\xi) \frac{\partial G_m}{\partial n'}(x,\xi)\, dC = b_m^k \int_{C_b} n_k'(\xi)\, G_m(x,\xi)\, dC \qquad \text{for x on } C_b \qquad (4.17)$$

Among these three alternatives, the source distribution method, involving the numerical solution of the line integral equation in (4.12) and the subsequent determination of the potential on $C_b$ based on (4.11), is most commonly adopted, and will be used in this thesis. A similar approach has been adopted in the corresponding scattering problem by Isaacson (1978), and is briefly mentioned in Appendix A.

## 4.2 Numerical Scheme

In a numerical solution of (4.12), the contour $C_b$ is discretized into a finite number of segments, with the function $f_m^k$ taken as uniform over each segment. Equation (4.12) is then applied at the centre of each segment in turn and the integral equation is reduced to a set of linear algebraic equations:

$$\sum_{j=1}^{N} B_{ij}^m\, f_m^k(\xi_j) = n_k'(x_i)\, b_m^k \qquad \text{for } i = 1, ..., N \qquad (4.18)$$

$x_i$ and $\xi_j$ are the values of $x$ and $\xi$ at the centres of the i-th and j-th segments respectively. The coefficients $B_{ij}^m$ are given as:

$$B_{ij}^m = \int_{\Delta C_j} \frac{\partial G_m}{\partial n}(x_i,\xi)\, dC \qquad (4.19)$$

where $\Delta C_j$ is the length of the j-th segment. When $i \neq j$, the integrand in (4.19) is taken as

constant over $\Delta C_j$ and thus $B_{ij}^m$ is approximated as:

$$B_{ij}^m = \Delta C_j \frac{\partial G_m}{\partial n}(x_i, \xi_j) \tag{4.20}$$

When $i = j$, the first term of (4.12) accounts for the influence of the source distribution on i-th segment on the centre of the segment, so that $B_{ii}^m$ is taken as:

$$B_{ii}^m = -1 \tag{4.21}$$

Once the matrix $B_{ij}^m$ has been evaluated, the source strength distribution function $f_m^k$ may be obtained from (4.18) by a standard matrix inversion procedure. The potentials themselves may then be obtained from a discretized form of (4.11):

$$\phi_m^k(x_i) = \sum_{j=1}^{N} A_{ij}^m \, f_m^k(\xi_j) \qquad\qquad i = 1, ..., N \tag{4.22}$$

in which:

$$A_{ij}^m = \int_{\Delta C_j} G_m(x_i, \xi) \, dC \tag{4.23}$$

As a consistent approximation, $A_{ij}^m$ may be evaluated as:

$$A_{ij}^m = \Delta C_j \, G_m(x_i, \xi_j) \qquad\qquad \text{for } i \neq j \tag{4.24}$$

$$A_{ii}^m = \frac{\Delta C_i}{\pi} \left\{ 1 - \ln\left[\frac{k_m \Delta C_i}{2}\right] \right\} \tag{4.25}$$

A derivation of the above expressions for $A_{ij}^m$ and $B_{ij}^m$ are given in Appendix B.

In a numerical scheme to calculate the corresponding hydrodynamic coefficients, the series expansions in (2.39) and (2.45) are truncated to a finite number of terms and the integrals are replaced by appropriate summations as follows:

40

$$I'_{jk} = \begin{cases} \displaystyle\sum_{m=0}^{M} \Big\{ \sum_{i=1}^{N} \phi_m^k(x_i)\, n_j'(x_i)\, \Delta C_i \Big\} Z_m(k_m z) & \text{for } k = 1, 2, 3, 6 \\[3ex] \displaystyle z \sum_{m=0}^{M} \Big\{ \sum_{i=1}^{N} \phi_m^k(x_i)\, n_j'(x_i)\, \Delta C_i \Big\} Z_m(k_m z) & \text{for } k = 4, 5 \end{cases} \tag{4.26}$$

$$I_{jk} = \sum_{m=0}^{M} b_m^j \Big\{ \sum_{i=1}^{N} \phi_m^k(x_i)\, n_j'(x_i)\, \Delta C_i \Big\} \tag{4.27}$$

Finally, the added masses and damping coefficients, $\mu'_{jk}$, $\lambda'_{jk}$, $\mu_{jk}$ and $\lambda_{jk}$, may be obtained directly from $I'_{jk}$ and $I_{jk}$ by means of (2.37), (2.38), (2.43) and (2.44). This completes an outline of the numerical evaluation of the hydrodynamic coefficients using the method of integral equations. The remainder of this chapter considers methods of improving the accuracy of numerical calculations; and the effects of the irregular frequencies.

# 4.3  Convergence of Numerical Results

The precision with which $C_b$ is discretized clearly has a significant effect on the accuracy of the numerical results. Sarpkaya and Isaacson (1981) have summarized general guidelines on the size and distribution of segments. In brief, a larger number of segments yields more accurate results, but at the expense of increased computer time and storage requirements. For example, for water wave scattering by a vertical circular cylinder, Isaacson (1978) has shown how the accuracy of numerical results for runup and exciting force improves with an increase in the number of segments used to describe the horizontal contour of the cylinder surface.

It is generally believed that a numerical result calculated on the basis of N segments will converge to a correct answer as N is continuously increased (Jefferys, 1987; Korsmeyer et al., 1988). Such a variation may be represented as some function of N, and the limiting value may be obtained by suitable extrapolation schemes (Dahlquist and Bjorck, 1974; Bender and Orszag, 1978). Two such schemes, namely the Shanks transformation and the Richardson extrapolation, seem particularly suited to this purpose, and are applied here in the present context.

## 4.3.1 Shanks Transformation

Consider a sequence A(N) whose N-th term is expressed in the form:

$$A(N) = \alpha_0 + \alpha_1 \varepsilon^N \qquad (4.28)$$

where $\alpha_0$, $\alpha_1$ and $\varepsilon$ are constants, such that $\alpha_1$ is non-zero, and $|\varepsilon| < 1$. Thus $A(N) \to \alpha_0$ as $N \to \infty$. When $\varepsilon$ is positive, the transient $\alpha_1 \varepsilon^N$ in (4.28) decays monotonically with increasing N; and when $\varepsilon$ is negative the transient has an oscillatory decay with increasing N. Since any member of this sequence depends on the three parameters $\alpha_0$, $\alpha_1$ and $\varepsilon$, it follows that $\alpha_0$, which represents the limiting value $A(N \to \infty)$, can be determined from three terms of the sequence, say $A(N_1)$, $A(N_2)$ and $A(N_3)$. In fact, if $N_1$, $N_2$ and $N_3$ are chosen in arithmetic progression, such that $N_3 - N_2 = N_2 - N_1$, then $\alpha_0$ is given by the nonlinear transformation:

$$\alpha_0 = S[A(N_2)] = \frac{A(N_1)\,A(N_3) - A^2(N_2)}{A(N_1) + A(N_3) - 2A(N_2)} \qquad (4.29)$$

where S[ ] denotes the Shanks transformation studied extensively by Shanks (1955).

In the present context, A(N) would represent a calculated variable, such as an added mass, damping coefficient or exciting force, estimated using N segments in a discretization scheme. Thus (4.28) represents an assumed form of variation of the estimated variable A(N) as a function of the number of segments; and (4.29) then represents the transformation which eliminates the assumed transient, and provides an estimate of $A(N \to \infty)$ in terms of $A(N_1)$, $A(N_2)$, and $A(N_3)$. The latter correspond to numerical values of hydrodynamic coefficients calculated using $N_1$, $N_2$, and $N_3$ segments respectively.

In fact, in the present context it turns out that (4.28) represents a poor approximation to the variation of A(N) with the number of facets. Rather, the leading term in the error in numerical solutions is expected to be inversely proportional to some power of N. This can be accomplished by replacing N by $\log_\upsilon(N)$ in (4.28), where $\upsilon$ is a constant and $\varepsilon$ is taken as positive. The

42

resulting variation of A(N) with N can then be re-cast in the alternative form:

$$A(N) = \alpha_0 + \frac{\alpha_1}{N^\sigma} \qquad\qquad (4.30)$$

where $\sigma = -\log_\upsilon(\varepsilon)$ is a positive constant. The expression for $\alpha_0$ given by (4.29) continues to hold provided that we now choose $N_1$, $N_2$, and $N_3$ in geometric progression with a common ratio $\upsilon = N_3/N_2 = N_2/N_1$. Of course, in any real application this transformation will not produce an exact result since the assumed form of variation with N may still be incorrect.

Indeed, one difficulty in applying the Shanks transformation is that the calculated value of $\alpha_0$ can become unduly large for certain sets of values of A(N). In particular, if the variation of A(N) with N is linear, such that $A(N_3) - A(N_2) = A(N_2) - A(N_1)$, then the denominator of (4.29) becomes zero, and the estimation of $\alpha_0$ fails.

When results are available at more than three levels of discretization, it is possible to apply the Shanks transformation procedure to a set of successive triads of A(N) in order to obtain a set of estimates of $\alpha_0$ corresponding to the Shanks transforms $S[A(N_l)]$; and then re-apply this procedure to a set of previously calculated Shanks transforms themselves. In this way a second level of transforms, denoted $S^2[A(N_l)]$, may be developed. More generally, the procedure may be applied repeatedly so as to produce a sequence of sets corresponding to $S[A(N_l)]$, $S^2[A(N_l)]$, ..., which may be more and more rapidly convergent. Thus L available values of A(N), with L odd, eventually yield at the highest level the single Shanks transform $S^J[A(N_K)]$ where $J = (L - 1)/2$ and $K = (L + 1)/2$.

As an example of the foregoing, when the variable A(N) has been obtained at five levels of discretization, $L = 5$, then the three sets $[A(N_1), A(N_2), A(N_3)]$, $[A(N_2), A(N_3), A(N_4)]$ and $[A(N_3), A(N_4), A(N_5)]$ give rise to the first level transforms $S[A(N_2)]$, $S[A(N_3)]$ and $S[A(N_4)]$. These three values in turn give rise to a second level transform $S^2[A(N_3)]$.

43

## 4.3.2 Richardson Extrapolation

As an alternative to the Shanks transformation, the Richardson extrapolation scheme, previously used by Breit *et al.* (1985), is based instead on a different assumption regarding the variation of the calculated variable A(N) with the number of facets N. This assumed variation is such that A(N) contains transients in inverse, known powers of N and thus may instead be expressed in the form:

$$A(N) = \alpha_0 + \frac{\alpha_1}{N^{\sigma_1}} + \frac{\alpha_2}{N^{\sigma_2}} + \dots \tag{4.31}$$

where $\alpha_l$ and $\sigma_l$ are constants, with $\sigma_l$ positive and increasing in magnitude for increasing $l$: $\sigma_{l+1} > \sigma_l$. The limiting value $A(N \to \infty)$ corresponds to $\alpha_0$ and is required. By retaining the first L terms of this series, and assuming known values of $\sigma_l$, L available values of A(N) at different values of N provides L equations for the unknown coefficients which can be used to solve for the required $\alpha_0$.

In the usual case, $\sigma_l = l$ is assumed (i.e. $\sigma_1 = 1$, $\sigma_2 = 2$, ...) so that (4.31) becomes:

$$A(N) = \alpha_0 + \frac{\alpha_1}{N} + \frac{\alpha_2}{N^2} + \dots \tag{4.32}$$

where $\alpha_l$ are unknown constants.

The simplest application of the above procedure is to estimate $\alpha_0$ from a knowledge of two values of A(N). Thus, by neglecting terms smaller than $\alpha_1/N$, the resulting two equations for $\alpha_0$ and $\alpha_1$ can be solved to yield:

$$\alpha_0 = R[A(N_2)] = \frac{\upsilon A(N_2) - A(N_1)}{\upsilon - 1} \tag{4.33}$$

where $\upsilon = N_2/N_1$ and R[ ] denotes the Richardson extrapolation. A key feature of this operation is that it is linear in A. If additional A(N) values are available, this procedure may be repeated by operating on successive pairs of A(N) in order to obtain a set of estimates of $\alpha_0$, with $R[A(N_l)]$ denoting the estimate obtained from the pair of values $A(N_l)$ and $A(N_{l-1})$. This represents a first level of extrapolation which provides a series of estimates of $\alpha_0$ corresponding to the use of

successive pairs of values of A(N). The following formula may be then applied to these Richardson transforms in order to obtain a second level of extrapolation, denoted $R^2[\ ]$.

$$R^2[A(N_l)] = \frac{\upsilon^2\, R[A(N_l)] - R[A(N_{l-1})]}{\upsilon^2 - 1} \tag{4.34}$$

This procedure may be repeated to higher levels of transformation in general. In fact the estimate $R^{L-1}[A(N_L)]$, which requires L values of A(N), is equivalent to an estimate of $\alpha_0 = A(N \rightarrow \infty)$ retaining the first L terms of the series on the right-hand side of (4.32).

In the particular case of three available values of A(N), the highest level of extrapolation corresponds to a neglect of terms smaller than $\alpha_2/N^2$. This provides three equations which yield:

$$R^2[A(N_3)] = \frac{\upsilon^3 A(N_3) - \upsilon(\upsilon+1)A(N_2) + A(N_1)}{(\upsilon+1)(\upsilon-1)^2} \tag{4.35}$$

And in the particular case when $\upsilon = 2$, (such that $N_3 = 2N_2 = 4N_1$) this corresponds to the simple result:

$$R^2[A(N_3)] = \frac{8A(N_3) - 6A(N_2) + A(N_1)}{3} \tag{4.36}$$

In calculating hydrodynamic coefficients, it is expected that it will generally suffice to use three values of A(N) as a reasonable compromise between accuracy and computational effort, and thus obtain the best estimate of $\alpha_0$ as $R^2[A(N_3)]$ given by (4.36).

It is noted that the formulae given for the Richardson extrapolation are linear with respect to the available values of A, and the difficulty of an irregularity as in the case of the Shanks transformation does not arise.

# 4.4  Irregular Frequencies

All three forms of integral equations in the solution of $\phi_m^k$, (4.12), (4.15) and (4.17), are plagued by the presence of irregular frequencies for the propagating mode potential corresponding to

m = 0. These are discrete frequencies at which the method fails to give a unique solution. The matrix equation becomes ill-conditioned within a narrow band near these values. In the first and third methods (source and mixed distributions) discussed in section 4.1, the surface integral equation to be solved is an inhomogeneous Fredholm equation of the second kind with identical kernels, one being the transpose of the other, and hence the same irregular frequencies are akin to both (Yeung, 1982). On the other hand, the dipole distribution leads to a Fredholm equation of the first kind which possesses a different set of irregular frequencies. The difficulties due to irregular frequencies are important because the irregular frequencies are unknown *a priori* for a complicated geometry, and the situation worsens at high frequencies when the irregular frequency values become more closely spaced.

## 4.4.1 Reasons for Occurrence

Copley (1968) has given reasons for the occurrence of irregular frequencies in three-dimensional acoustic problems, and Mei (1983) has explained their occurrence in three-dimensional problems involving surface gravity waves. Somewhat similar causes account for the occurrence of irregular behaviour in the horizontal plane problem for $\phi_0^k$. It is to be noted though that the boundary value problem for $\phi_0^k$ posed by (2.23), (2.26) and (2.29) is uniquely solvable (e.g. Kolton and Kress, 1983), and the irregularities arise rather in the method used for representing the solution.

For all three integral equation methods mentioned in 4.1, the irregular frequencies are related to the properties of the corresponding interior problem for the potential $\bar{\phi}_0^k$.

Thus, the viability of the source distribution method depends on the inhomogeneous interior problem with the Dirichlet condition (4.10) on $C_b$. The homogeneous counterpart of this interior problem, with the Dirichlet condition $\bar{\phi}_0^k = 0$ on $C_b$, admits non-trivial solutions at a set of frequencies called the eigenfrequencies. At these frequencies, the inhomogeneous problem itself cannot be solved unless the following condition is satisfied:

$$\int_{C_b} \phi_0^k \frac{\partial \overline{\psi}_D}{\partial n'} dC = 0 \qquad (4.37)$$

where $\overline{\psi}_D$ is the interior eigenfunction of the corresponding eigenfrequency. Since there is then no finite potential $\overline{\phi}_0^k$ that satisfies the inhomogeneous interior problem, it follows that a source distribution, developed on the basis of a difference in the derivatives of the exterior and interior potentials as in (4.9), cannot then be realized. Thus the source distribution method fails at the eigenfrequencies of the interior Dirichlet problem which do not satisfy (4.37).

Similar remarks apply to the case of the dipole distribution method. In this case, the relevant inhomogeneous problem for the interior region is defined instead by the Neumann condition (4.13) on $C_b$. The dipole distribution method will fail at the eigenfrequencies of the corresponding homogeneous problem that do not now satisfy:

$$\int_{C_b} \frac{\partial \phi_0^k}{\partial n'} \overline{\psi}_N dC = 0 \qquad (4.38)$$

where $\overline{\psi}_N$ is the interior eigenfunction of the corresponding eigenfrequency.

Finally, in the case of the mixed distribution method, the homogeneous counterpart of the integral equation (4.17) admits non-trivial solutions at a set of frequencies. These frequencies turn out to be the same frequencies as the eigenfrequencies of the interior Dirichlet problem. Any solution to (4.17) is then not unique and the mixed distribution method fails.

Thus in the source and dipole distribution methods, in general, solutions do not exist in the first place whereas for the mixed distribution method, the problem is one of non-uniqueness of solution. Neither situation is desirable, but it has been observed that in actual numerical computations (Adachi and Ohmatsu, 1979) the mixed distribution yields less perturbed results.

It has been stated that irregular frequencies arise in the solution to $\phi_0^k$, but not in solutions to

$\phi_m^k$, $m \geq 1$. In order to prove the absence of irregularities in the integral equations for $\phi_m^k$, $m \geq 1$, it suffices to show that $\overline{\phi}_m^k$, which satisfies (2.24) in $\overline{S}$ and either a homogeneous Dirichlet or Neumann condition on $C_b$, vanishes uniformly in $\overline{S}$. This may indeed be shown by a simple application of Green's theorem (see, for example, Bateman, 1932).

## 4.4.2 Determination of Irregular Frequencies

For vertical cylinders of circular and elliptic sections, the irregular values can be determined exactly from available analytical solutions to the interior eigenvalue problem. Murphy (1978) thereby predicted the irregular values in the source distribution method for wave scattering by a vertical circular cylinder as the zeros of $J_m(k_0 a)$, $m = 0, 1, 2, ...$, where a denotes the cylinder radius. The first few zeros are tabulated in Table I. In the scattering problem, although the scattered potential is irregular at these values of $k_0 a$, the calculated overall force involves a term like $\int_0^{2\pi} \Phi \cos\theta \, d\theta$ and therefore by orthogonality will show discrepancies only at the zeros of $J_1(k_0 a)$. In the radiation problem, the radiated potential itself is irregular only at the zeros of $J_1(k_0 a)$ due to the condition in (4.37). In a similar way, irregular frequencies for an elliptic cylinder may be determined as corresponding to the zeros of the appropriate Mathieu function. In the case of a cylinder of arbitrary section, the irregular frequency values cannot be calculated easily. However, suitable upper and lower bounds may readily be obtained by considering the limiting circular or elliptic sections which completely enclose, and which are completely enclosed by, the water-line contour (Jones, 1974).

In the case of more general geometries, Wu and Price (1986) have calculated the irregular frequencies in the source representation for a rectangular box, circular tank, sector of a circular tank, and a horizontal triangular prism. They have noted that in calculations of the hydrodynamic coefficients for various oscillatory modes of motion, singular behaviour may not occur if the mode of body motion is of opposite symmetry to the interior potential solution, a condition analogous to (4.37) and (4.38). An 'equivalent box formula' to calculate irregular values for a general geometry has also been presented.

## 4.4.3 Methods to Nullify Irregular Behaviour

Thus it would seem that the irregular frequencies are a common problem associated with the Green kernel function. Except at low frequencies, they are so close together that it would appear impractical to use the method of integral equations in its basic form. Various means of circumventing these difficulties have been proposed. These may be broadly classified into three categories as described below.

### (a)    Addition of Null-field Equations

Schenck (1968) suggested such an approach to eliminating irregularities in the context of acoustic applications. These can be applied to water wave situations without essential changes. The general approach is to remedy the deficiencies of the mixed distribution method by imposing extra constraints through the application of Green's integral equation at certain strategic interior points. The idea is that, out of the set of solutions that satisfy the Fredholm equation resulting from the mixed distribution, only one will also satisfy the Green's integral equation for all points interior to the obstacle. The non-square or overdetermined system of equations is then solved by a least squares orthonormalizing procedure. However, the choice of the interior points is then critical. In short, at an irregular value, they should not lie on the nodal surface of the interior standing wave. At higher irregular values the nodal surfaces get closer and hence, for sufficiently short waves, it may become impractical to obtain enough useful points inside the obstacle (Chertock, 1970). This may pose a severe limitation on this approach.

### (b)    Modification to the Integral Equation

In a method proposed by Burton and Miller (1971), a new integral equation is formed at the outset by taking the normal gradient, with respect to the field point, of the Fredholm equation resulting from the mixed distribution. This, weighted by a coupling parameter $\alpha$, is then added to the original equation. Although each of the two integral equations has a set of irregular frequencies, these sets are distinct and the resulting formulation will yield unique solutions for all wave

49

numbers when $\alpha$ is chosen such that its imaginary part is non-zero. Good results at higher wave numbers were obtained by taking $\alpha = i/k_0$ where $k_0$ is the wave number (Meyer, Bell, Stallybrass and Zinn, 1979). In a recent study, Lee and Sclavounos (1989) have found that the optimum value of the coupling parameter is dependent on the body shape. The optimum value is in fact taken to be that which minimizes the condition number of the matrix equation at the first irregular frequency of the mixed distribution. They recommend $\alpha = 0.1i$ and $0.15i$ for the three-dimensional cases of a floating sphere and a floating vertical circular cylinder respectively. However, for an arbitrary geometry the method requires an estimation of the value of the irregular frequency, followed by a determination of the condition number of the matrix equation over a range of values of $\alpha$. This may involve substantial computational effort. Somewhat similar efforts were reported by Panich (1965), who proposed the use of a linear combination of source and dipole distributions with the dipole strength proportional to the source strength, and by Wu and Price (1987) who used a linear combination of Green's integral equation and separate integral equations applied to interior points.

*(c)    Modification to the Kernel*

Jones (1974) has shown that by adding a sufficiently large series of outgoing wave functions to the free space Green's function, any required number of characteristic frequencies may be eliminated in the source distribution method for the exterior acoustic problem. Jones' treatment of the two-dimensional problem is particularly suitable for water wave scattering and radiation by vertical cylinders and involves replacing the Green's function in (4.2) for the propagating mode corresponding to $m = 0$ with a modified form:

$$G_0'(x,\xi) = \frac{i}{2}H_0^{(1)}(k_0 \mid x-\xi \mid) + \sum_{m=0}^{M_1} c_m H_m^{(1)}(k_0 \mid x \mid)\cos(m\theta_x) H_m^{(1)}(k_0 \mid \xi \mid)\cos(m\theta_\xi)$$

$$+ \sum_{m=1}^{M_2} s_m H_m^{(1)}(k_0 \mid x \mid)\sin(m\theta_x) H_m^{(1)}(k_0 \mid \xi \mid)\sin(m\theta_\xi) \qquad (4.39)$$

Here, $\mid x \mid$, $\theta_x$ are polar coordinates of $x$, and similarly for $\xi$. If $L = \min(M_1+2, M_2+2)$, then no irregular behaviour occurs for at least the first $L-1$ irregular frequencies provided $c_m$ and $s_m$ are

real or their imaginary part is positive. The integral equation to be solved is again given by (4.12), but now the integral will be taken to be principal value only whenever necessary. There is considerable latitude over the choice of the constants $c_m$ and $s_m$, and an optimum range of values for these coefficients may have to be identified by actual numerical calculations for various fundamental configurations. Ursell (1978) simplified the proof of one of the principal results of Jones (1974), and Kleinman and Roach (1982) presented an explicit choice of coefficients of the added terms that is optimal in the sense of minimizing the least-square difference between the modified and exact Green's functions. In an adaptation of the work to water waves, Ursell (1981) treated the case of a semi-submerged horizontal cylinder of infinite length making simple harmonic heave oscillations. The additional multipole wave singularities introduced are complicated on account of the free surface and bottom boundary conditions. Other efforts in this direction include those due to Ogilvie and Shin (1978), Sayer and Ursell (1977) and Ursell (1953). Certain difficulties in some numerical solutions based on (4.39) have been reported by Brandt *et al.* (1985).

Angell *et al.* (1986) has shown that irregular frequencies do not occur in three-dimensional floating body problems if a simple Green's function is used i.e. one that satisfies only the boundary conditions at the sea bottom and the far field. The surface of integration should then be extended over both the ship hull and the free surface.

It has been indicated that the difficulties due to irregular frequencies become more serious at higher frequencies, when the irregular frequencies become more closely spaced. For the particular case of a vertical cylinder of arbitrary section, which is the focus of the present work, alternative approaches to circumventing the irregularities by use of various high frequency approximations are considered in the next chapter.

# Chapter 5

# HIGH FREQUENCY APPROXIMATIONS

In certain applications, such as those involving ice impact or earthquake excitation, or for very large structural concepts (e.g. Chow *et al.*, 1991), hydrodynamic coefficients are required at relatively high frequencies. However, difficulties with the integral equation methods may then arise on account of the presence of irregular frequencies described in the previous chapter. Various attempts to remove these have been mentioned. All these methods entail additional computational effort. In this chapter, alternative approaches to circumventing these irregularities, all of which are based on various high frequency approximations, are described for the special case of vertical cylinders of arbitrary section.

## 5.1 Damping Coefficients

At sufficiently high frequencies, damping coefficients may be calculated by a short-wave asymptotic solution relating to the local form of waves generated by the oscillating structure. As an alternative, they may also be obtained on the basis of the Haskind relations from the exciting forces of the related scattering problem, with these forces at high frequencies obtained by a geometrical optics approximation. These approaches provide simple and viable alternatives to the complete numerical solution in the high frequency range over which irregular frequencies are encountered.

### 5.1.1 Ursell's Short-wave Solution

Ursell (1957) has deduced the leading term in a short-wave asymptotic expansion of the solution to the horizontal plane problem posed by (2.23), (2.26), and (2.29). Ursell's solution is valid on $C_b$ and may be used to obtain damping coefficients of vertical cylinders of arbitrary section. Ursell (1957) gives the short-wave solution as:

$$\phi_0^k(C) = -\frac{i}{k_0} n_k'(C) \, b_0^k \tag{5.1}$$

where C is the arc length along $C_b$ measured from an arbitrary starting point. Equation (5.1) is valid provided that $C_b$ is an arbitrary closed convex curve satisfying certain regularity conditions, and that the right-hand side of (2.26) varies slowly along $C_b$.

The above result follows from a simple physical argument. For high frequency motions, short waves radiate outward from $C_b$ normal to it, so that the resulting potential $\phi_0^k$ at a general point $x = (x,y)$ near $C_b$ may be expressed as:

$$\phi_0^k(x) = \phi_0^k(C) \exp(ik_0 n) \tag{5.2}$$

where n denotes perpendicular distance to x from $C_b$. Invoking the boundary condition on $C_b$ (2.26), we obtain:

$$ik_0 \, \phi_0^k(C) = n_k'(C) \, b_0^k \tag{5.3}$$

Substituting for $\phi_0^k(C)$ from (5.3), the potential given by (5.2) now becomes:

$$\phi_0^k(x) = -\frac{i}{k_0} n_k'(C) \, b_0^k \exp(ik_0 n) \tag{5.4}$$

and hence the result (5.1) follows.

For the case of a vertical cylinder, the damping coefficients were given in terms of the potential component $\phi_0^k$ by (2.44) and (2.45). By applying the form of $\phi_0^k$ given by (5.1), the damping coefficients may be obtained from (2.44) with $I_{jk}$ now given as:

$$
\begin{aligned}
I_{jk} &= b_0^j \int_{C_b} \phi_0^k \, n_j' \, dC \\[2ex]
&= -\frac{i}{k_0} b_0^j \, b_0^k \int_{C_b} n_j' \, n_k' \, dC
\end{aligned}
\tag{5.5}
$$

Thus:

$$\frac{\lambda_{jk}}{\rho\omega a l'} = \frac{c_{jk}}{(k_0 a)^{l-1}} f_0^{(l)}(k_0 d) \tag{5.6}$$

where $l' = l + \delta_{6j} + \delta_{6k}$ and:

$$l = \begin{cases} 3 & j,k = 1,2,6 \\ 5 & j,k = 4,5 \\ 4 & j = 1,2,6, \ k = 4,5; \ \text{or} \ j = 4,5, \ k = 1,2,6 \end{cases} \tag{5.7}$$

$a$ is a characteristic length, $\delta_{jk}$ is the Kronecker delta function, and $c_{jk}$ is a function of the contour $C_b$ only and is given as:

$$c_{jk} = \frac{1}{a^{1+\delta_{6j}+\delta_{6k}}} \int_{C_b} n'_j n'_k \, dC \tag{5.8}$$

*Circular Cylinder*

In the particular case of a vertical circular cylinder, substituting for $n_k'$ from (3.8) into (5.8), the coefficients $c_{jk}$ are obtained as:

$$c_{11} = c_{55} = c_{15} = \pi \tag{5.9}$$

These may be used in (5.6) to obtain expressions for $\lambda_{11}$, $\lambda_{55}$, and $\lambda_{15}$. These expressions reduce to the corresponding analytical forms in (3.26) - (3.28) if the functions $f_0^{(l)}(k_0 d)$ are replaced by their high frequency approximations from (3.23) - (3.25). The complete set of damping coefficients may be obtained based on (3.44).

*Elliptic Cylinder*

For the case of a vertical elliptic cylinder, substituting for $n_k'$ from (3.55) into (5.8), the damping coefficients are again expressed in the form (5.6) with the coefficients $c_{jk}$ now obtained in terms of

54

elliptic coordinates as:

$$c_{11} = c_{55} = c_{15} = \Sigma_1 \sinh\xi_0 \tanh\xi_0 \tag{5.10}$$

$$c_{22} = c_{44} = c_{24} = \Sigma_2 \cosh\xi_0 \tag{5.11}$$

$$c_{22} = \Sigma_2 \frac{1}{4\cosh^3\xi_0} \tag{5.12}$$

where:

$$\Sigma_1 = \int_0^{2\pi} \frac{\cos^2\eta}{(\cosh^2\xi_0 - \cos^2\eta)^{1/2}} \, d\eta \tag{5.13}$$

$$\Sigma_2 = \int_0^{2\pi} \frac{\sin^2\eta}{(\sinh^2\xi_0 + \sin^2\eta)^{1/2}} \, d\eta \tag{5.14}$$

These integrals require a numerical evaluation. Once the coefficients $c_{jk}$ are calculated, they may be used in (5.6), and based on (3.70) the complete set of damping coefficients may be obtained.

*Square Cylinder*

For a square cylinder with a pair of sides perpendicular to the x axis, provided a is now the side length of the square, the coefficients $c_{jk}$ to be applied to (5.6) are obtained as:

$$c_{11} = c_{55} = c_{15} = 2 \tag{5.15}$$

$$c_{66} = 1/3 \tag{5.16}$$

These may be used in (5.6) to obtain expressions for $\lambda_{11}$, $\lambda_{55}$, $\lambda_{15}$ and $\lambda_{66}$. Bearing in mind the symmetry of the damping coefficient matrix in general and the symmetry of the structure in particular, the complete set of damping coefficients are then given as:

$$[\lambda_{jk}] = \begin{bmatrix} \lambda_{11} & 0 & 0 & 0 & \lambda_{15} & 0 \\ 0 & \lambda_{11} & 0 & -\lambda_{15} & 0 & 0 \\ 0 & 0 & 0 & 0 & 0 & 0 \\ 0 & -\lambda_{15} & 0 & \lambda_{55} & 0 & 0 \\ \lambda_{15} & 0 & 0 & 0 & \lambda_{55} & 0 \\ 0 & 0 & 0 & 0 & 0 & \lambda_{66} \end{bmatrix}$$ (5.17)

The expressions for $\lambda_{11}$, $\lambda_{55}$, $\lambda_{15}$ and $\lambda_{66}$ are unchanged if the square cylinder is reoriented with a diagonal perpendicular to the x axis.

## 5.1.2 Geometrical Optics

The diagonal terms of the damping coefficient matrix may also be obtained by first considering the exciting force of the corresponding scattering problem, and then applying (2.47) deriving from the Haskind relations. The exciting force itself may be calculated based on a high frequency asymptotic solution to the scattering problem described by (A.4) - (A.6). Asymptotic methods for a variety of scattering problems have been described by Keller, Lewis and Seckler (1956). The general method is based on the postulate that fields propagate along rays or wave orthogonals, i.e. curves orthogonal to wave fronts. A field value is assigned to each point on a ray. The total field at a point is then the sum of the fields due to all rays which pass through that point. The resulting expansion is the so-called Luneburg-Kline expansion and its leading term corresponds to the geometrical optics solution.

According to the geometrical optics approximation, (e.g. Chung, 1986), the incident potential is completely reflected on the exposed (illuminated) side of $C_b$, while the potential is zero on the sheltered (shadow) side of $C_b$. Thus

$$\Phi_i + \Phi_s = \begin{cases} 2\Phi_i & \text{on the exposed surface} \\ 0 & \text{on the sheltered surface} \end{cases}$$ (5.18)

where $\Phi_i$ is the incident potential which is known, and $\Phi_s$ is the corresponding scattered potential.

Equation (5.18) may be used to find the exciting force $F_k$ to be used in (2.47). Thus, in particular, for translational modes corresponding to k = 1, 2:

$$F_k(\alpha) = -\rho g H d \frac{\tanh(k_0 d)}{k_0 d} \int_{C_e(\alpha)} \exp[ik_0(x \cos\alpha + y \sin\alpha)] \, n'_k \, dC \qquad (5.19)$$

where $C_e(\alpha)$ represents the exposed portion of the contour $C_b$. Applying (5.19) to (2.47), the damping coefficients for translational modes are expressed as:

$$\frac{\lambda_{kk}}{\rho a^3 \omega} = \frac{1}{2\pi} \frac{f_0^{(3)}(k_0 d)}{k_0 a} \frac{1}{a^2} \int_0^{2\pi} \left| \int_{C_e(\alpha)} \exp[ik_0(x \cos\alpha + y \sin\alpha)] \, n'_k \, dC \right|^2 \, d\alpha \qquad (5.20)$$

where a is a characteristic length of the structure and k = 1, 2.

A simple check on the validity of (5.19) and (5.20) may be made by considering the case of a vertical circular cylinder. For a wave train propagating in the x direction, the force predicted by (5.19) is:

$$\frac{F_1(0)}{\rho g H a d \tanh(k_0 d)/k_0 d} = - \int_{\pi/2}^{3\pi/2} \exp(ik_0 a \cos\theta) \cos\theta \, d\theta \qquad (5.21)$$

This can be evaluated by making use of the following identities:

$$\int_{\pi/2}^{3\pi/2} \cos(m\theta) \cos\theta \, d\theta = \begin{cases} -2 & \text{for m = 0} \\[2mm] \dfrac{\pi}{2} & \text{for m = 1} \\[2mm] 0 & \text{for m = 3, 5, 7 ...} \\[2mm] \dfrac{2(-1)^{m/2}}{m^2-1} & \text{for m = 2, 4, 6 ...} \end{cases} \qquad (5.22)$$

57

$$\exp(ik_0 a \cos\theta) = \sum_{m=0}^{\infty} \beta_m J_m(k_0 a) \cos(m\theta) \qquad (5.23)$$

Substituting (5.23) into (5.21) and evaluating the resulting definite integrals of $\cos(m\theta)\cos\theta$, the force $F_1(0)$ may be expressed as:

$$\frac{F_1(0)}{\rho g Had \, \tanh(k_0 d)/k_0 d} = 2J_0(k_0 a) - i\pi J_1(k_0 a) - \sum_{m=2,4,\ldots}^{\infty} \frac{4}{m^2-1} J_m(k_0 a) \qquad (5.24)$$

Since the geometrical optics approximation is only valid for large $k_0 a$, (5.24) may be simplified by replacing the Bessel functions in (5.24) by their principal asymptotic forms (Abramowitz and Stegun, 1972). Use can then be made of the following identity:

$$\sum_{m=2,4,\ldots}^{\infty} \frac{(-1)^{m/2}}{m^2-1} = \frac{1}{2} - \frac{\pi}{4} \qquad (5.25)$$

Carrying out this procedure, the force may be reduced to the form:

$$|F_1(0)| = \sqrt{\frac{2\pi}{k_0 a}} \; \rho g Had \, \tanh(k_0 d)/k_0 d \qquad (5.26)$$

which corresponds to the high frequency limit of the analytical solution obtained in (A.12). The result in (5.26) may be applied to (5.20) to evaluate the corresponding damping coefficient $\lambda_{11}$. For a circular cylinder, the exciting force $F_1(\alpha)$ varies with the angle of wave incidence $\alpha$ as:

$$F_1(\alpha) = F_1(0) \cos\alpha \qquad (5.27)$$

Using the high frequency approximation for $f_0^{(3)}(k_0 d)$ given in (3.23), (5.20) may be then shown to yield an identical result for $\lambda_{11}/\rho a^3 \omega$ as the corresponding analytical form in (3.26):

$$\frac{\lambda_{11}}{\rho a^3 \omega} = \frac{2\pi}{(k_0 a)^2} \qquad (5.28)$$

58

# 5.2 Added Masses

Consideration is now given to the corresponding evaluation of the high frequency added masses. The preceding methods used to obtain the damping coefficients cannot be used to obtain the added masses. However, it is possible to calculate the added masses either by discarding the propagating mode potential and using evanescent mode potentials alone, or by utilizing the Kramers-Kronig relations. Both approaches circumvent the numerical difficulties due to irregular frequencies.

## 5.2.1 Added Masses from Evanescent Modes

The argument presented in 5.1.1 which led to Ursell's approximation (5.1) indicates that the potential $\phi_0^k$ on $C_b$ becomes wholly imaginary at high frequencies. On the other hand, the added masses, given by (2.43) and (2.45), depends only on the real part of $\phi_0^k$. Consequently, at sufficiently high frequencies the component $\phi_0^k$ does not contribute to the added masses, and thus the term corresponding to $m = 0$ may be discarded from the sum in (2.45). Thus (2.45) may be replaced by:

$$\mu_{jk} = -\rho \sum_{m=1}^{\infty} b_m^j \int_{C_b} \phi_m^k n_j' \, dC \tag{5.29}$$

The potential $\phi_0^k$ corresponds to a propagating mode and is distinctly different from the remaining potentials $\phi_m^k$, $m \geq 1$, which correspond to evanescent modes. It was indicated in section 4.4.1 that the irregular frequencies in the boundary integral method are associated with the propagating component, $m = 0$, only, and do not arise for the evanescent components, $m \geq 1$. This is because the propagating component is a solution to the Helmholtz equation (2.23), which exhibits irregular behaviour at frequencies equal to the eigen-frequencies of the corresponding interior problem (which describes hypothetical, free surface fluid motions in the region within the body). On the other hand, the evanescent components are solutions to (2.24) which does not exhibit irregular behaviour.

Taking account of both factors described above, it follows that at sufficiently high frequencies, the added masses may be computed by discarding the term m = 0 in (2.45), and furthermore that this approach will circumvent the usual numerical difficulties associated with irregular frequencies since these will not arise in the calculation of the potentials $\phi_m^k$, m ≥ 1.

At higher frequencies, the added masses reach a steady value $\mu_{jk}(\infty)$. These may be determined using (5.29) above, but the eigenvalues may now be calculated, in place of (2.22), from:

$$k_m d = \frac{(2m - 1)\pi}{2} \tag{5.30}$$

This approach is tantamount to discarding gravitational effects and corresponds to using $\Phi = 0$ as the free surface boundary condition which is based on $\omega^2 d/g \gg 1$. The method corresponds to Garrison and Berklite's (1973) method for an arbitrary structure, but is simpler in the present case due to the restricted geometry considered here.

## 5.2.2 Kramers-Kronig Relations

It is possible to calculate the added masses at all frequencies by utilizing the Kramers-Kronig relations (Kotik and Mangulis, 1962). These relate the added masses and damping coefficients, and provide one of these at one frequency in terms of an integral of the other over all frequencies. In the case of sway motion, these are given as:

$$\bar{\mu}(Ka) - \bar{\mu}(\infty) = \frac{1}{\pi} \int_0^\infty \frac{\bar{\lambda}(u)}{u - Ka} du \tag{5.31}$$

$$\bar{\lambda}(Ka) = \frac{\sqrt{Ka}}{\pi} \int_0^\infty \frac{\bar{\mu}(\infty) - \bar{\mu}(u)}{\sqrt{u} (u - Ka)} du \tag{5.32}$$

where the integrals are principal value integrals, and $\bar{\mu}$ and $\bar{\lambda}$ are the dimensionless added mass and damping coefficient respectively, defined as $\bar{\mu} = \mu_{22}/\rho a^3$, and $\bar{\lambda} = \lambda_{22}/\rho a^3 \omega$. Also u is a variable

of integration, and $K = \omega^2/g$ is the deep water wave number.

Greenhow (1984, 1986) has used these relations to show that a knowledge of the high or low frequency expansion for the added mass or damping coefficient, enables the corresponding asymptotic expansion of the other to be easily determined; and furthermore that the coefficients in these expansions may be determined by evaluating known integrals that involve intermediate frequencies. For example, Greenhow (1984) gives:

$$\bar{\mu}(Ka) = \bar{\mu}(\infty) + \frac{A}{Ka} \qquad\qquad Ka \to \infty \qquad\qquad (5.33)$$

where:

$$A = -\frac{1}{\pi} \int_0^\infty \bar{\lambda}(u)\, du \qquad\qquad\qquad (5.34)$$

Rather than adopt any such assumption about the form of $\bar{\mu}(Ka)$, the approach adopted here is to use (5.31) directly to calculate the added mass. In order to apply (5.31), the damping coefficient is needed over the entire frequency range and may be obtained by a suitable combination of the integral equation method for lower frequencies and Ursell's solution for higher frequencies. However, the right-hand side of (5.31) has the same form as the one-sided Hilbert transform of $\bar{\lambda}$ and its direct numerical evaluation is tedious, since this would need to be repeated for each value of $Ka$ at which the added mass is required. As an alternative, a suitable application of Fourier transforms may be used to express (5.31) in a more convenient form. The right-hand side of (5.31) may be recognized as the convolution of $\bar{\lambda}(u)$ with $-1/\pi u$. The convolution theorem may therefore be used to express the Fourier transform of the right-hand side of (5.31) as the product of the Fourier transforms of $\bar{\lambda}(u)$ and $-1/\pi u$. The Fourier transform of $-1/\pi u$ is i[sign(s)] (Bracewell, 1986), where s is the transform variable, while the Fourier transform of $\bar{\lambda}(u)$ is denoted $\bar{A}(s)$ and defined as:

61

$$\overline{\Lambda}(s) = \int_{-\infty}^{\infty} \overline{\lambda}(u) \, \exp(-i2\pi su) \, du \tag{5.35}$$

The convolution theorem then gives:

$$D(s) = i[\text{sign}(s)] \, \Lambda'(s) \tag{5.36}$$

where $D(s)$ is the Fourier transform of the right-hand side of (5.31). Equation (5.36) may then be inverse transformed to obtain an expression for $\overline{\mu}(Ka) - \overline{\mu}(\infty)$:

$$\overline{\mu}(u) - \overline{\mu}(\infty) = \int_{-\infty}^{\infty} i[\text{sign}(s)] \, \overline{\Lambda}(s) \, \exp(i2\pi su) \, ds \tag{5.37}$$

In order to carry out the corresponding computations, the Fourier transform in (5.35) is expressed in discrete form in terms of damping coefficient values calculated at equal intervals over a sufficiently large range of u:

$$\overline{\Lambda}(m\Delta s) = \frac{1}{N} \sum_{n=0}^{N-1} \overline{\lambda}(n\Delta u) \, \exp(-\frac{i2\pi mn}{N}) \Delta u \qquad m = 0, 1, 2, ..., N-1 \tag{5.38}$$

where N is the number of discrete values of the damping coefficient, $\Delta u$ is the sampling interval and $\Delta s$ is the interval between successive values of the transform variable s. Since the use of (5.38) requires $\overline{\lambda}$ to be periodic with period $N\Delta u$, N must be chosen such that $N\Delta u$ is sufficiently large, while $\Delta u$ must be sufficiently small so as to describe accurately the damping coefficient variation with u. Since $\Delta s = 1/N\Delta u$, this ensures that the discrete Fourier transforms are obtained at sufficiently small intervals for a sufficiently large range of the transform variable s.

Likewise, the Fourier integral in (5.37) is replaced by a Fourier series:

$$\overline{\mu}(u) - \overline{\mu}(\infty) = \sum_{m=1}^{N/2} \left[ a_m \cos\left(\frac{2\pi mu}{N\Delta u}\right) + b_m \sin\left(\frac{2\pi mu}{N\Delta u}\right) \right] \tag{5.39}$$

where the coefficients $a_m$ and $b_m$ are real and are given by (e.g. Cooley *et al.*, 1967):

$$a_m = -2 \; \text{Im}\{\bar{\Lambda}(m\Delta s)\} \left.\vphantom{\begin{array}{c} a \\ b \end{array}}\right\}$$
$$b_m = -2 \; \text{Re}\{\bar{\Lambda}(m\Delta s)\}$$
$$\text{for } m = 1, 2, \dots, N/2 - 1 \qquad (5.40)$$

$$a_{N/2} = 0 \left.\vphantom{\begin{array}{c} a \\ b \end{array}}\right\}$$
$$b_{N/2} = -\bar{\Lambda}(N\Delta s/2) \qquad (5.41)$$

Equation (5.38) may be evaluated using a Fast Fourier Transform routine. The damping coefficient, required in order to apply the above equation, is obtained by the integral equation method described in Chapter 4 for lower frequencies, $u < u_0$, where $u_0$ is a transition value of $u$; and by Ursell's short-wave solution described in section 5.1.1 for higher frequencies, $u > u_0$. A suitable choice of $u_0$ may be made from an inspection of coefficient values obtained by the two methods. In brief, $u_0$ must be less than the value corresponding to the lowest irregular frequency of the body; and at the same time it must be sufficiently high for Ursell's solution to hold. In this regard, prior knowledge of the lowest irregular frequency value is useful. Some available methods to estimate this are mentioned in section 4.4.2. In principle, further reduction in the computational effort would have been possible if a simple method were available to deduce the low frequency asymptotic behaviour of the damping coefficient, thereby reducing the frequency range in which solutions have to be obtained by the integral equation method.

Finally, in order to obtain $\bar{\mu}(u)$ from (5.39), the limiting value $\bar{\mu}(\infty)$ is also required, and may be determined by the integral equation method using the eigenvalues calculated from (5.30) as indicated in section 5.2.1.

The alternative approaches described in this chapter apply to an incompressible fluid, and do not predict the variation of the added masses and damping coefficients due to compressibility effects at sufficiently high frequencies. Effects of fluid compressibility are addressed separately in the next chapter.

# Chapter 6

# COMPRESSIBILITY EFFECTS

In the solutions described in the previous chapters, the fluid surrounding the structure is assumed to be incompressible. The only form of damping then is due to surface waves propagating away from the structure. As the frequency of excitation is increased, these outward propagating waves become insignificant and the entire hydrodynamic force is then accounted for by the added mass as indicated in section 5.2.1. At still higher frequencies, a further modification to the hydrodynamic loading arises from the effects of compressibility of the water.

The significance of fluid compressibility at high excitation frequencies has been demonstrated in several studies of vertical circular cylinders and vertical axisymmetric structures undergoing forced harmonic motions, not to mention numerous studies of dam-reservoir systems. Goto and Toki (1963) formulated the problem considering surface waves and fluid compressibility, and indicated the form of the analytical solution for a vertical circular cylinder. Kotsubo (1965) provided the corresponding analytical solution for an elliptic cylinder. More recently, extensive results for a circular cylinder were obtained by Liaw and Chopra (1974), and Tanaka and Hudspeth (1988). These studies are useful in providing an indication of the conditions under which compressibility effects become important. Briefly, modifications to the solution for an incompressible fluid start to become necessary approximately when $\omega d/c > 0.5$, i.e. $\omega/\omega_1 > 0.3$, where $\omega$ is the angular frequency of excitation, d is the water depth, c is the speed of sound in water and $\omega_1$ is the first cut-off frequency for acoustic waves. A marked effect is observed for squatty cylinders corresponding to a/d > 0.25, where a is the cylinder radius, in comparison to slender cylinders with small values of a/d. The case of a submerged circular cylinder subject to horizontal and vertical harmonic ground excitation has been investigated by Williams and Moubayed (1990) using an axisymmetric Green's function. Kokkinowrachos and Thanos (1990) adopted a 'macro element method' for general axisymmetric structures which uses an eigenfunction expansion for a stepped composite cylinder in the limit of small step size. Mei et al. (1979) proposed a hybrid element

method based on a localized variational principle for a general elastic structure.

The case of a vertical cylinder of arbitrary section appears not to have been specifically addressed in the literature. For this particular class of structure, extensions to the methods already described in the previous chapters to account for compressibility may readily be made and are now described.

# 6.1 Modifications to Governing Equations

In order to account for the effects of compressibility, the governing Laplace equation for the velocity potential (2.1) may readily be extended to include an additional term (see, for example, Morse and Ingard, 1968):

$$\nabla^2 \Phi - \frac{1}{c^2} \frac{\partial^2 \Phi}{\partial t^2} = 0 \qquad\qquad \text{within the fluid region} \qquad\qquad (6.1)$$

When the adopted representation of $\Phi$ given by (2.11) and (2.17) are applied to this, the governing equations (2.23) and (2.24) for $\phi_m^k$ are replaced respectively by:

$$\frac{\partial^2 \phi_0^k}{\partial x^2} + \frac{\partial^2 \phi_0^k}{\partial y^2} + \left( k_0^2 + \frac{\omega^2}{c^2} \right) \phi_0^k = 0 \qquad\qquad (6.2)$$

$$\frac{\partial^2 \phi_m^k}{\partial x^2} + \frac{\partial^2 \phi_m^k}{\partial y^2} - \left( k_m^2 - \frac{\omega^2}{c^2} \right) \phi_m^k = 0 \qquad\qquad m = 1, 2, \dots \qquad\qquad (6.3)$$

The solution to these may readily be obtained by continuing to apply the procedures already described for an incompressible fluid. In the case of $\phi_0^k$, a comparison between (2.23) and (6.2) indicates that both equations have the same form, with the eigenvalue $k_0$ now replaced by an effective value $k_0'$ given by:

$$k_0' = \sqrt{k_0^2 + \frac{\omega^2}{c^2}} \qquad\qquad (6.4)$$

In the case of $\phi_m^k$, $m \geq 1$, a comparison between (2.24) and (6.3) indicates that both equations have the same form only when $k_m > \omega/c$, in which case the eigenvalue $k_m$ is replaced by an effective value:

$$k_m' = \sqrt{\left| k_m^2 - \frac{\omega^2}{c^2} \right|} \tag{6.5}$$

On the other hand, when $k_m < \omega/c$, the effective eigenvalue $k_m'$ given by (6.5) continues to apply, but now (6.3) instead takes the form of the Helmholtz equation (2.23). Thus overall, when $m = 0$ or when $m \geq 1$ and $k_m < \omega/c$, the solution to $\phi_m^k$ corresponds to that of the Helmholtz equation (2.23) with a suitably modified eigenvalue given either by (6.4) for $m = 0$ or by (6.5) for $m \geq 1$; or when $m \geq 1$ and $k_m > \omega/c$, the solution corresponds to that of (2.24) with modified eigenvalues given by (6.5). For the particular case, when $m \geq 1$ and $k_m = \omega/c$, the effective eigenvalue in (6.5) vanishes. The corresponding potential $\phi_m^k$ may then be obtained as solution to the two-dimensional Laplace equation.

The potentials are still subject to the body surface boundary condition (2.26) and similar radiation conditions as before. Thus $\phi_0^k$ and $\phi_m^k$, $m \geq 1$, with $k_m < \omega/c$ are subject to the radiation condition (2.29) with $k_0$ replaced by the modified eigenvalue $k_m'$. The potentials $\phi_m^k$, $m \geq 1$, with $k_m \geq \omega/c$ are subject to the radiation condition (2.30).

Thus overall, it is noted that when fluid compressibility is taken into account, there are acoustic propagating modes in addition to the usual gravitational propagating mode, with the number of such acoustic propagating modes corresponding to the number of $k_m$ values which are less than $\omega/c$ and thus dependent on the excitation frequency. Thus no acoustic propagating modes occur when $\omega \leq k_1 c$ and one acoustic propagating mode occurs for $k_1 c < \omega \leq k_2 c$. As the frequency is increased above $k_2 c$, more and more acoustic propagating modes occur, such that $\overline{M} - 1$ acoustic propagating modes are present when $k_{\overline{M}-1} c < \omega \leq k_{\overline{M}} c$, where $\overline{M}$ is the smallest integer value of $m \geq 1$, for which $k_m d \geq \omega d/c$.

In an investigation of the effects of fluid compressibility on the hydrodynamic loads, a simplification to the solution is possible by neglecting gravitational effects. At the very high frequencies when fluid compressibility becomes a dominant factor, gravitational effects are then relatively unimportant, and hence may be ignored (see, for example, Liaw and Chopra, 1974).

This is tantamount to discarding the propagating mode potential $\phi_0^k$, and using the high frequency limit (5.30) to calculate $k_m$ to be used in (6.5).

It follows that the general methods indicated earlier for an incompressible fluid may still be applied, provided that due attention is given to the form of the governing equation and to the effective eigenvalue for any particular value of m.

# 6.2 Modifications to Analytical Solutions

## 6.2.1 Circular Cylinder

For the case of a vertical circular cylinder, the added masses and damping coefficients continue to be given in the same form as (3.11), but with suitable modifications made to the number of propagating and evanescent modes and with effective eigenvalues used as appropriate. Thus:

$$\frac{\mu_{jk} + i\,\lambda_{jk}/\omega}{\rho a^l} = -\sum_{m=0}^{\overline{M}-1} \frac{\pi}{k_m'a\,(k_ma)^{l-2}} \frac{H_1^{(1)}(k_m'a)}{H_1^{(1)'}(k_m'a)}\, f_m^{(l)}(k_md)$$

$$-\sum_{m=\overline{M}}^{\infty} \frac{\pi}{k_m'a\,(k_ma)^{l-2}} \frac{K_1(k_m'a)}{K_1'(k_m'a)}\, f_m^{(l)}(k_md) \qquad j,\,k = 1,\,5 \qquad (6.6)$$

where:

$$l = \begin{cases} 3 & j,\,k = 1 \\ 5 & j,\,k = 5 \\ 4 & j = 1,\,k = 5 \end{cases} \qquad (6.7)$$

In the above, the first sum on the right-hand side corresponds to the propagating modes including the gravitational mode and $\overline{M} - 1$ acoustic modes, and the second sum corresponds to the evanescent modes.

## 6.2.2 Elliptic Cylinder

For the case of a vertical elliptic cylinder, the added masses and damping coefficients continue to be given in the same form as (3.66) - (3.68), but with suitable modifications as follows:

$$\frac{\mu_{jk} + i\,\lambda_{jk}/\omega}{\rho a^l} = -\sum_{m=0}^{\overline{M}-1} \frac{\pi}{(k_m a)^{l-2}}\frac{b^2}{a^2} \sum_{n=0}^{\infty} \frac{A_1^{(2n+1)}(q_m')^2}{Mc_{2n+1}^{(3)'}(\xi_0,q_m')}\, Mc_{2n+1}^{(3)}(\xi_0,q_m')\, f_m^{(l)}(k_m d)$$

$$-\sum_{m=\overline{M}}^{\infty} \frac{\pi}{(k_m a)^{l-2}}\frac{b^2}{a^2} \sum_{n=0}^{\infty} \frac{A_1^{(2n+1)}(-q_m')^2}{Mc_{2n+1}^{(3)'}(\xi_0,-q_m')}\, Mc_{2n+1}^{(3)}(\xi_0,-q_m')\, f_m^{(l)}(k_m d) \qquad j,k = 1,5 \qquad (6.8)$$

$$\frac{\mu_{jk} + i\,\lambda_{jk}/\omega}{\rho a^l} = (-1)^l \sum_{m=0}^{\overline{M}-1} \frac{\pi}{(k_m a)^{l-2}} \sum_{n=0}^{\infty} \frac{B_1^{(2n+1)}(q_m')^2}{Ms_{2n+1}^{(3)'}(\xi_0,q_m')}\, Ms_{2n+1}^{(3)}(\xi_0,q_m')\, f_m^{(l)}(k_m d)$$

$$+(-1)^l \sum_{m=\overline{M}}^{\infty} \frac{\pi}{(k_m a)^{l-2}} \sum_{n=0}^{\infty} \frac{B_1^{(2n+1)}(-q_m')^2}{Ms_{2n+1}^{(3)'}(\xi_0,-q_m')}\, Ms_{2n+1}^{(3)}(\xi_0,-q_m')\, f_m^{(l)}(k_m d) \qquad j,k = 2,4 \qquad (6.9)$$

$$\frac{\mu_{66} + i\,\lambda_{66}/\omega}{\rho a^5} = -\sum_{m=0}^{\overline{M}-1} \frac{\pi}{4\,k_m a}\,\frac{1}{\cosh^4\xi_0} \sum_{n=0}^{\infty} \frac{B_2^{(2n+2)}(q_m')^2}{Ms_{2n+2}^{(3)'}(\xi_0,q_m')}\, Ms_{2n+2}^{(3)}(\xi_0,q_m')\, f_m^{(3)}(k_m d)$$

$$-\sum_{m=\overline{M}}^{\infty} \frac{\pi}{4\,k_m a}\,\frac{1}{\cosh^4\xi_0} \sum_{n=0}^{\infty} \frac{B_2^{(2n+2)}(-q_m')^2}{Ms_{2n+2}^{(3)'}(\xi_0,-q_m')}\, Ms_{2n+2}^{(3)}(\xi_0,-q_m')\, f_m^{(3)}(k_m d) \qquad (6.10)$$

where:

$$l = \begin{cases} 3 & \text{for } j,k = 1; \text{ or } j,k = 2 \\ 5 & \text{for } j,k = 5; \text{ or } j,k = 4 \\ 4 & \text{for } j = 1,\ k = 5; \text{ or } j = 2,\ k = 4 \end{cases} \qquad (6.11)$$

and $q_m'$ is defined as follows:

$$q_m' = \frac{k_m'^2 h^2}{4} \qquad\qquad m = 0, 1, 2, \dots \qquad (6.12)$$

# 6.3 Modifications to Numerical Solutions

The method of integral equations described in Chapter 4 continues to apply provided it is recognized that now, in addition to the usual gravitational propagating mode, there are also acoustic propagating modes corresponding to $\phi_m^k$, $m = 1, 2, ..., \overline{M} - 1$. Since all the propagating modes are governed by the Helmholtz equation with $k_0$ replaced by the effective eigenvalue $k_m'$, the choice of Green's functions should now be based on:

$$G_m(x,\xi) = \begin{cases} \dfrac{i}{2} H_0^{(1)}(k_m'R) & m < \overline{M} \\[3mm] \dfrac{1}{\pi} K_0(k_m'R) & m \geq \overline{M} \end{cases} \tag{6.13}$$

instead of (4.2). Furthermore, $k_m$ in the various equations describing the numerical solution should now be replaced by the effective eigenvalue $k_m'$. Numerical irregularities now occur in the calculations for each of the propagating modes when any of the corresponding modified eigenvalues coincides with an irregular frequency. For the reference case of a circular cylinder with $a/d = 2$, where $a$ is now the radius, the first few irregular frequencies in the first two acoustic propagating modes when gravitational effects are omitted are tabulated in Table II.

# 6.4 Modifications to High Frequency Approximations

The two high frequency methods for estimating the damping coefficients were based on, firstly, Ursell's short-wave solution to the Helmholtz equation and, secondly, the application of the Haskind relations to a geometrical optics solution. Of these, the Haskind relations and the geometrical optics solution cannot be applied in their present forms and would require careful reconsideration if compressibility effects are to be accounted for. In any event, the approach based on Ursell's short-wave solution has been found to be superior to the approach based on the Haskind relations in obtaining solutions with compressibility discarded, and hence the latter method is not considered here.

The method based on Ursell's short-wave solution may readily be modified to provide estimates of

the damping coefficients when compressibility is included in the analysis. Ursell's solution may now be applied to each propagating mode separately to obtain the asymptotic value of the corresponding potential $\phi_m^k$ on $C_b$. Thus:

$$\phi_m^k(C) = -\frac{i}{k_m'}\, n_k'(C)\, b_m^k \qquad\qquad 0 \leq m \leq \bar{M}-1 \qquad\qquad (6.14)$$

The damping coefficients continue to be given by (2.44):

$$\lambda_{jk} = -\rho\,\omega\,\text{Im}\{I_{jk}\} \qquad\qquad (6.15)$$

but now (5.5), which accounts for the gravitational propagating mode potential only, is extended to:

$$I_{jk} = \sum_{m=0}^{\bar{M}-1} b_m^j \int_{C_b} \phi_m^k\, n_j'\, dC$$

$$= -i \sum_{m=0}^{\bar{M}-1} \frac{1}{k_m'}\, b_m^j\, b_m^k \int_{C_b} n_j'\, n_k'\, dC \qquad\qquad (6.16)$$

Thus the damping coefficients are extended from (5.6) to:

$$\frac{\lambda_{jk}}{\rho\omega a^{l'}} = c_{jk} \sum_{m=0}^{\bar{M}-1} \frac{1}{k_m' a\,(k_m a)^{l-2}}\, f_m^{(l)}(k_m d) \qquad\qquad (6.17)$$

where $l' = l + \delta_{6j} + \delta_{6k}$ and:

$$l = \begin{cases} 3 & j,k = 1,2,6 \\ 5 & j,k = 4,5 \\ 4 & j = 1,2,6,\ k = 4,5;\ \text{or}\ j = 4,5,\ k = 1,2,6 \end{cases} \qquad\qquad (6.18)$$

Nevertheless, (6.17) will not give accurate estimates for a range of frequencies immediately following the emergence of each propagating mode since it is valid only when the effective eigenvalues in the denominators are sufficiently large.

The two high frequency methods for estimating the added masses were based on, firstly, the use of evanescent modes alone and, secondly, an application of the Kramers-Kronig relations. Of these, the Kramers-Kronig relations in their present forms do not apply when compressibility is accounted for, and hence the latter approach cannot be adopted. The approach based on the use of evanescent modes alone may yield reasonable estimates at frequencies sufficiently high in relation to the emergence of a progressive wave, whereas discarding the progressive waves in calculations of added masses will lead to erroneous results at frequencies closely following each cut-off frequency.

Thus overall, of the various methods considered in Chapter 5, the method based on Ursell's short-wave solution for the damping coefficients and the method based on the use evanescent modes alone for the added masses are applicable when compressibility effects are accounted for, although the usefulness of the latter approach may be limited.

The calculations including compressibility effects may be somewhat simplified if gravitational effects can be omitted. The gravitational propagating mode corresponding to $m = 0$ may then be discarded and the eigenvalues $k_m$, $m \geq 1$, may be obtained using (5.30). This is in fact valid when $\omega^2 d/g \gg 1$ which is invariably the case when fluid compressibility effects start to become dominant i.e. $\omega d/c > 0.5$. Thus at the very high frequencies when fluid compressibility becomes a dominant factor, gravitational effects are then relatively unimportant, and hence may be ignored.

# Chapter 7

# RESULTS AND DISCUSSION

Results obtained by the various methods described in chapters 3-6 for a number of fundamental configurations are now presented, compared with each other and discussed. These include the following:

(a)   the analytical solution based on a separation of variables technique for circular and elliptic section cylinders,

(b)   the boundary integral method based on a continuous distribution of sources for arbitrary sections,

(c)   high frequency approximations to the damping coefficients based on Ursell's short-wave solution and geometrical optics,

(d)   alternative approaches to obtain the added masses based on the use of evanescent modes alone and the Kramers-Kronig relations, and

(e)   extensions to methods (a), (b), (c), and (d) above to account for fluid compressibility.

## 7.1  Analytical Solutions

### 7.1.1  Circular Cylinder

The dimensionless total surge added mass and damping coefficient are functions of $k_0a$ and $a/d$ only, and are presented as solid lines in Figs. 5a and 5b respectively as functions of $k_0a$ for $a/d$ values of 0.2, 0.5, 1, 2 and 5. The values of the hydrodynamic coefficients agree closely with Yeung's (1981) results for his particular case of a bottom clearance to water depth ratio of 0.001. [Yeung's solution applies to a circular cylinder raised above the seabed, and is more complicated than that for a cylinder extending to the seabed because of the need to account for the fluid region directly beneath the cylinder.]

As $k_0a$ approaches zero, the dimensionless surge added mass approaches a value of $\pi d/a$, which

corresponds to the known value for a two-dimensional flow about a circular section. As $k_0a$ increases, the added mass reaches a maximum, then a minimum, and eventually approaches its limiting value, which is smaller than the corresponding zero frequency value $\pi d/a$. The damping coefficient is zero at zero frequency, attains its maximum value in the region of $k_0a$ approximately equal to 1 and eventually decreases as $1/(k_0a)^2$ at higher values of $k_0a$.

*High Frequency Approximations*

The high frequency approximations to the surge added mass and damping coefficient given by (3.26) and (3.33) respectively are also shown in Figs. 5a and 5b as broken lines. Fig. 5a shows how the added mass approaches its limiting values as $k_0a$ increases. Although the added mass based on the complete solution appears to be in reasonable agreement with the limiting values over the higher values of $k_0a$ shown in the figure, the convergence between the two values is relatively slow. It turns out that the agreement between the two predictions depends primarily on the relative water depth $k_0d$ or $\omega^2d/g$. The limiting value of the added mass differs from the complete solution by less than 5% for $k_0d$ or $\omega^2d/g$ greater than about 40; by less than 2% for $k_0d$ or $\omega^2d/g$ greater than about 100; and by less than 1% for $k_0d$ or $\omega^2d/g$ greater than about 200.

Fig. 5b shows how the damping coefficient approaches its high frequency approximation as $k_0a$ increases. The agreement between the damping coefficient based on the high frequency approximation (3.26) and the complete solution is relatively good for the higher values of $k_0a$ shown in the figure.

Also of interest is the possibility of employing the very simple large cylinder approximation to the added mass, valid for large $\omega^2d/g$ and large $a/d$ and given by (3.38). The added mass predictions based on this and the added mass given by (3.33) are compared in Fig. 6. In the figure, the dimensionless added mass is expressed in the form $\mu_{22}/\rho ad^2$ as a function of $a/d$ so that (3.38) predicts a constant value of this dimensionless added mass. The figure indicates that the predictions based on (3.33) and (3.38) differ by less than 5% when $a/d$ is greater than about 8. It

73

is noted, though, that in most engineering applications a/d is generally not so large so that (3.38) will usually not be useful.

*Vertical Distribution of Hydrodynamic Coefficients*

Vertical distributions of the dimensionless sectional surge added mass and damping coefficient are shown in Figs. 7 and 8 respectively for various values of $k_0a$ and a/d.

Fig. 7 indicates that the sectional added mass is generally non-zero at all depths, even at high frequencies. This is associated with the $\cos(k_mz)$ terms appearing in (3.41). It is of interest to note that the figure also indicates that the sectional added mass near the free surface becomes negative at high frequencies. It might be expected that at high frequencies, the sectional added mass near the seabed should not depend on free surface effects and should thus take on a value equal to $\pi\rho a^2$, corresponding to a two-dimensional flow about a circular section. This is found to be the case for small values of a/d (see Fig. 7a), whereas for large a/d values the sectional added mass is considerably smaller (see Fig. 7d).

Figure 8 shows how the sectional surge damping coefficient has a hyperbolic cosine variation with depth as indicated in (3.41). At high frequencies, this corresponds to the sectional damping coefficient becoming zero below an elevation of about half a wave length below the still water level. In fact, at the high frequency limit this feature implies that the total damping coefficient depends only on the water-line curve of the structure and not on its configuration below the still water level, as indicated by Davis (1976). The sectional damping coefficient at the still water level varies with $k_0a$ and a/d in a similar manner to that indicated for the total damping coefficient in Fig. 5b: for a given value of $k_0a$ it decreases monotonically with increase in a/d; while for a given value of a/d it decreases with increasing values of $k_0a$, except for $k_0a$ less than about 1.

*Free Surface Elevation*

As an illustration of the propagating and evanescent waves, Fig. 9 shows the water surface

elevation associated with the propagating mode and the first three evanescent modes as a function of the distance along the radial line, $\theta = 0$. The surface profiles are for time $t = 0$, in the particular case of surge oscillations of a circular cylinder with $k_0 a = 2$ and $a/d = 0.5$. As expected the evanescent waves decay rapidly with distance from the cylinder and are negligible at distances greater than twice the depth.

## 7.1.2 Elliptic Cylinder

The chief task in the evaluation of the expressions for the added masses and damping coefficients of an elliptic cylinder is the computation of the Mathieu functions. Clemm (1969) has published a set of FORTRAN routines to calculate the even and odd periodic Mathieu functions $ce_r(\eta,q)$ and $se_r(\eta,q)$ and the corresponding radial Mathieu functions $Mc_r^{(i)}(\xi,q)$ and $Ms_r^{(i)}(\xi,q)$ for real non-negative values of the parameter $q$ (see also Sale, 1970). However, the evanescent terms in (3.66) - (3.68) contain radial Mathieu functions with negative values of this parameter, for which neither tabulations nor computer programs are generally available. Hence a new set of double precision FORTRAN routines were developed to calculate $Mc_r^{(i)}(\xi,-q)$ and $Ms_r^{(i)}(\xi,-q)$ based on equations 20.8.5, 20.8.9, and 20.8.11 of Abramowitz and Stegun (1972). The routines are designed with the same general structure as Clemm's routines and have to be used in conjunction with these.

The dimensionless sway added masses and damping coefficients are now functions of $b/a$, $k_0 a$ and $a/d$ only and are presented in Figs. 10a and 10b respectively as functions of $k_0 a$ for $a/d$ values of 0.5, 1 and 2, for a particular value of $b/a = 0.2$ where $a$ and $b$ are the semi-major and semi-minor axes of the ellipse. As $k_0 a$ approaches zero, the dimensionless sway added mass approaches a value of $\pi d/a$, which corresponds to the value for a two-dimensional flow about an elliptic section. As $k_0 a$ increases, the added mass reaches a maximum, then a minimum, and eventually approaches its limiting value, which is smaller than the corresponding zero frequency value $\pi d/a$. The damping coefficient is zero at zero frequency, attains its maximum value in the region of $k_0 a = 1.25$ and eventually decreases at higher values of $k_0 a$.

75

## 7.2 Numerical Solutions

A computer program based on the boundary integral method described in section 4.2 has been developed for cylinders of arbitrary cross-section. The program is applied here to structures of various fundamental configurations and the corresponding results are presented and discussed.

### 7.2.1 Circular Cylinder

Initially, results have been obtained for a circular cylinder for which a closed-form solution is available. The added masses and damping coefficients of a circular cylinder, expressed in dimensionless form, are presented in Figs. 11 - 13 as functions of $k_0a$ for various values of a/d, where a is the radius of the cylinder. In the computations, 64 segments were used to describe the circular section and M = 9 was used in the approximation to the infinite series expansion given in (4.27) for the added masses.

Figure 11 shows the surge added mass and damping coefficient for $k_0a$ ranging from 0 to 3 and for a/d ratios of 0.5, 1, 2 and 5. Results based on the closed-form solution of section 7.1 are also given for comparison. Fig. 12 shows the pitch added moment of inertia and damping coefficient for $k_0a$ ranging from 0 to 3 and for a/d values of 0.5 and 1 along with the corresponding analytical solution. Similar results for the coupling added mass and damping coefficient between surge and pitch are given in Fig. 13. The agreement with the closed-form solution is seen to be very good, even though relatively few terms of the infinite series expansion have been used.

The effect of number of segments on computed values of hydrodynamic coefficients has also been investigated. Fig. 14 shows the ratios of the surge added mass and damping coefficient calculated using various numbers of segments N to the corresponding results of the complete solution for the particular case of $k_0a = 0.5$ and a/d = 0.5. Also shown are the damping coefficients derived from the corresponding exciting forces using (2.47) based on the Haskind relations, where the exciting forces themselves have been calculated numerically following Isaacson (1978). Using the present method, for the particular choice of $k_0a$ and a/d, the added mass is estimated to within 6% of the

complete solution using as little as 16 segments, whereas the evaluation of the damping coefficient requires at least 128 segments for the same level of accuracy. Thus it would seem to be advantageous to solve the scattering problem and then derive the damping coefficient from the corresponding exciting force. However, in order to apply (2.47) to an arbitrary section, the scattering problem would have to be solved for a series of incident wave directions and the results then integrated numerically with respect to wave direction, so that such an approach would not be particularly efficient. Extrapolation schemes to obtain accurate estimates of the added masses and damping coefficients from results calculated using moderate levels of discretization are evaluated in section 7.3. For the present, new results are given for added masses of a square cylinder, as an indication of an important configuration for which an analytical solution is not available.

## 7.2.2 Square Cylinder

The added masses of a square cylinder are presented in dimensionless form in Fig. 15. In the calculations, 64 segments were used to discretize the square contour, and once more $M = 9$ was used in the approximation to the infinite series expansion given in (4.27). Results for two orientations corresponding in turn to motions parallel to a pair of sides, $\beta = 0°$, and motions parallel to a diagonal, $\beta = 45°$, where $\beta$ is the angle between a pair of sides and the direction of motion, have been found to be identical. Fig. 15a shows the surge added mass as a function of $k_0 a$, where $a$ is the side length, for $\beta = 0°$ or $\beta = 45°$ and for $b/d$ ratios of 0.5, 1, 2 and 5. As $k_0 a$ approaches zero, the dimensionless surge added mass $\mu_{11}/\rho a^3$ approaches a value of 1.19 $d/a$, which corresponds to the value for a two-dimensional flow about a square section. Corresponding results for the pitch added moment of inertia are given in Fig. 15b for $a/d$ ratios of 0.5, 1 and 2. The surge-pitch added mass is presented in Fig. 15c and the yaw added moment of inertia in Fig. 15d. Again as $k_0 a$ approaches zero, the dimensionless yaw added moment of inertia $\mu_{66}/\rho a^5$ approaches a value of 0.045 $d/a$ which is the correct result for the corresponding two-dimensional problem without a free surface.

# 7.3 Convergence of Numerical Results

Two schemes to accelerate the convergence of numerical results described in section 4.3 have been evaluated by applying them to circular and elliptic cylinders, and corresponding results are now presented in order to assess the suitability of the two methods.

## 7.3.1 Circular Cylinder

Table III shows results of calculations based on the boundary integral method of the surge exciting force, added mass and damping coefficient for a vertical circular cylinder using different numbers of segments N for $a/d = 1$ and for various values of $k_0a$. The exciting force $F_1$, the added mass $\mu_{11}$ and the damping coefficient $\lambda_{11}$ are presented in dimensionless form as $|F_1|k_0d / \rho gHadtanh(k_0d)$, $\mu_{11}/\rho a^3$ and $\lambda_{11}/\rho a^3\omega$ respectively. Results of the closed-form solution, based on (A.9) for the exciting force, and on (3.11) for the added mass and damping coefficient, are included in the table, together with the results of applying the Shanks transformation and the Richardson extrapolation to the numerical values. The results of the Shanks transformation given correspond to $S[(A(N_2)]$ using (4.29); while those of the Richardson extrapolation correspond to $R^2[A(N_3)]$ using (4.36). $N_1$, $N_2$ and $N_3$ are chosen to be 32, 64, and 128 respectively.

For the case of the exciting force, the Richardson extrapolation is found to give results correct to 4 or 5 significant digits for $k_0a$ up to 5. When $k_0a$ equals 10, the numerical results are in error since $k_0a = 10.2$ corresponds to an irregular frequency in the method of integral equations (see section 7.4). On the other hand, the Shanks transformation does not give consistent improvements in accuracy, and for most of the $k_0a$ values shown, gives results inferior to the Richardson extrapolation.

For the case of added mass and damping coefficient, both Shanks transformation and Richardson extrapolation are found to give improved results, although the latter once more appears to be superior. It is for the damping coefficient that the most substantial improvements are observed. In

fact, for the $k_0a$ values shown, the damping coefficient calculated using 128 segments is consistently less than the corresponding analytical value and is typically correct to a single decimal digit, whereas the Shanks transformation gives results correct to at least 2 digits and the Richardson extrapolation gives 3 or 4 correct decimal digits. Again, the numerical results for a $k_0a$ value of 10 are in error due to the proximity to an irregular frequency. In calculations of added mass, the propagating mode and a maximum of 16 evanescent modes have been included, except for the limiting value $\mu_{22}(\infty)$ which is obtained by discarding the potential $\phi_0^k$ and using (5.30) to calculate $k_m$ (see section 5.2.1). The calculation of the damping coefficient requires solution to the propagating mode only.

## 7.3.2 Elliptic Cylinder

Corresponding results have also been obtained for an elliptic cylinder which represents a more general case for which an analytical solution is available. Figure 16 shows the ratio of sway exciting force, added mass and damping coefficient values calculated numerically using different numbers of segments N to the corresponding analytical values for the case $b/a = 0.2$ and $a/d = 2$, where a and b represent the semi-major and semi-minor axes respectively. The results of applying the Richardson extrapolation to the numerical values are also shown. The analytical values of exciting force used for comparison are based on the solution of Chen and Mei (1971) indicated in (A.16). The analytical values of added mass and damping coefficient are based on (3.67). In calculations of added mass, the propagating mode and a maximum of 20 evanescent modes have been included.

The extrapolated results for the exciting force are found to be accurate except at the two highest frequencies corresponding to $k_0a = 16$ and $k_0a = 20$. The first irregular frequency in this case occurs at $k_0a = 16.2$, and accounts for the large error in the numerical results near that frequency.

The extrapolated results for the added mass are found to be accurate for all the $k_0a$ values shown. The numerical values of damping coefficient are found to be consistently less than the

corresponding analytical values, except for $k_0a = 16$, and the application of the Richardson extrapolation gives substantially improved estimates. The erratic convergence at $k_0a = 16$ is again due to the proximity of the irregular frequency.

## 7.4 Irregular Frequencies

Irregular frequencies in the method of integral equations are manifested in actual calculations as spurious peaks in the curves of exciting forces, added masses, and damping coefficients as functions of wave frequency. The irregular behaviour may be clearly demonstrated if the numerical results described in section 7.2 are extended to include high $k_0a$ values. For example, Fig. 17a shows the surge damping coefficient of a circular cylinder with $a/d = 1$ for $k_0a$ ranging from 0 to 8, and Fig. 17b shows the corresponding propagating mode potential $\phi_0^k$ at $(r,\theta) = (a,\pi/2)$ suitably scaled to give the resulting surface elevation. The solid line is the analytical solution and the dashed line represents numerical results obtained using 64 segments. The dotted line in both figures is an approximation to Turing's N-condition number (Turing, 1948) for the coefficient matrix in the matrix solution. The condition number is a measure of the ill-conditioning of the system, such that a condition number of 1 corresponds to a well-conditioned system of equations while a condition number which is greater than or equal to the order of the matrix indicates an ill-conditioned system. In the present case, the matrix condition number is approximately 1 except near $k_0a$ values corresponding to the zeros of the Bessel functions, $J_m(k_0a)$, m = 0, 1, 2, ... However, the damping coefficient as well as the propagating mode potential show irregularities only at the zeros of $J_1(k_0a)$ due to the condition in (4.37). Figure 18 indicates improvements to numerical results in the neighbourhood of the first irregular frequency due to an application of the Richardson extrapolation. The solid line in the figure represents the analytical solution, the dotted line shows numerical values obtained using 128 segments, and the dashed line represents the results of applying the Richardson extrapolation to numerical values obtained using 32, 64 and 128 segments.

It is also of interest to examine the effect of irregular frequencies on the computed force and the

potential in the corresponding scattering problem described in Appendix A. Figure 19a shows the exciting force on a circular cylinder due to an incident wave of height H and Fig. 19b shows the corresponding wave runup, which is proportional to the potential, at $(r,\theta) = (a,\pi)$. The solid line is the analytical solution of MacCamy and Fuchs (1954) and the dashed line represents numerical results obtained using the integral equation method of Isaacson (1978). The dotted line is again the approximation to Turing's N-condition number for the coefficient matrix in the matrix solution. Unlike the radiation problem, the condition (4.37) is no longer satisfied and hence the runup shows irregular oscillations in the neighbourhood of the zeros of $J_m(k_0a)$, m = 0, 1, 2, ..., whereas the integrated force has irregularities only near the zeros of $J_1(k_0a)$.

It appears that the occurrence of an irregular frequency in numerical calculations for an arbitrary structure may be detected by monitoring the variation of the condition number as well as the variation of the numerical result for a range of frequencies preceding and following the particular frequency of interest. Hydrodynamic coefficients at the irregular frequency may then be interpolated from a number of values calculated sufficiently away from the irregular region. The Richardson extrapolation is beneficial in narrowing the bandwidth of the irregular region. However, such an approach is not particularly efficient. Available methods to eliminate the occurrence of irregular frequencies have been summarized in 4.4.3, but all of them entail additional computational effort. Alternative approaches based on high frequency approximations are evaluated in the next section.

# 7.5  High Frequency Approximations

Alternative approaches for calculating high frequency added masses and damping coefficients of vertical cylinders have been outlined in Chapter 5, and corresponding results for various fundamental configurations are presented here and discussed.

## 7.5.1  Circular Cylinder

Initially, results are presented for a vertical circular cylinder for which an analytical solution is

available. Figure 20 shows the dimensionless surge damping coefficient as a function of $k_0a$ for the particular case $a/d = 1$. In the figure, the solid line represents the analytical solution. The dashed line indicates the numerical solution obtained by the integral equation method using 32, 64 and 128 segments and then applying the Richardson extrapolation to accelerate convergence. Irregular behaviour occurs near $k_0a = 3.83$ and 7.02, corresponding to the first two zeros of $J_1(k_0a)$. The dotted line corresponds to damping coefficient values obtained using (2.47), with the exciting force $F_1$ calculated by the integral equation method (Isaacson, 1978) using 64 segments. As expected, this exhibits irregularities near the same critical frequencies. The chain-dotted line shows results obtained using (5.20) based on the geometrical optics approximation. This is seen to be accurate only for relatively high frequencies, corresponding approximately to $k_0a > 6$. On the other hand, the chain-dashed line shows results based on Ursell's short-wave solution (5.6), which is seen to agree with the complete solution over a wider frequency range corresponding approximately to $k_0a > 2$. It appears from Fig. 20 that the geometrical optics approximation is generally unsuitable for use in calculating the added masses using the Kramers-Kronig relations, whereas Ursell's short-wave approximation is accurate at frequencies well below the lowest irregular frequency, and so could be used for this purpose.

Figure 21 presents the corresponding surge added mass of a circular cylinder as a function of $k_0a$, again for the particular case $a/d = 1$. The solid line indicates the analytical solution, and the dashed line indicates the results based on the integral equation method. A maximum of 17 terms were used in the infinite series expansion for the added mass in (4.27) and the Richardson extrapolation was applied to numerical results obtained using 32, 64 and 128 segments. As in the case of the damping coefficient, the numerical solution once more exhibits irregular behaviour near the known irregular frequencies. The chain-dotted line, practically indistinguishable from the solid line corresponding to the analytical solution, shows the added mass calculated by applying the Kramers-Kronig relation, using analytical values of the damping coefficient. Damping coefficients at 512 discrete values of Ka ranging from 0 to 51.2 have been used, and 16 terms were considered in the analytical series for $\mu_{11}(\infty)$ in (3.33). The added mass has also been calculated by applying

the Kramers-Kronig relation using instead numerical values of the damping coefficient, as would more generally be available for arbitrary sections. The damping coefficient at low frequencies and the limiting added mass were obtained by the integral equation method with the Richardson extrapolation applied to results calculated using 32, 64 and 128 segments, while the damping coefficient at high frequencies was obtained using Ursell's short-wave solution (5.6). Sixteen terms were considered in the series in (5.29) in order to calculate the limiting value of the added mass, and the transition frequency $u_0$ was taken as 2.5. The results, indicated by a dotted line in the figure, are indistinguishable from the solid line corresponding to the analytical solution. The circular symbols represent the added mass calculated numerically using evanescent modes alone and using 64 segments to describe the horizontal contour. The error is less than 5% for $k_0a \geq 5$ and less than 1% for $k_0a \geq 10$.

## 7.5.2 Elliptic Cylinder

Corresponding results have also been obtained for an elliptic cylinder which represents a more general case for which an analytical solution is available, although not all results based on the available methods used in Figs. 20 and 21 are presented. Results are presented here for the case $a/d = 2$ and $b/a = 0.2$, where a and b are the semi-major and semi-minor axes respectively. The sway damping coefficient, expressed in dimensionless form, is presented in Fig. 22 as a function of $k_0a$. The solid line corresponds to the analytical solution, while the dashed line corresponds to the numerical solution based on the integral equation method obtained by applying the Richardson extrapolation to results calculated using 32, 64 and 128 segments. The latter shows irregular behaviour near $k_0a = 16.2$ and 18.3 corresponding to the zeros of the radial Mathieu functions of the first kind, $Ms_1^{(1)}(\xi_0,q_0)$ and $Ms_3^{(1)}(\xi_0,q_0)$. The dotted line shows the damping coefficient based on Ursell's short-wave solution and given by (5.6). This method is found to be accurate for $k_0a > 4$.

Figure 23 presents the corresponding sway added mass of an elliptic cylinder as a function of $k_0a$, for the same case corresponding to $a/d = 2$ and $b/a = 0.2$. The solid line shows the analytical

83

solution, and the dashed line shows the results based on the integral equation method. A maximum of 21 terms were used in the infinite series expansion for the added mass in (4.27) and the Richardson extrapolation was applied to numerical results obtained using 32, 64 and 128 segments. The numerical results once more exhibit irregular behaviour near the known irregular frequencies. The chain-dotted line, practically indistinguishable from the solid line corresponding to the analytical solution, indicates the added mass calculated by applying the Kramers-Kronig relation and using analytical values of the damping coefficient. Damping coefficients at 1024 discrete values of Ka ranging from 0 to 102.4 have been used, and the limiting value of the added mass, $\mu_{22}(\infty)$, was determined numerically by considering 20 terms in (5.29) and applying the Richardson extrapolation. The dotted line indicates the added mass calculated by applying the Kramers-Kronig relation and using numerical values of the damping coefficient. In this case, the damping coefficients at low frequencies were obtained by using the integral equation method and then applying the Richardson extrapolation, while the damping coefficients at high frequencies were obtained using Ursell's short-wave solution. The transition frequency $u_0$ was taken as 4, and once more, the results agree well with analytical predictions such that the dotted line is indistinguishable from the solid line. The circular symbols represent the added mass calculated numerically using evanescent modes alone and using 64 segments to describe the horizontal contour. The error is found to be less than 5% for $k_0a \geq 10$.

## 7.5.3 Square Cylinder

Finally, the various methods described have been used to provide results for a square cylinder for which an analytical solution is not available. Figure 24 shows the dimensionless surge damping coefficient as a function of $k_0a$ for a/d values of 1, 2, and 5 where a now denotes the side of the square. The solid line corresponds to the numerical solution based on applying the Richardson extrapolation to results obtained by the integral equation method calculated using 32, 64 and 128 segments. Based on Jones (1974), the lowest irregular frequency occurs within the range $5.42 < k_0a < 7.66$. In actual calculations, numerical irregularities occur at $k_0a = 7.0$. The dashed

84

line is Ursell's short-wave solution given by (5.6).

Figure 25 presents the corresponding surge added mass of a square cylinder as a function of $k_0a$, for the same cases corresponding to $a/d = 1, 2$, and 5. The dashed line shows the results based on the integral equation method. A maximum of 17 terms were used in the infinite series expansion for the added mass in (4.27) and a Richardson extrapolation was applied to numerical results obtained using 32, 64 and 128 segments. The numerical results once more exhibit irregular behaviour near $k_0a = 7$. The solid line indicates the added mass calculated by applying the Kramers-Kronig relation and using numerical values of the damping coefficient. Damping coefficients at 512 discrete values of $Ka$ ranging from 0 to 51.2 have been used. The damping coefficients at low frequencies were obtained by using the integral equation method and then applying the Richardson extrapolation, while the damping coefficients at high frequencies were obtained using Ursell's short-wave solution. The limiting value of the added mass, $\mu_{22}(\infty)$, was determined numerically by considering 16 terms in (5.29) and applying the Richardson extrapolation. The added mass obtained from evanescent modes alone and using 64 segments to describe the horizontal contour is indicated for $k_0a = 5, 6, ..., 10$ and shows excellent agreement with the previous solutions.

## 7.6 Compressibility Effects

When fluid compressibility is taken into account, an additional physical quantity, the speed of sound c in water, enters the analysis. Hence the dimensionless added masses and damping coefficients or the corresponding dimensionless forces are now functions of $c^2/ga$ in addition to $k_0a$ and $a/d$. Furthermore, since gravitational effects are relatively unimportant at the very high frequencies at which fluid compressibility effects become dominant, it is convenient to use the dimensionless quantity $\omega/\omega_1$ (where $\omega_1$ is the first cut-off frequency for acoustic waves), which is independent of g, in place of $k_0a$.

## 7.6.1 Circular Cylinder

Figure 26 shows the amplitude of the force due to surge oscillations of a vertical circular cylinder as a function of $\omega/\omega_1$ for $a/d = 0.1, 0.25, 0.5$, and $1.0$, and may be compared to Fig. 10 of Tanaka and Hudspeth (1988). The solid line represents the analytical solution described in section 6.2.1 which takes account of both fluid compressibility ($c = 1447$ m/s) and gravity, with $c^2/ga = 10^5$. A total of about 24 terms were included in the series expansion of (6.6). The rapid variation in the dimensionless force at small values of the dimensionless frequency is due to gravitational effects. The subsequent gradual increase indicates the effect of fluid compressibility. For squatty cylinders with larger $a/d$ ratios, the rate of this increase is more pronounced and the maximum is reached sooner after the first cut-off frequency. For a cylinder with $a/d = 1$, the maximum force occurs at $\omega/\omega_1 = 1.05$, and is 2.5 times the corresponding value for an incompressible fluid. For a cylinder with $a/d = 0.25$, the maximum occurs at $\omega/\omega_1 = 1.66$, and is only 1.36 times the value for an incompressible fluid. After reaching a maximum, the dimensionless force decreases. For a squatty cylinder, a secondary peak is observed following the second cut-off frequency, and is believed to be due to the emergence of the second acoustic propagating mode, rather than 'an artifice of the eigenseries' as suggested by Tanaka and Hudspeth (1988). The dip in the curve near $\omega/\omega_1 = 3$ for a slender cylinder observed in Tanaka and Hudspeth's figure is not found in the present results. It appears that their results at $\omega/\omega_1 = 3$ do not include the contribution of the term corresponding to m = 2 in (6.6).

In Fig. 26, the dashed line corresponds to the numerical solution described in section 6.3 obtained after ignoring gravitational effects. 64 segments were used to describe the cross-section, and M in (4.27) was taken to be about 10 such that the contribution from the last term included in the sum was less than 0.1%. The agreement with the analytical solution is seen to be particularly good for frequencies of oscillation less than the frequency corresponding to the maximum force. For higher frequencies, numerical values tend to underestimate the force. This is because the propagating modes which are dominant at such frequencies require a finer discretization than do the evanescent

modes for the same level of accuracy. For squatty cylinders, a secondary peak occurs following the second cut-off frequency. For $a/d = 1$, an irregular frequency occurs in the first propagating mode at $\omega/\omega_1 = 2.64$, since $k_1'a$ is then approximately equal to 3.83 corresponding to the first zero of $J_1$.

In Figs. 27 and 28, the force is presented as an added mass and a damping coefficient for the particular case of $a/d = 2$. In Fig. 27, the solid line represents the damping coefficient obtained from the analytical solution taking both compressibility and gravitational effects into account and with $c^2/ga = 10^5$. The effects of gravity are confined to small dimensionless frequencies $\omega/\omega_1$ and cannot be noticed on the adopted scale, with the damping coefficient virtually zero for all $\omega \leq \omega_1$. At $\omega = \omega_1$, the first acoustic progressive wave emerges and the damping coefficient rises steeply to a maximum due to fluid compressibility. Subsequently the damping coefficient falls. At $\omega/\omega_1 = 3$, the second acoustic progressive wave emerges and causes the damping coefficient to climb before falling again. The dashed line represents the numerical solution based on an omission of gravitational effects, and obtained by applying the Richardson extrapolation of section 4.3.2 to results obtained using 32, 64, and 128 segments. This shows excellent agreement with the analytical solution except at the irregular frequencies as expected. These correspond to $\omega/\omega_1 = 1.58$, 2.45, 3.24, 3.39, and 3.74. The dotted line in Fig. 25 corresponds to the asymptotic solution given in (6.17) and based on Ursell's short-wave solution. This coincides with the analytical solution (solid line) except in the vicinity of each cut-off frequency when the denominator of one of the terms on the right-hand side of (6.17) vanishes.

In Fig. 28, the solid line represents the added mass obtained from the analytical solution taking both compressibility and gravitational effects into account, again with $c^2/ga = 10^5$, and using about 24 terms in the series expansion of (6.6). The effect of gravity at low dimensionless frequencies $\omega/\omega_1 \ll 1$ is hardly noticeable on the adopted scale. Thus, the added mass appears to rise from its limiting value for an incompressible fluid and reaches a maximum near $\omega = \omega_1$. Subsequently it decreases and falls well below its limiting value in incompressible fluid. A small secondary peak

occurs when $\omega/\omega_1$ is approximately equal to 3 due to the second acoustic progressive mode. The dashed line represents the numerical solution based on an omission of gravitational effects and obtained by applying the Richardson extrapolation of section 4.3.2 to results obtained using 32, 64, and 128 segments. This shows excellent agreement with the analytical solution except at the irregular frequencies. These results are based on M in (4.27) taken to be about 11 such that the contribution from the last term included in the sum was less than 0.1%. Finally, the circular symbols denote the added mass calculated numerically using 64 segments after discarding the propagating modes which are present when $\omega > \omega_1$, and is found to give somewhat reasonable estimates at frequencies sufficiently after the emergence of each progressive wave.

## 7.6.2 Elliptic Cylinder

Corresponding results have also been obtained for an elliptic cylinder which represents a more general case for which an analytical solution is available. Figures 29 and 30 show the dimensionless damping coefficient and added mass respectively as functions of dimensionless frequency $\omega/\omega_1$ for an elliptic cylinder with $b/a = 0.2$ and $a/d = 2$. In Fig. 29, the solid line represents the sway damping coefficient obtained from the analytical solution with gravitational effects omitted. The damping coefficient is zero for $\omega \leq \omega_1$. At $\omega = \omega_1$, the first acoustic progressive wave emerges and the damping coefficient rises steeply to a maximum due to fluid compressibility. Subsequently the damping coefficient falls. At $\omega/\omega_1 = 3$, the second acoustic progressive wave emerges and causes the damping coefficient to climb before falling again. The dashed line represents the numerical solution, again with gravitational effects omitted, and obtained by applying the Richardson extrapolation to results obtained using 32, 64, and 128 segments. For this particular configuration, the first irregular frequency is expected only near $\omega/\omega_1 = 5.3$, and hence the dashed line is practically indistinguishable from the solid line over the entire range of frequencies shown. The dotted line corresponds to the asymptotic solution given in (6.17) based on Ursell's short-wave solution and coincides with the solid line except in the vicinity of each cut-off frequency.

In Fig. 30, the solid line represents the corresponding added mass obtained from the analytical solution with gravitational effects omitted. Terms corresponding to m ranging from 1 to 15 and n ranging from 0 to 31 were included in the series expansion of (6.9). The added mass is found to increase from its limiting value in an incompressible fluid and reach a maximum near $\omega = \omega_1$. Subsequently it decreases and falls well below its limiting value in incompressible fluid. A small secondary peak occurs when $\omega/\omega_1$ is approximately equal to 3 due to the second acoustic progressive mode. The dashed line represents the numerical solution obtained by applying the Richardson extrapolation to results obtained using 32, 64, and 128 segments, and is practically indistinguishable from the analytical solution. Effect of gravity was ignored and M in (4.27) was taken to be about 10 such that the contribution from the last term included in the sum was less than 0.1%. The circular symbols denote the added mass calculated numerically using 64 segments after discarding the propagating modes which are present when $\omega > \omega_1$, and is found to give somewhat reasonable estimates at frequencies sufficiently after the emergence of each progressive wave.

## 7.6.3 Square Cylinder

Finally, the methods have been used to provide results for a square cylinder for which an analytical solution is not available. Figures 31 and 32 show the dimensionless surge damping coefficient and added mass respectively as functions of dimensionless frequency $\omega/\omega_1$ for a square cylinder with a/d = 2. In Fig. 31, the solid line represents the surge damping coefficient obtained numerically with gravitational effects omitted, using 32, 64 and 128 segments, and applying Richardson extrapolation. The damping coefficient is zero for $\omega \leq \omega_1$. At $\omega = \omega_1$, the first acoustic progressive wave emerges and the damping coefficient rises steeply to a maximum due to fluid compressibility. Subsequently the damping coefficient falls. At $\omega/\omega_1 = 3$, the second acoustic progressive wave emerges and causes the damping coefficient to climb before falling again. The rapid oscillations found at $\omega/\omega_1 = 2.44$ and 3.74 are due to irregular frequencies in the method of integral equations. The dotted line is the asymptotic solution given in (6.17) based on Ursell's short-wave solution, and provides a useful estimate of the damping coefficient except in the

vicinity of each cut-off frequency.

In Fig. 32, the solid line represents the corresponding added mass calculated by including about 12 terms in the series expansion of (4.27) and applying Richardson extrapolation to results obtained using 32, 64, and 128 segments. The added mass is found to increase from its limiting value in an incompressible fluid and reach a maximum near $\omega = \omega_1$. Subsequently it decreases and falls well below its limiting value in incompressible fluid. A small secondary peak occurs when $\omega/\omega_1$ is approximately equal to 3 due to the second acoustic progressive mode. The rapid oscillations found at $\omega/\omega_1 = 2.44$ and 3.74 are due to irregular frequencies in the method of integral equations. The circular symbols denote the added mass calculated using 64 segments after discarding the propagating modes which are present when $\omega > \omega_1$, and is found to give somewhat reasonable estimates at frequencies sufficiently after the emergence of each progressive wave.

## 7.7 Available Experimental Data

In the previous sections, theoretical predictions using several methods have been compared and found to be in excellent agreement. In principle, a validation of the theoretical basis by comparison with experimental results is also required. Several such comparisons are available for the case of surge oscillations of a circular cylinder (e.g. Garrison and Berklite (1973), and Tanaka and Hudspeth (1988) for frequencies at which neither gravitational effects nor compressibility effects are significant; and Pegg (1983) for lower frequencies at which gravitational effects have to be accounted for). Garrison and Berklite (1973) have also compared the corresponding results for a cone and a sphere. As an example, Fig. 33 shows a comparison between the analytical solution described in section 3.1.1 and the experimental results of Pegg (1983) for the particular case of a circular cylinder with a/d = 0.28. The figure indicates that the theoretical and experimental values of added mass and damping coefficient are generally in good agreement. Thus, in general, available experimental data serves to justify the application of linear potential flow theory to problems of small amplitude oscillations of large offshore structures. However, there is a lack of experimental data for frequencies at which fluid compressibility has a significant effect. Since the

90

compressibility of water is not scalable, similitude at such frequencies is inhibited by requirements of prohibitively high excitation frequencies in the model.

# Chapter 8

# EXAMPLE APPLICATION

Various methods of calculating the hydrodynamic coefficients of a bottom-founded vertical cylinder of arbitrary section extending to the free surface have been described and corresponding results have been presented in Chapter 7. It is appropriate to summarize limitations in applying these methods to engineering situations, and to illustrate a typical ocean engineering application of these solutions.

The assumption of potential flow is reasonable for an oscillation amplitude to cylinder characteristic radius ratio of less than about 0.6, corresponding to the absence of flow separation or to flow separation effects generally being unimportant (e.g. Sarpkaya and Isaacson, 1981). Even though flow separation may still occur for structures with sharp corners, these effects then become relatively localized. The linearization assumption is consistent with small ratios of oscillation amplitude to cylinder characteristic radius, but is in addition based on generated surface waves of small steepness which may be shown to correspond to cylinder accelerations which are small in relation to g. In fact, experience has indicated that such linear solutions are often quite reasonable even when this condition is not formally satisfied. Bearing these in mind, the approaches described here are valid approximately for $\zeta/a < 0.6$ and $\omega^2\zeta/g << 1$ (perhaps not essential) where $\zeta$ is the amplitude of the (translatory) motion and a is the cylinder characteristic radius. These ranges of validity apply to many engineering applications

An omission of surface tension effects is justified for sufficiently long surface waves. For example, when the period T > 0.35 sec and d > 0.02 m, the change in wave length of propagating surface waves due to capillary effects is less than 1% (Le Méhauté, 1976). On the other hand, at high frequencies when the propagating surface waves are sufficiently short for capillary effects to be felt, then the propagating surface waves themselves are of little consequence to the overall problem which is then primarily influenced by the evanescent modes alone. Thus an omission of

surface tension is usually justified at all frequencies.

A further engineering limitation of the approaches described here relates to the configuration which is treated, since many offshore structures may not correspond to vertical cylinders. Nevertheless, even for structures of general shape it will often be appropriate to apply the present method in order to assess the influence of sectional shape on modifications to the predicted hydrodynamic coefficients.

Finally, some useful guidelines on the relative importance of gravity and fluid compressibility may be summarized. Gravitational effects are no longer important when $\omega^2 d/g \gg 1$. In practice, an accounting for gravitational effects produces less than 5% reduction in the added mass when $\omega^2 d/g > 40$. On the other hand, fluid compressibility is not significant when $\omega/\omega_1 \ll 1$, and an accounting for fluid compressibility produces less than 5% increase in the added mass when $\omega/\omega_1 < 0.3$. When both $\omega^2 d/g > 40$ and $\omega/\omega_1 < 0.3$, then neither gravity nor compressibility need be accounted for. The added masses are then given by frequency-independent limiting values and the damping coefficients vanish. The three regimes are indicated in Fig. 34 in which the ordinate represents water depth in metres, the abscissa represents frequency in Hertz, and the solid lines correspond to $\omega^2 d/g = 40$ and $\omega/\omega_1 = 0.3$. However, for slender cylinders, the ranges indicated are conservative.

In order to illustrate the present approach in the context of a typical ocean engineering application, consideration is given to a case similar to the Molikpaq structure which has been deployed in the Beaufort Sea. The Molikpaq has a typical octagonal section contained within a square of side 111 m as indicated in Fig. 35. Although the Molikpaq does not have vertical sides, it is approximated here as a vertical cylinder with the depicted cross-section, located in a water depth of 20 m with surge (motion parallel to a pair of long sides) excitation frequencies from earthquake loading ranging from 0.1 - 20 Hz.

The surge added mass and damping coefficient of the octagonal section vertical cylinder are initially

calculated with gravitational effects accounted for and fluid compressibility effects omitted. Figure 36 shows the dimensionless surge damping coefficient as a function of $k_0a$ where a is now the distance between a pair of long sides of the octagon. The solid line corresponds to the numerical solution based on the integral equation method, obtained by applying the Richardson extrapolation to results calculated using 32, 64 and 128 segments. The broken line corresponds to Ursell's short-wave approximation, given by (5.6) with $c_{11} = 1.77$. Based on Jones (1974), the lowest irregular frequency occurs within the range $6.56 < k_0a < 7.66$. In actual calculations, numerical irregularities occur at $k_0a = 7.1$, as indicated in the figure, corresponding to a frequency of 0.12 Hz. Results are not shown for $k_0a > 20$, and over such a range the damping coefficient $\lambda_{11}$ is given on the basis of (5.6) simply by $\lambda_{11}/\rho\omega a^3 = 3.54/(k_0a)^2$.

Figure 37 presents the corresponding surge added mass of the octagonal cylinder as a function of $k_0a$. The solid line shows the results based on the Richardson extrapolation applied to numerical results obtained using 32, 64 and 128 segments, with a maximum of 20 terms used in the infinite series expansion in (4.27). Once more, irregular frequencies are apparent in the curve based on the integral equation method. The broken line corresponds to the evanescent mode approximation. The figure indicates that over the relatively low $k_0a$ range shown, the evanescent mode approximation is not yet sufficiently accurate. However, it becomes more suitable for large $k_0a$, and at a sufficiently high $k_0a$ value the added mass $\mu_{11}$ reaches its limiting value in incompressible fluid corresponding to $\mu_{11}/\rho a^3 = 0.0267$.

Based on Figs. 36 and 37, the ranges of validity of the principal high frequency approximations which have been described in Chapter 5 may be summarized for the present case as follows:

Damping coefficient − Ursell's approximation, (5.6):        valid for $k_0a > 3.5$

Added mass − evanescent mode approximation, (5.29):        valid for $k_0a > 20$

Finally, the corresponding surge added mass and damping coefficient are calculated with fluid compressibility effects accounted for and gravitational effects omitted. Figures 38 and 39 show the

94

dimensionless surge damping coefficient and added mass respectively as functions of dimensionless frequency $\omega/\omega_1$. In Fig. 38, the solid line represents the surge damping coefficient obtained numerically using 32, 64 and 128 segments, and applying Richardson extrapolation. The damping coefficient is zero for $\omega \leq \omega_1$. At $\omega = \omega_1$, the first acoustic progressive wave emerges and the damping coefficient rises steeply to a maximum due to fluid compressibility. Subsequently the damping coefficient falls. At $\omega/\omega_1 = 3$, the second acoustic progressive wave emerges and causes the damping coefficient to climb before falling again. The other rapid oscillations are due to irregular frequencies in the method of integral equations, the first occurring at $\omega/\omega_1 = 1.29$ corresponding to $k_1' a = 7.1$. The dotted line is the asymptotic solution given in (6.17) based on Ursell's short-wave solution, and provides a useful estimate of the damping coefficient except in the vicinity of each cut-off frequency.

In Fig. 39, the solid line represents the corresponding added mass calculated by including about 20 terms in the series expansion of (4.27) and applying Richardson extrapolation to results obtained using 32, 64, and 128 segments. Once again, the peaks in the added mass curve, except those at $\omega/\omega_1 = 1$ and 3, are due to the effects of irregular frequencies. The broken line denotes the added mass calculated using 64 segments after discarding the propagating modes which are present when $\omega > \omega_1$, and is found to give somewhat reasonable estimates at frequencies sufficiently after the emergence of each progressive wave.

For the particular frequencies 0.02, 0.1, 1, 5, 10, and 20 Hz, the predicted values of added mass and damping coefficient obtained from the above results are indicated in Table IV. The added mass is calculated by the integral equation method with the propagating and evanescent modes for 0.02 and 0.1 Hz, with evanescent modes alone and the modified eigenvalues in (5.30) for 1 and 5 Hz, and by the modified integral equation method accounting for compressibility effects and omitting gravitational effects for 10 and 20 Hz. The damping coefficient is calculated by the integral equation method for 0.02 Hz, by Ursell's short-wave solution for 0.1 and 1 Hz, and by the modified integral equation method accounting for compressibility effects and omitting gravitational

95

effects for 20 Hz. The damping coefficient is zero for 5 and 10 Hz since there are no acoustic propagating modes and the gravitational propagating mode does not have any significant effect.

Once the coefficients have been obtained as functions of frequency, they may be applied to an analysis in either the frequency or time domain in order to determine the loads due to either periodic, random, or transient oscillations. In fact, the corresponding analysis may be carried out in the frequency domain for the periodic or random motions, and in the time domain for transient motions. The corresponding procedures are briefly illustrated here for the case of a single degree of freedom system with the excitation provided through a specified motion.

*(a)* *Harmonic Excitation*

For the case of harmonic excitation, if the displacement and the resulting base shear are expressed as $\zeta \exp(-i\omega t)$ and $F \exp(-i\omega t)$ respectively, then the equation of motion is:

$$[-\omega^2(m + \mu(\omega)) - i\omega\lambda(\omega)] \zeta = F \tag{8.1}$$

where m represents the structural mass, $\mu(\omega)$ is the added mass, and $\lambda(\omega)$ is the damping coefficient, which are both functions of frequency. Since $\mu$ and $\lambda$ are known at the excitation frequency $\omega$, then F may be obtained directly from the above equation, for any specified value of $\zeta$.

*(b)* *Random Excitation*

In the case of a stationary, random excitation, the solution for harmonic excitation is initially used to provide a complex frequency response function which may be applied directly to a spectral analysis. For harmonic base motion, the complex amplitude of the base shear F is related to the complex amplitude of the displacement $\zeta$ by:

$$F = H(i\omega) \zeta \tag{8.2}$$

where $H(i\omega)$ is the complex frequency response function relating displacement to base shear. On

96

the basis of (8.1), this is given as:

$$H(i\omega) = -\omega^2(m + \mu(\omega)) - i\omega\lambda(\omega) \qquad (8.3)$$

With the complex frequency response function known from (8.3), the case of a stationary random process may be treated such that the power spectral density function of the force $S_F(\omega)$ is related to that of the displacement $S_\zeta(\omega)$ as:

$$S_F(\omega) = |H(i\omega)|^2 S_\zeta(\omega) \qquad (8.4)$$

*(c)    Time-domain Solution*

A time-domain solution corresponding to a specified base motion record may also be developed. In this case, the complex frequency response function may be used to obtain the corresponding impulse response function, which can subsequently be applied to Duhamel's integral in order to develop a time history of the force. For the linear system described here, the time domain solution for the base shear F(t) may be related to the known acceleration record $\ddot\alpha(t)$ in terms of Duhamel's integral as:

$$[m + \mu(\infty)]\ \ddot\alpha(t) + \int_0^t h(t-\tau)\ \ddot\alpha(\tau)\ d\tau = F(t) \qquad (8.5)$$

where h(t) is an impulse response function which is related to integrals of the added mass or damping coefficient over frequency:

$$h(t) = \frac{2}{\pi}\int_0^\infty [\mu(\omega) - \mu(\infty)]\ \cos(\omega t)\ d\omega = \frac{2}{\pi}\int_0^\infty \frac{\lambda(\omega)}{\omega}\ \sin(\omega t)\ d\omega \qquad (8.6)$$

Equation (8.5) may be used in a time-stepping procedure to obtain a force record from a displacement record once the impulse response function is evaluated based on (8.6) with $\mu(\omega)$, $\mu(\infty)$, and $\lambda(\omega)$ obtained by the methods outlined in this study.

# Chapter 9

# CONCLUSIONS AND RECOMMENDATIONS

## 9.1 Conclusions

The present thesis addresses the problem of determining hydrodynamic loads on a large structure oscillating in water, which may be approximated as a vertical cylinder of arbitrary section extending from the seabed to the free surface. By assuming that the body motions are of small amplitude, that the fluid is incompressible and inviscid, and that the fluid motion is irrotational, the problem is initially formulated in the frequency domain as a three-dimensional linear radiation problem. By exploiting the restriction to the geometry of the structure, the three-dimensional problem is simplified and reformulated as a series of two-dimensional problems in the horizontal plane. The first of these correspond to a propagating mode potential and the others to evanescent mode potentials.

Analytical solutions are first obtained for circular and elliptic sections, and a set of corresponding results for the sway mode are presented. These are used as the basis of assessing the suitability of various methods subsequently described which are applicable to cylinders of arbitrary section.

For the case of an arbitrary section, a solution may be obtained by applying the method of integral equations. Because of the restriction to a vertical cylinder, only the cross-sectional contour of the structure is required to be discretized instead of the entire submerged surface. Besides, the Green's function of the problem is simply proportional to a Bessel function and hence easily calculated. These factors afford considerable economy of effort, both in the complexity of programming as well as in computer time and storage requirements. Numerical results obtained for several fundamental configurations indicate that the added masses are accurately predicted using moderate levels of discretization, whereas the damping coefficients are consistently underpredicted and requires a finer discretization to achieve the same level of accuracy. This is because only the

propagating mode potential contributes to damping and this is more sensitive than the evanescent mode potentials to the level of discretization. On the other hand, both the propagating mode potential and the evanescent mode potentials contribute to the added masses.

Two extrapolation schemes, namely Shanks transformation and Richardson extrapolation, for accurately estimating the added masses and damping coefficients from results calculated using moderate levels of discretization are evaluated, and the Richardson extrapolation scheme is found to be superior. A Richardson extrapolation scheme applied to results calculated using 32, 64, and 128 segments is found to be extremely effective.

Irregular frequencies in the method of integral equations arise in the solution to the propagating mode potential only, leaving a separate set of evanescent mode potentials free of numerical irregularities. The occurrence and possible removal of irregular frequencies are described, but not developed. Application of the Richardson extrapolation is sometimes beneficial in narrowing the bandwidth of such irregularities.

To circumvent numerical difficulties associated with the irregular frequencies, alternative approaches to calculating the hydrodynamic coefficients at higher frequencies are investigated. Two schemes for estimating damping coefficients are outlined: a short-wave solution to the propagating mode potential and a method based on geometrical optics. The former is found to be particularly suitable for calculation of the damping coefficients. The two methods cannot be used to obtain the added masses. Instead two alternative methods are proposed. One is by discarding the propagating mode and using the evanescent modes alone which are free of irregular frequencies. The other is by a somewhat more elaborate procedure based on an application of the Kramers-Kronig relations valid for the entire frequency range. The one-sided Hilbert transform of the damping coefficient which occurs in one of the Kramers-Kronig relations may be conveniently evaluated by a suitable application of discrete Fourier transforms. This requires the calculation of the damping coefficient at sufficiently small intervals up to a frequency which is about 5 times the maximum frequency of interest to avoid errors due to truncation effects. However, this is not too

restrictive since a solution by the integral equation method is required only at low frequencies, and for most of the frequency range, a simple calculation based on Ursell's short-wave solution suffices.

When the oscillation frequency is sufficiently high, a further modification to the hydrodynamic loading arises from the effects of compressibility of the water, and extensions of the various methods to account for the effects of compressibility may readily be made and are described. At such frequencies gravitational effects are usually relatively unimportant, and may be omitted. When the motion frequency is less than the first cut-off frequency, there are no acoustic propagating modes to cause damping, and the added masses are accurately predicted by using moderate levels of discretization in a numerical method. At higher frequencies, acoustic propagating modes are present, and require a finer discretization for a given level of accuracy. Unlike the two-dimensional straight gravity dam problem, unbounded values for the force at a set of discrete resonant frequencies are not found to occur for an isolated cylinder. Numerical irregularities now occur at a set of discrete frequencies corresponding to the irregular frequencies of each propagating mode. Alternative approaches to circumvent numerical difficulties are based on the use of a short-wave solution for each of the propagating potentials in the calculation of the damping coefficient and the use of evanescent modes alone in added mass calculation. Such an approach provides useful estimates of the damping coefficients except in the vicinity of cut-off frequencies, but estimates of added masses are then accurate only at frequencies sufficiently after the emergence of a progressive wave.

As an example of the application of the various methods to arbitrary sections, a set of new results has been presented for a square cylinder. Possible limitations and guidelines in applying the present solution to engineering situations have been summarized, and a typical ocean engineering application of the solution illustrated.

## 9.2 Recommendations for Further Study

In this thesis, the problem of determining hydrodynamic loads on a large vertical cylinder of arbitrary section, oscillating in water, has been addressed. Only isolated rigid structures have been treated. However, the methods described are amenable to extensions to account for various additional effects.

The elasticity of the structure should be accounted for in many practical engineering applications (Liaw and Chopra, 1974; Tanaka and Hudspeth, 1988). For example, the structure may be treated as a cantilevered tower with an arbitrary cross-section and in response to horizontal base motion may undergo distortions in its various modes of lateral vibration. The frequencies and mode shapes may be taken as those obtained by elementary beam theory for uniform cantilevered beams in air. The added masses and damping coefficients for such elastic modes may then be readily calculated by continuing to apply the methods in this study, but with a modified boundary condition on the horizontal contour of the structure. The corresponding generalized loads may then be substituted into the equation of motion in order to obtain the dynamic response.

In some applications, the hydrodynamic loads on a structure are affected by the proximity of other neighbouring structures which themselves may be either fixed or oscillating. Provided that such structures can be approximated as vertical cylinders of arbitrary section, their interaction can be accounted for simply by extending a boundary condition, similar to the one already used, to the horizontal contours of neighbouring cylinders.

The influence of ice cover on the water surface requires an assessment in the design of structures for the arctic seas. In particular, if ice cover is present when a large earthquake occurs, hydrodynamic forces may be increased significantly because of coupling effects between the ice cover and fluid compressibility (Kiyokawa and Inada, 1989). Ice cover may be accommodated in the theoretical model by applying a homogeneous Neumann condition on the free surface and modifying the eigenfunctions that represent the vertical variation of the potential accordingly.

Another factor which may require attention in some situations is the elasticity of the foundation medium (Bi *et al.*, 1991), since ground compliance provides an additional damping mechanism.

An important extension of the methods of this study is a modification to treat truncated vertical cylinders of arbitrary section either floating or resting on the seabed: configurations which will adequately model barges, submerged oil storage tanks etc. Separate outer and inner fluid domains may then be defined as in Garrett (1971): an inner domain comprising of the fluid region directly above or beneath the cylinder; and an outer infinite domain encompassing the rest of the fluid region. Separate problems may be set up for the velocity potentials in these two regions which should now satisfy, in addition to the usual boundary conditions, two matching conditions at the boundary between inner and outer regions ensuring continuity of the potential as well as its normal derivative. By employing separate sets of eigenfunctions to represent the vertical variation of the inner and outer potentials, and by carrying out suitable vertical integrations of the boundary condition on the vertical sides of the structure and the matching conditions, the problem may be reduced to two sets of horizontal plane problems: one set associated with the inner potential; and another set associated with the outer potential. These two-dimensional problems are coupled due to the matching conditions. Nevertheless, solving the two sets of coupled two-dimensional problems using the methods of this study will be more efficient than adopting a conventional approach based on a three-dimensional formulation.

Finally, the radiation problem of a structure of arbitrary three-dimensional shape which intersects the free surface vertically is related to that of a vertical cylinder of the same cross-section at the waterplane, in so far as the radiated waves in the far field become asymptotically equivalent when the oscillation frequency is increased (Davis, 1976). Since the damping coefficients are associated with energy radiation away from the structure due to the propagating waves, it follows that the high frequency damping coefficients of the three-dimensional problem may be then obtained in principle by solving a simpler horizontal plane problem to which the methods of this study apply.

# Bibliography

Abramowitz, M. and Stegun, I.A., (Eds.), Handbook of Mathematical Functions, Dover Publications, New York, 1972, 1046 pp.

Adachi, H. and Ohmatsu, S., "On the Influence of Irregular Frequencies in the Integral Equation Solutions of the Time-Dependent Free-Surface Problems", Journal of the Society of Naval Architects of Japan, Vol. 145, 1979, pp. 127-136.

Angell, T. S., Hsiao, G. C. and Kleinman, R. E., "An Integral Equation for the Floating Body Problem", Journal of Fluid Mechanics, Vol. 166, 1986, pp. 161-171.

Bai, K.J., "Diffraction of Oblique Waves by an Infinite Cylinder", Journal of Fluid Mechanics, Vol. 68, 1975, pp. 513-535.

Bai, K.J., "Zero-Frequency Hydrodynamic Coefficients of Vertical Axisymmetric Bodies at a Free Surface", Journal of Hydronautics, Vol. 11, 1977, pp. 53-57.

Bateman, H., Partial Differential Equations of Mathematical Physics, Cambridge University Press, 1932, p. 139, 522 pp.

Beck, R.F. and Liapis, S., "Transient Motions of Floating Bodies at Zero Forward Speed", Journal of Ship Research, Vol. 31, No. 3, 1987, pp. 164-176.

Behrendt, L., "A Finite Element Model for Water Wave Diffraction Including Boundary Absorption and Bottom Friction", Series Paper No. 37, Institute of Hydrodynamics and Hydraulic Engineering, Technical University Of Denmark, 1985.

Bender, C.M. and Orszag, S.A., Advanced Mathematical Methods for Scientists and Engineers, McGraw-Hill, New York, 1978, 593 pp.

Bettess, P., "Finite and Infinite Elements for Fluid Loading on Offshore Structures - an Assessment of Accuracy", in Integrity of Offshore Structures - 3, Eds. D. Faulkner, M.J. Cowling and A. Incecik, Elsevier Applied Science, 1988, pp. 95-114.

Bi, J.J., Zhuang, H. and Weng, X.L., "Hydrodynamic Characteristics and Seismic Analysis of Offshore Cylindrical Structure-Fluid-Soil Systems", Proceedings of the First International Offshore and Polar Engineering Conference, ISOPE'91, Edinburgh, Vol. 3, 1991, pp. 264-269.

Black, J.L., "Wave Forces on Vertical Axisymmetric Bodies", Journal of Fluid Mechanics, Vol. 67, 1975, pp. 369-376.

Black, J.L., Mei, C.C. and Bray, M.C.G., "Radiation and Scattering of Water Waves by Rigid Bodies", Journal of Fluid Mechanics, Vol. 46, 1971, pp. 151-164.

Blanch, G., "On the Computation of Mathieu Functions", Journal of Mathematical Physics, Vol. 25, 1946, pp. 1-20.

Bowman, J.J., Senior, T.B.A. and Uslenghi, P.L.E., (Eds.), Electromagnetic and Acoustic Scattering by Simple Shapes, North-Holland Publishing Company, Amsterdam, 1969, 728 pp.

Bracewell, R.N., The Fourier Transform and its Applications, McGraw-Hill, New York, 1986, 474 pp.

Brandt, D. W., Eftimiu, C. and Huddleston, P. L., "Electromagnetic Scattering by Closed Conducting Bodies: The Problem of Internal Resonances", Fourth International Conference on Antennas and Propagation, ICAP 85, Coventry (UK), 1985, pp. 434-437.

Brebbia, C.A. and Dominguez, J., Boundary Elements: an Introductory Course, Computational Mechanics Publications, Southampton, 1989, 292 pp.

Breit, S.R., Newman, J.N. and Sclavounos, P.D., "A New Generation of Panel Programs for Radiation-Diffraction Problems", Proceedings of the Fourth International Conference on Behaviour of Offshore Structures, BOSS'85, Delft, 1985, pp. 531-544.

Burton, A.J. and Miller, G.F., "The Application of Integral Equation Methods to the Numerical Solutions of Some Exterior Boundary Value Problems", Proceedings of the Royal Society of London, Ser. A, Vol. 323, 1971, pp. 201-210.

Calisal, S.M., and Sabuncu, T., "Hydrodynamic Coefficients for Vertical Composite Cylinders", Ocean Engineering, Vol. 11, No. 5, 1984, pp. 529-542.

Chakrabarti, S.K., "Wave Forces on Multiple Vertical Cylinders", Journal of the Waterway, Port, Coastal and Ocean Division, ASCE, Vol. 104, No. WW2, 1978, pp. 147-161.

Chakrabarti, S.K., Hydrodynamics of Offshore Structures, Computational Mechanics Publications and Springer-Verlag, Berlin, 1987, 440 pp.

Chen, H.S. and Mei, C.C., "Scattering and Radiation of Gravity Waves by an Elliptic Cylinder", Report No. 140, Ralph M. Parsons Laboratory, Department of Civil Engineering, M.I.T., 1971, 149 pp.

Chen, H.S. and Mei, C.C., "Wave Forces on a Stationary Platform of Elliptical Shape", Journal of Ship Research, Vol. 17, No. 2, 1973, pp. 61-71.

Chertock, G., "Sound Radiation from Vibrating Surfaces", The Journal of the Acoustical Society of America, Vol. 36, No. 7, 1964, pp. 1305-1313.

Chertock, G., "Solutions for Sound Radiation Problems by Integral Equations at the Critical Wave Numbers", The Journal of the Acoustical Society of America, Vol. 47, 1970, pp. 387-388.

Chopra, A.K. and Chakrabarti, P. , "Dynamics of Gravity Dams - Significance of Compressibility of Water and Three-Dimensional Effects", International Journal of Earthquake Engineering and Structural Dynamics, Vol. 2, 1973, pp. 103-104.

Chung, Y.K., "Theory of Short Wave Excitation", Journal of Ship Research, Vol. 30, No. 3, 1986, pp. 147-152.

Chung, Y.K. and Rhee, K.P., "New Approach to Short Wave Diffraction Problems", Proceedings of the Fifth International Offshore Mechanics and Arctic Engineering Symposium, Tokyo, Vol. 1, 1986, pp. 182-185.

Clemm, D.S., "Characteristic Values and Associated Solutions of Mathieu's Differential Equation", Algorithm 352 [S22], Communications of the ACM, Vol. 12, No. 7, 1969, pp. 399-407.

Colton, D. and Kress, R., Integral Equation Methods in Scattering Theory, John Wiley, New York, 271 pp.

Copley, L.G., "Fundamental Results Concerning Integral Representations in Acoustic Radiation", The Journal of the Acoustical Society of America, Vol. 44, No. 1, 1968, pp. 28-32.

Dahlquist, G. and Bjorck, A., Numerical Methods, Prentice-Hall, New Jersey, 1974, 573 pp.

Davis, A.M.J., "On the Short Surface Waves due to an Oscillating, Partially Immersed Body", Journal of Fluid Mechanics, Vol. 75, Part 4, 1976, pp. 791-807.

Eatock Taylor, R. and Dolla, J.P., "Hydrodynamic Loads on Vertical Bodies of Revolution", Report No. OEG/78/6, Department of Mechanical Engineering, University College, London, 1978.

Fenton, J.D., "Wave Forces on Vertical Bodies of Revolution", Journal of Fluid Mechanics, Vol. 85, 1975, pp. 241-255.

Faltinsen, O.M., Sea Loads on Ships and Offshore Structures, Cambridge University Press, 1990, 328 pp.

Garrett, C.J.R., "Wave Forces on a Circular Dock", Journal of Fluid Mechanics, Vol. 46, 1971, pp. 129-139.

Garrison, C.J. and Berklite, R.B., "Impulsive Hydrodynamics of Submerged Rigid Bodies", Journal of the Engineering Mechanics Division, ASCE, Vol. 99, No. EM1, 1973, pp. 99-120.

Goto, H. and Toki, K., "Vibration Characteristics and a Seismic Design of Submerged Bridge Piers", Proceedings of the Third World Conference on Earthquake Engineering, New Zealand, Vol. 2, 1965, pp. 107-125.

Houston, J.R., "Combined Refraction and Diffraction of Short Waves Using the Finite Element Method", Applied Ocean Research, Vol. 3, 1981, pp. 163-170.

Hulme, A., "The Wave Forces Acting on a Floating Hemisphere Undergoing Forced Periodic Oscillations", Journal of Fluid Mechanics, Vol. 121, 1982, pp. 443-463.

Humar, J.L. and Jablonski, A.M., "Boundary Element Reservoir Model for Seismic Analysis of Gravity Dams", Earthquake Engineering and Structural Dynamics, Vol. 16, 1988, pp. 1129-1156.

Ince, E.L., "Tables of the Elliptic Cylinder Functions", Proceedings of the Royal Society of Edinburgh, Vol. 52, 1932, pp. 355-423.

Ince, E.L., "Zeros and Turning Points", Proceedings of the Royal Society of Edinburgh, Vol. 52, 1932, pp. 424-433.

Isaacson, M., "Vertical Cylinders of Arbitrary Section in Waves" Journal of the Waterway, Port, Coastal and Ocean Division, ASCE, Vol. 104, No. WW4, 1978, pp. 309-324.

Isaacson, M., "Wave Forces on Compound Cylinders", Proceedings of the Conference: Civil Engineering in the Oceans IV, ASCE, San Francisco, Vol. 1, 1979, pp. 518-530.

Isaacson, M., "Fixed and Floating Axisymmetric Structures in Waves", Journal of the Waterway, Port, Coastal and Ocean Division, ASCE, Vol. 108, No. WW2, 1982, pp. 180-199.

Jefferys, E.R., "Numerical Problems of First Order Diffraction Theory", Proceedings of the Second International Workshop on Water Waves and Floating Bodies, Report No. AM-87-06, University of Bristol, 1987.

John, F., "On the Motion of Floating Bodies II", Communications on Pure and Applied Mathematics, Vol. 3, 1950, pp. 45-101.

Jones, D.S., "Integral Equations for the Exterior Acoustic Problem", Quarterly Journal of Mechanics and Applied Mathematics, Vol. 27, 1974, pp. 129-142.

Keller, J.B., Lewis, R.M. and Seckler, B.D., "Asymptotic Solutions of Some Diffraction Problems", Communications on Pure and Applied Mathematics, Vol. 9, 1956, pp. 207-265.

Keller, J.B., "Diffraction by a Convex Cylinder", IRE Transactions on Antennas and Propagation, Vol. AP-4, 1956, pp. 312-321.

Keller, J.B. and Levy, B.R., "Decay Exponents and Diffraction Coefficients for Surface Waves on Surfaces of Nonconstant Curvature", IRE Transactions on Antennas and Propagation, Vol. AP-7, 1959, pp. S52-S61.

Kim, C.H., "Hydrodynamic Forces and Moments for Heaving, Swaying and Rolling Cylinders on Water of Finite Depth", Journal of Ship Research, Vol. 13, 1969, pp. 137-154.

Kim, W.D., "On the Harmonic Oscillations of a Rigid Body on a Free Surface", Journal of Fluid Mechanics, Vol. 21, 1965, pp. 427-451.

Kiyokawa, T. and Inada, H., "Hydrodynamic Forces Acting on Axisymmetric Bodies Immersed in Ice-covered Sea During Earthquakes", Proceedings of the Eighth International Conference on Offshore Mechanics and Arctic Engineering, The Hague, 1989, pp. 153-160.

Kleinman, R.E. and Roach, G.F., "On Modified Green Functions in Exterior Problems for the Helmholtz Equation", Proceedings of the Royal Society of London, Ser. A, Vol. 383, 1982, pp. 313-332.

Kokkinowrachos, K. and Thanos, I., "Structure-Wave Interaction Under Earthquake Excitation", Journal of Offshore Mechanics and Arctic Engineering, Vol. 112, 1990, pp. 65-73.

Korsmeyer, F.T., Lee, C.-H., Newman, J.N. and Sclavounos, P.D., "The Analysis of Wave Effects on Tension Leg Platforms", Seventh International Conference on Offshore Mechanics and Arctic Engineering, Houston, 1988, pp. 1-14.

Kotik, J. and Mangulis, V., "On the Kramers-Kronig Relations for Ship Motions", International Shipbuilding Progress, Vol. 9, No. 97, 1962, pp. 361-368.

Kotsubo, S., "Seismic Force Effect on Submerged Bridge Piers with Elliptic Cross Sections", Proceedings of the Third World Conference on Earthquake Engineering, New Zealand, Vol. 2, 1965, pp. 342-356.

Lax, M. and Feshback, H., "On the Radiation Problem at High Frequencies", The Journal of the Acoustical Society of America, Vol. 19, No. 4, 1947, pp. 682-690.

Le Méhauté, B., "Similitude in Coastal Engineering", Journal of the Waterway, Port, Coastal and Ocean Division, ASCE, Vol. 102, No. WW3, 1976, pp. 317-335.

Lee, C.-H. and Sclavounos, P.D., "Removing the Irregular Frequencies from Integral Equations in Wave-body Interactions", Journal of Fluid Mechanics, Vol. 207, 1989, pp. 393-418.

Levy, B.R. and Keller, J.B., "Diffraction by a Smooth Object", Communications on Pure and Applied Mathematics, Vol. 12, 1959, pp. 159-209.

Liaw, C-Y. and Chopra, A.K., "Dynamics of Towers Surrounded by Water", Earthquake Engineering and Structural Dynamics, Vol. 3, 1974, pp. 33-49.

MacCamy, R.C. and Fuchs, R.A., "Wave Forces on Piles: a Diffraction Theory", U.S. Army Corps of Engineers, Beach Erosion Board, Technical Memorandum Number 69, 1954.

Maeda, H., "Hydrodynamical Forces on a Cross Section of a Stationary Structure", Proceedings of the International Symposium on the Dynamics of Marine Vehicles and Structures in Waves, University College, London, 1974, pp. 80-90.

Martin, P.A., "On the Null-Field Equations for Water-Wave Radiation Problems", Journal of Fluid Mechanics, Vol. 113, 1981, pp. 315-332.

McCormick, M.E., "Hydrodynamic Coefficients of a Monolithic Circular Offshore Structure", Earthquake Engineering and Structural Dynamics, Vol. 18, 1989, pp. 199-216.

Mei, C.C., "Numerical Methods in Water-Wave Diffraction and Radiation", Annual Review of Fluid Mechanics, Vol. 10, 1978, pp. 393-416.

Mei, C.C., "Reciprocity Relations for Offshore Structures Vibrating at Acoustic Frequencies", Proceedings of the Second International Conference on Behaviour of Offshore Structures, BOSS'79, London, 1979, Paper 56, pp. 125-138.

Mei, C.C., Foda, M.A. and Tong, P., "Exact and Hybrid-Element Solutions for the Vibration of a Thin Elastic Structure Seated on the Sea Floor", Applied Ocean Research, Vol. 1, No. 2, 1979, pp. 79-88.

Mei, C.C., The Applied Dynamics of Ocean Surface Waves, John Wiley, NY, 1983, 740 pp.

Meyer, W.L., Bell, W.A., Stallybrass, M.P. and Zinn, B.T., "Prediction of the Sound Field Radiated from Axisymmetric Surfaces", The Journal of the Acoustical Society of America, Vol. 65, 1979, pp. 631-638.

Miao, G.P., Liu, Y.Z. and Mi, Z.X., "The Computation of Hydrodynamic Forces on Vibrating Multiple Large Vertical Cylinders of Arbitrary Section", Proceedings of the First International Workshop on Very Large Floating Structures, VLFS'91, Hawaii, 1991, pp. 355-366.

Morison, J.R., O'Brien, M.P., Johnson, J.W. and Schaaf, S.A., "The Forces Exerted by Surface Waves on Piles", Petroleum Trans., AIME, Vol. 189, pp. 149-157.

Morse, P.M. and Ingard, K.U., Theoretical Acoustics, McGraw-Hill Book Company, New York, 1968, 927 pp.

Murphy, J.E., "Integral Equation Failure in Wave Calculations", Journal of the Waterway, Port, Coastal and Ocean Division, ASCE, Vol. 104, 1978, pp. 330-334.

Naftzger, R.A. and Chakrabarti, S.K., "Scattering of Waves by Two-Dimensional Circular Obstacles in Finite Water Depths", Journal of Ship Research, Vol. 23, 1979, pp. 32-42.

Newman, J.N., Marine Hydrodynamics, The MIT Press, Cambridge, Massachusetts, 1977, 402 pp.

Ogilvie, T.F. and Shin, Y.S.,"Integral Equation Solutions for Time-Dependent Free Surface Problems", Journal of the Society of Naval Architects of Japan, Vol. 143, 1978, pp. 41-51.

Panich, O.I., "The Problem of Solvability of Exterior Boundary Value Problems for the Wave Equation and for Systems of Maxwell's Equations", Russian Mathematical Surveys, Vol. 20, No. 1, 1965, pp. 221-226.

Pegg, N.G., An Experimental Study of the Seismic Forces on Submerged Structures, M.A.Sc. Thesis, Department of Civil Engineering, University of British Columbia, Vancouver, Canada, 1983, 102 pp.

Sabuncu, T. and Calisal, S.M., "Hydrodynamic Coefficients for Vertical Circular Cylinders at Finite Depth", Ocean Engineering, Vol. 8, No. 1, 1981, pp. 25-63.

Sale, A.H.J., "Remark on Algorithm 352 [S22]", Communications of the ACM, Vol. 13, No. 12, 1970, pp. 750.

Sarpkaya, T. and Isaacson, M., Mechanics of Wave Forces on Offshore Structures, Van Nostrand Reinhold, New York, NY, 1981, 651 pp.

Sayer, P. and Ursell, F., "Integral Equation Methods for Calculating Virtual Mass in Water of Finite Depth", Proceedings of the Second International Conference on Numerical Ship Hydrodynamics, Berkeley, 1977, pp. 176-184.

Schenck, H.A., "Improved Integral Formulation for Acoustic Radiation Problems", The Journal of the Acoustical Society of America, Vol. 44, 1968, pp. 41-58.

Shanks D., "Non-linear Transformations of Divergent and Slowly Convergent Sequences", Journal of Mathematics and Physics, Vol. 34, 1955, pp. 1-42.

Spring, B.H. and Monkmeyer, P.L., "Interaction of Plane Waves with Vertical Cylinders", Proceedings of the Fourteenth Coastal Engineering Conference, Copenhagen, Vol. 3, 1974, pp. 1828-1847.

Spring, B.H. and Monkmeyer, P.L., "Interaction of Plane Waves with a Row of Cylinders", Proceedings of the Conference: Civil Engineering in the Oceans III, ASCE, University of Delaware, Vol 3, 1975, pp. 979-998.

Stiassnie, M. and Dagan, G., "Wave Forces on a Submerged Vertical Plate", Journal of Engineering Mathematics, Vol. 7, No. 3, 1973, pp. 235-247.

Sun, K. and Nogami, T., "Earthquake Induced Hydrodynamic Pressure on Axisymmetric Offshore Structures", Earthquake Engineering and Structural Dynamics, Vol. 20, 1991, pp. 429-440.

Tanaka, Y. and Hudspeth, R.T., "Restoring Forces on Vertical Circular Cylinders Forced by Earthquakes", Earthquake Engineering and Structural Dynamics, Vol.16, 1988, pp. 99-119.

Tung, C.C., "Hydrodynamic Forces on Submerged Vertical Cylindrical Tanks Under Ground Excitation", Applied Ocean Research, Vol. 1, No. 2, 1979, pp. 75-78.

Turing, A.M., "Rounding-off Errors in Matrix Processes", Quarterly Journal of Mechanics and Applied Mathematics, Vol. 1, 1948, pp. 287-308.

Ursell, F., "Short Surface Waves due to an Oscillating Immersed Body", Proceedings of the Royal Society of London, Ser. A, Vol. 220, 1953, pp. 90-103.

Ursell, F., "On the Short-Wave Asymptotic Theory of the Wave Equation $(\nabla^2 + k^2) \phi = 0$", Proceedings of the Cambridge Philosophical Society, Vol. 53, 1957, pp. 115-133.

Ursell, F., "On the Exterior Problems of Acoustics II", Mathematics Proceedings of the Cambridge Philosophical Society, Vol. 84, 1978, pp. 545-548.

Ursell, F., "Irregular Frequencies and the Motion of Floating Bodies", Journal of Fluid Mechanics, Vol. 105, 1981, pp. 143-156.

Ursell, F., "Integrals with a Large Parameter: Hilbert Transforms", Mathematics Proceedings of the Cambridge Philosophical Society, Vol. 93, 1983, pp. 141-149.

Vugts, J.H., "The Hydrodynamic Coefficients for Swaying, Heaving and Rolling Cylinders in a Free Surface", International Shipbuilding Progress, Vol. 15, No. 97, 1968, pp. 251-276.

Werner, P.W. and Sundquist, K.J., "On Hydrodynamic Earthquake Effects", Transactions, American Geophysical Union, Vol. 30, No. 5, 1949, pp. 636-657.

Williams, A.N., "Wave Forces on an Elliptic Cylinder", Journal of Waterway, Port, Coastal and Ocean Engineering, ASCE, Vol. 111, No. 2, 1985a, pp. 433-449.

Williams, A.N., "Wave Diffraction by Elliptical Breakwaters in Shallow Water", Ocean Engineering, Vol. 12, No. 1, 1985b, pp. 25-43.

Williams, A.N. and Darwiche, M.K., "Three-dimensional Wave Scattering by Elliptical Breakwaters", Ocean Engineering, Vol. 15, No. 2, 1988, pp. 103-118.

Williams, A.N. and Darwiche, M.K., "Wave Radiation by Truncated Elliptical Cylinder", Journal of Waterway, Port, Coastal and Ocean Engineering, ASCE, Vol. 116, No. 1, 1990, pp. 101-119.

Williams, A.N. and Moubayed, W.I., "Earthquake-induced Hydrodynamic Pressures on Submerged Cylindrical Storage Tanks", Ocean Engineering, Vol. 17, No. 3, 1990, pp. 181-199.

Wong, R., "Asymptotic Expansion of the Hilbert Transform", SIAM Journal of Mathematical Analysis, Vol. 11, No. 1, 1980, pp. 92-99.

Wu, X.J. and Price, W.G., "An Equivalent Box Approximation to Predict Irregular Frequencies in Arbitrarily-Shaped Three-Dimensional Marine Structures", Applied Ocean Research, Vol. 8, 1986, pp. 223-231.

Wu, X.J. and Price, W.G., "A Multiple Green's Function Expression for the Hydrodynamic Analysis of Multi-Hull Structures", Applied Ocean Research, Vol. 9, No. 2, 1987, pp. 58-66.

Yeung, R.W., "Added Mass and Damping of a Vertical Cylinder in Finite-Depth Waters", Applied Ocean Research, Vol. 3, No. 3, 1981, pp. 119-133.

Yeung, R.W., "Numerical Methods in Free Surface Flows", Annual Review of Fluid Mechanics, Vol. 14, 1982, pp. 395-442.

Yu, Y.S. and Ursell, F., "Surface Waves Generated by an Oscillating Circular Cylinder on Water of Finite Depth: Theory and Experiment", Journal of Fluid Mechanics, Vol. 11, 1961, pp. 529-551.

Zienkiewicz, O.C., Bettess, P. and Kelly, D.W., "The Finite Element Method for Determining Fluid Loadings on Rigid Structures. Two- and Three- Dimensional Formulations", in Numerical Methods in Offshore Engineering, Eds. O.C. Zienkiewicz, R.W. Lewis and K.G. Stagg, John Wiley, 1978, pp. 141-183.

# Appendix A

## WATER WAVE SCATTERING BY VERTICAL CYLINDERS

## A.1 Theoretical Formulation

The problem of plane wave scattering by a vertical cylinder of arbitrary section (see Fig. 1) is much simpler to treat than the general three-dimensional problem, since the problem is readily reduced to one in the horizontal plane by means of a known variation of the solution in the vertical direction (Isaacson, 1978). The velocity potential $\Phi$ is first represented as the sum of incident wave and scattered wave potentials as follows:

$$\Phi = \Phi_i + \Phi_s \tag{A.1}$$

where the incident potential $\Phi_i$ is known and corresponds to a regular two-dimensional wave train:

$$\Phi_i(x,y,z,t) = -\frac{igH}{2\omega}\frac{\cosh(k_0z)}{\cosh(k_0d)}\exp(ik_0x)\exp(-i\omega t) \tag{A.2}$$

The boundary value problem is then set up for the scattered potential $\Phi_s$. In order to satisfy the seabed and free surface boundary conditions, the scattered potential has a hyperbolic cosine variation with depth:

$$\Phi_s(x,y,z,t) = -\frac{igH}{2\omega}\frac{\cosh(k_0z)}{\cosh(k_0d)}\phi_s(x,y)\exp(-i\omega t) \tag{A.3}$$

where $\phi_s(x,y)$ is a spatial potential independent of the z coordinate. Then a solution to $\phi_s$ is desired subject to:

$$\frac{\partial^2\phi_s}{\partial x^2} + \frac{\partial^2\phi_s}{\partial y^2} + k_0^2\phi_s = 0 \qquad \text{within the fluid region} \tag{A.4}$$

$$\frac{\partial\phi_s}{\partial n} = -\frac{\partial\phi_i}{\partial n} \qquad \text{on } C_b \tag{A.5}$$

$$\underset{r\to\infty}{\text{Limit}}\ \sqrt{r}\ (\frac{\partial\phi_s}{\partial r} - ik_0\phi_s) = 0 \tag{A.6}$$

Here, n denotes distance normal to $C_b$ and directed into the fluid, and r is radial distance.

111

# A.2 Analytical Solutions

## A.2.1 Circular Cylinder

An analytical solution to the scattering problem posed by (A.4) - (A.6) is available when $C_b$ is a circle, and may be used to obtain wave-induced loads and moments (MacCamy and Fuchs, 1954). In this section, the classical MacCamy and Fuchs' solution is indicated together with its high frequency asymptotic form. If a denotes the cylinder radius, the analytical form of the spatial potential $\phi_S$ is then given as:

$$\phi_S = -\sum_{m=0}^{\infty} \beta_m \frac{J'_m(k_0 a)}{H_m^{(1)'}(k_0 a)} H_m^{(1)}(k_0 r) \cos(m\theta) \tag{A.7}$$

where:

$$\beta_m = \begin{cases} 1 & \text{for } m = 0 \\ 2 i^m & \text{for } m \geq 1 \end{cases} \tag{A.8}$$

The amplitudes of the force component in the x direction and the moment component about the y axis are simply:

$$|F_1| = 2 \frac{A(k_0 a)}{k_0 a} \rho g H a d \tanh(k_0 d)/k_0 d \tag{A.9}$$

$$|F_5| = 2 \frac{A(k_0 a)}{k_0 a} \frac{\rho g H a d^2 [k_0 d \sinh(k_0 d) - \cosh(k_0 d) + 1]}{(k_0 d)^2 \cosh(k_0 d)} \tag{A.10}$$

where:

$$A(k_0 a) = [J_1'^2(k_0 a) + Y_1'^2(k_0 a)]^{-1/2} \tag{A.11}$$

High frequency approximations to (A.9) and (A.10) are obtained by replacing $A(k_0 a)$ by the corresponding asymptotic form for large $k_0 a$ (section 9.2.30 of Abramowitz and Stegun, 1972), and ignoring all but the leading term:

$$|F_1| = \sqrt{\frac{2\pi}{k_0 a}} \rho g H a d \tanh(k_0 d)/k_0 d \tag{A.12}$$

$$|F_5| = \sqrt{\frac{2\pi}{k_0 a}} \frac{\rho g H a d^2 [k_0 d \sinh(k_0 d) - \cosh(k_0 d) + 1]}{(k_0 d)^2 \cosh(k_0 d)} \tag{A.13}$$

## A.2.2 Elliptic Cylinder

The form of the analytical solution for an elliptic cylinder, i.e. when $C_b$ is an ellipse, is given by Chen and Mei (1971), and is summarized here. Elliptic coordinates $(\xi, \eta)$ are first introduced as follows:

$$x = h\cosh\xi\cos\eta; \qquad y = h\sinh\xi\sin\eta \qquad (A.14)$$

where the semi-focal distance of the ellipse $h = \sqrt{a^2 - b^2}$, and a and b are respectively the semi-major and semi-minor axes of the ellipse. The generalized forces $F_1$, $F_2$, $F_3$ which denote the force components in the x, y, z directions respectively, and $F_4$, $F_5$, $F_6$ which denote the moment components about the x, y, z axes respectively are obtained as follows:

$$F_1 = \rho g H a d \left[ \frac{\tanh(k_0 d)}{k_0 d} \right] C_x \exp(-i\omega t) \qquad (A.15)$$

$$F_2 = \rho g H a d \left[ \frac{\tanh(k_0 d)}{k_0 d} \right] C_y \exp(-i\omega t) \qquad (A.16)$$

$$F_4 = -\rho g H a d^2 \left[ \frac{k_0 d \sinh(k_0 d) - \cosh(k_0 d) + 1}{(k_0 d)^2 \cosh(k_0 d)} \right] C_y \exp(-i\omega t) \qquad (A.17)$$

$$F_5 = \rho g H a d^2 \left[ \frac{k_0 d \sinh(k_0 d) - \cosh(k_0 d) + 1}{(k_0 d)^2 \cosh(k_0 d)} \right] C_x \exp(-i\omega t) \qquad (A.18)$$

$$F_6 = \rho g H a^2 d \left[ \frac{\tanh(k_0 d)}{k_0 d} \right] C_{xy} \exp(-i\omega t) \qquad (A.19)$$

where:

$$C_x = 2\frac{b}{a} \sum_{n=0}^{\infty} \left[ (-1)^n \frac{A_1^{(2n+1)}(q_0)}{Mc_{2n+1}^{(3)'}(\xi_0, q_0)} ce_{2n+1}(\alpha, q_0) \right] \qquad (A.20)$$

$$C_y = 2 \sum_{n=0}^{\infty} \left[ (-1)^n \frac{B_1^{(2n+1)}(q_0)}{Ms_{2n+1}^{(3)'}(\xi_0, q_0)} se_{2n+1}(\alpha, q_0) \right] \qquad (A.21)$$

$$C_{xy} = \frac{i}{\cosh^2(\xi_0)} \sum_{n=0}^{\infty} \left[ (-1)^n \frac{B_2^{(2n+2)}(q_0)}{Ms_{2n+2}^{(3)'}(\xi_0, q_0)} se_{2n+2}(\alpha, q_0) \right] \qquad (A.22)$$

$ce_r(\eta, q_0)$ and $se_r(\eta, q_0)$ are the even and odd periodic Mathieu functions based on the notations of Ince (1932): the order r is of the form $2n+p$, where n is an integer and p is a parameter equal to 0 or 1 indicating that the period of the Mathieu function is $\pi$ or $2\pi$ respectively. $Mc_r^{(i)}(\xi, q_0)$ and $Ms_r^{(i)}(\xi, q_0)$ are the corresponding radial Mathieu functions of the i-th kind based on Blanch's

(1962) notations. The coordinate $\xi = \xi_0$ conforms to the horizontal contour of the cylinder, $\alpha$ is the angle the incident wave direction makes with the x axis, and $q_0$ is a parameter defined as:

$$q_0 = \frac{k_0^2 h^2}{4}$$ 
(A.23)

$A_{2l+p}^{(2n+p)}$ and $B_{2l+p}^{(2n+p)}$ are Fourier coefficients obtained from:

$$ce_{2n+p}(\eta,q_0) = \sum_{l=0}^{\infty} A_{2l+p}^{(2n+p)}(q_0) \cos [\ (2l+p)\eta\ ]$$ 
(A.24)

$$se_{2n+p}(\eta,q_0) = \sum_{l=0}^{\infty} B_{2l+p}^{(2n+p)}(q_0) \sin [\ (2l+p)\eta\ ]$$ 
(A.25)

with:

$$\int_0^{2\pi} [ce_r(\eta,q_0)]^2\, d\eta = \int_0^{2\pi} [se_r(\eta,q_0)]^2\, d\eta = \pi$$ 
(A.26)

and $A_0$, $A_1$, $B_2$ and $B_1$ positive.

# A.3 Numerical Solution

Wave exciting forces on a vertical cylinder of general cross-section have been obtained by Isaacson (1978) using the method of integral equations. In the solution, the scattered potential is expressed as:

$$\phi_s(x) = \int_{C_b} f(\xi)\ G(x,\xi)\ dC$$ 
(A.27)

where x represents a general point in the fluid and $\xi$ represents a point on the contour of integration. The Green's function G is simply:

$$G = \frac{i}{2} H_0^{(1)}(k_0 R)$$ 
(A.28)

where $R = |\ x - \xi\ |$. Application of the body surface boundary condition (A.5), then yields a Fredholm integral equation of the second kind for the unknown source strength distribution function f. This is solved on a computer after discretizing the cross-sectional contour $C_b$ into a finite number of segments and assuming that f is constant over each segment. For the case of a vertical circular cylinder, using 16 segments to discretize $C_b$, the maximum departure from the analytical solution is only about 0.6% for the exciting force over the range $0 < k_0 a \le 2$.

114

# Appendix B

# DETERMINATION OF MATRIX ELEMENTS

In the solution of horizontal plane water wave problems, only a single line integral equation corresponding to m = 0 require to be solved in the scattering case whereas a set of line integral equations corresponding to m = 0, 1, 2 ... need to be solved in the radiation case. Frequently, the Green's function chosen is:

$$G_m(x,\xi) = \begin{cases} \dfrac{i}{2} H_0^{(1)}(k_0 R) & m = 0 \\[2mm] \dfrac{1}{\pi} K_0(k_m R) & m \geq 1 \end{cases} \tag{B.1}$$

where $R = | x - \xi |$.

In a numerical scheme, the cylinder section is divided into a number of small segments each of length $\Delta C_j$ in which j ranges from 1 to N. If $x_i$ and $\xi_j$ are the values of x and $\xi$ at the centres of the i-th and j-th segments respectively, then the following terms are required:

$$B_{ij}^m = \int_{\Delta C_j} \frac{\partial G_m}{\partial n}(x_i,\xi) \, dC \tag{B.2}$$

$$A_{ij}^m = \int_{\Delta C_j} G_m(x_i,\xi) \, dC \tag{B.3}$$

When $i \neq j$, the integrands in (B.2) and (B.3) are taken as constant over $\Delta C_j$ and thus:

$$B_{ij}^m = \Delta C_j \frac{\partial G_m}{\partial n}(x_i,\xi_j)$$

$$= \Delta C_j \frac{\partial G_m}{\partial R}(x_i,\xi_j) \cos \gamma \tag{B.4}$$

$$A_{ij}^m = \Delta C_j \, G_m(x_i,\xi_j) \tag{B.5}$$

where $\Delta C_j$ is the length of the j-th segment and $\gamma$ is the angle between the outward normal vector at the point $x_i$ and a straight line from $\xi_j$ through $x_i$. Hence for $i \neq j$:

$$
B_{ij}^m = \begin{cases} \dfrac{-ik_o}{2} H_1^{(1)}(k_oR_{ij}) \cos \gamma \, \Delta C_j & m = 0 \\[2em] \dfrac{-k_m}{\pi} K_1(k_mR_{ij}) \cos \gamma \, \Delta C_j & m \geq 1 \end{cases}
\qquad\qquad (B.6)
$$

$$
A_{ij}^m = \begin{cases} \dfrac{i}{2} H_0^{(1)}(k_oR_{ij}) \, \Delta C_j & m = 0 \\[2em] \dfrac{1}{\pi} K_0(k_mR_{ij}) \, \Delta C_j & m \geq 1 \end{cases}
\qquad\qquad (B.7)
$$

where $R_{ij} = |\, x_i - \xi_j \,|$.

When $i = j$, the integrals in (B.4) and (B.5) require an analytical evaluation. In order to carry this out, consider local coordinates $(C, n)$, with origin at the centre of the i-th segment, $C$ measured along the segment and $n$ perpendicular to the segment, as shown in Fig. B.1. Consider a field point $x$ on the $n$ axis at $n = \delta$.
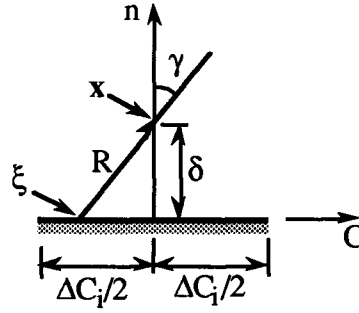


Fig. B.1. Local coordinates.

Using this notation, the matrix element $B_{ii}^m$ may be written as:

$$
B_{ii}^m = \lim_{\delta \to o} \int_{-\Delta C_i/2}^{\Delta C_i/2} \frac{\partial G_m}{\partial n}(x,\xi) \, dC
\qquad\qquad (B.8)
$$

Writing $\partial G_m/\partial n$ as $(\partial G_m/\partial R) \cos\gamma$, and using a small argument approximation for the Bessel function in $G_m$ (Abramowitz and Stegun, 1972), this gives:

$$
B_{ii}^m = \lim_{\delta \to o} -\frac{1}{\pi} \int_{-\Delta C_i/2}^{\Delta C_i/2} \frac{\delta}{R^2} \, dC
\qquad\qquad (B.9)
$$

116

Writing $R^2 = C^2 + \delta^2$ in (B.9) and performing the integration, we eventually obtain:

$$B_{ii}^m = \underset{\delta \to o}{Limit} -\frac{1}{\pi}(2\theta) \tag{B.10}$$

where $\theta$ is $\tan^{-1}(\Delta C_i/2\delta)$. Thus $\theta \to \pi/2$ as $\delta \to 0$, so that:

$$B_{ii}^m = -1 \tag{B.11}$$

A corresponding expression for $A_{ii}^m$ may be obtained in a similar way. Thus:

$$A_{ii}^m = \underset{\delta \to o}{Limit} \int_{-\Delta C_i/2}^{\Delta C_i/2} G_m(x,\xi)\, dC \tag{B.12}$$

Again, a small argument approximation of the Bessel function (Abramowitz and Stegun, 1972) may be used. Writing $R^2 = C^2 + \delta^2$ and carrying out the integration:

$$A_{ii}^m = \frac{\Delta C_i}{\pi}\left[1 - \ln\left(\frac{k_m \Delta C_i}{2}\right)\right] \tag{B.13}$$

117

| r | 0 | 1 | 2 | 3 | 4 | 5 |
|---|---|---|---|---|---|---|
| | 2.40 | 3.83 | 5.14 | 6.38 | 7.59 | 8.77 |
| | 5.52 | 7.02 | 8.42 | 9.76 | 11.1 | 12.3 |
| $k_0a$ | 8.65 | 10.2 | 11.6 | 13.0 | 14.4 | 15.7 |
| | 11.8 | 13.3 | 14.8 | 16.2 | 17.6 | 19.0 |
| | 14.9 | 16.5 | 18.0 | 19.4 | 20.8 | 22.2 |

Table I. The first few zeros of $J_r(k_0a)$.

| $k_1'a$ | $\omega/\omega_1$ | $k_2'a$ | $\omega/\omega_1$ |
|---|---|---|---|
| 3.83 | 1.58 | 3.83 | 3.24 |
| 7.02 | 2.45 | 7.02 | 3.74 |
| 10.2 | 3.39 | 10.2 | 4.41 |
| 13.3 | 4.36 | 13.3 | 5.19 |

Table II. Irregular frequencies of a vertical circular cylinder with a/d = 2 when fluid compressibility is included and gravitational effects excluded.

| $k_0a$ | Numerical Result Using Various N | | | Closed-form | Shanks Transformation | | Richardson Extrapolation | |
|---|---|---|---|---|---|---|---|---|
| | 32 | 64 | 128 | Result | Result | % error | Result | % error |
| 0.2 | 0.64653 | 0.64543 | 0.64447 | 0.64326 | 0.63823 | -0.78170 | 0.64323 | -0.00400 |
| 0.5 | 1.58466 | 1.58092 | 1.57829 | 1.57522 | 1.57207 | -0.20030 | 1.57516 | -0.00410 |
| 1.0 | 2.15672 | 2.15567 | 2.15510 | 2.15453 | 2.15442 | -0.00490 | 2.15450 | -0.00130 |
| 2.0 | 1.76508 | 1.76329 | 1.76252 | 1.76191 | 1.76197 | 0.00290 | 1.76185 | -0.00340 |
| 5.0 | 1.11318 | 1.11668 | 1.11954 | 1.12302 | 1.13241 | 0.83650 | 1.12314 | 0.01120 |
| 10.0 | 2.03002 | 1.42061 | 1.04077 | 0.79313 | 0.41229 | -48.0169 | 0.61084 | -22.9834 |
| 12.0 | 0.74253 | 0.73569 | 0.72967 | 0.72390 | 0.68596 | -5.24060 | 0.72193 | -0.27210 |
| 15.0 | 0.65071 | 0.65217 | 0.65009 | 0.64738 | 0.65131 | 0.60650 | 0.64613 | -0.19310 |

(a)      Exciting force

| $k_0a$ | Numerical Result Using Various N | | | Closed-form | Shanks Transformation | | Richardson Extrapolation | |
|---|---|---|---|---|---|---|---|---|
| | 32 | 64 | 128 | Result | Result | % error | Result | % error |
| 0.2 | 3.40875 | 3.38352 | 3.36899 | 3.35353 | 3.34924 | -0.12780 | 3.35318 | -0.01060 |
| 0.5 | 3.57584 | 3.52468 | 3.49828 | 3.47165 | 3.47012 | -0.04420 | 3.47132 | -0.00940 |
| 1.0 | 2.01340 | 1.97207 | 1.95303 | 1.93511 | 1.93676 | 0.08540 | 1.93507 | -0.00190 |
| 2.0 | 0.53062 | 0.54328 | 0.55023 | 0.55736 | 0.55868 | 0.23580 | 0.55759 | 0.04000 |
| 5.0 | 0.73104 | 0.72861 | 0.72792 | 0.72720 | 0.72765 | 0.06110 | 0.72758 | 0.05210 |
| 10.0 | 0.83036 | 0.89098 | 0.93235 | 0.97779 | 1.02132 | 4.45200 | 0.98110 | 0.33890 |
| 12.0 | 1.00098 | 1.01055 | 1.01580 | 1.02086 | 1.02218 | 0.12930 | 1.02136 | 0.04900 |
| 15.0 | 1.04931 | 1.05597 | 1.05990 | 1.06441 | 1.06556 | 0.10780 | 1.06423 | -0.01680 |
| $\infty$ | 1.20690 | 1.21556 | 1.21885 | 1.22205 | 1.22088 | -0.09570 | 1.22146 | -0.04820 |

(b)      Added mass

Table III.  Estimates of surge hydrodynamic coefficients of a vertical circular cylinder.

| $k_0 a$ | Numerical Result Using Various N | | | Closed-form | Shanks Transformation | | Richardson Extrapolation | |
|---|---|---|---|---|---|---|---|---|
| | 32 | 64 | 128 | Result | Result | % error | Result | % error |
| 0.2 | -0.11343 | 0.04953 | 0.12893 | 0.20688 | 0.20437 | -1.21380 | 0.20694 | 0.02710 |
| 0.5 | 0.95620 | 1.10235 | 1.17183 | 1.23902 | 1.23479 | -0.34120 | 1.23891 | -0.00880 |
| 1.0 | 2.10191 | 2.19288 | 2.23645 | 2.27873 | 2.27650 | -0.09770 | 2.27874 | 0.00050 |
| 2.0 | 1.19929 | 1.25258 | 1.27892 | 1.30505 | 1.30465 | -0.03030 | 1.30505 | 0.00010 |
| 5.0 | 0.18809 | 0.22020 | 0.23614 | 0.25198 | 0.25183 | -0.05800 | 0.25199 | 0.00440 |
| 10.0 | 0.06934 | 0.06869 | 0.06565 | 0.06291 | 0.06951 | 10.5026 | 0.06079 | -3.35600 |
| 12.0 | 0.01940 | 0.03180 | 0.03778 | 0.04367 | 0.04334 | -0.76440 | 0.04361 | -0.14720 |
| 15.0 | 0.00778 | 0.01804 | 0.02302 | 0.02794 | 0.02773 | -0.74300 | 0.02791 | -0.10600 |

(c)    Damping coefficient

Table III. Estimates of surge hydrodynamic coefficients of a vertical circular cylinder.

|  | frequency (Hz) | | | | | |
| --- | --- | --- | --- | --- | --- | --- |
|  | 0.02 | 0.1 | 1 | 5 | 10 | 20 |
| $k_0 a$ | 1.0 | 5.75 | 447 | 11,171 | ... | ... |
| $\omega/\omega_1$ | ... | ... | ... | ... | 0.553 | 1.11 |
| $\mu_{22}/\rho a^3$ | $1.88\times10^{-1}$ | $8.55\times10^{-3}$ | $2.67\times10^{-2}$ | $2.67\times10^{-2}$ | $3.25\times10^{-2}$ | $1.92\times10^{-2}$ |
| $\lambda_{22}/\rho a^3 \omega$ | $7.77\times10^{-2}$ | $5.43\times10^{-2}$ | $1.77\times10^{-5}$ | 0 | 0 | $6.54\times10^{-2}$ |
| $\mu_{22}$ ($10^6$ kg) | 257 | 11.7 | 36.5 | 36.5 | 44.4 | 26.3 |
| $\lambda_{22}$ ($10^6$ kg/sec) | 13.4 | 46.7 | 0.152 | 0 | 0 | 11200 |

Table IV. Added mass and damping coefficient in example application.
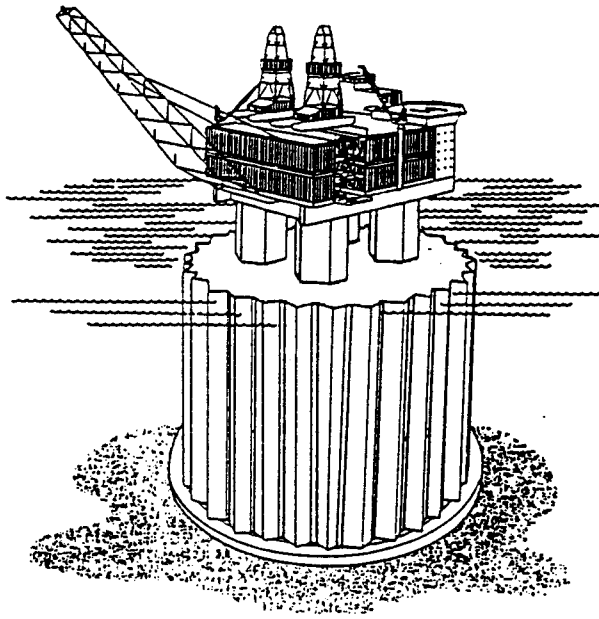
(a)
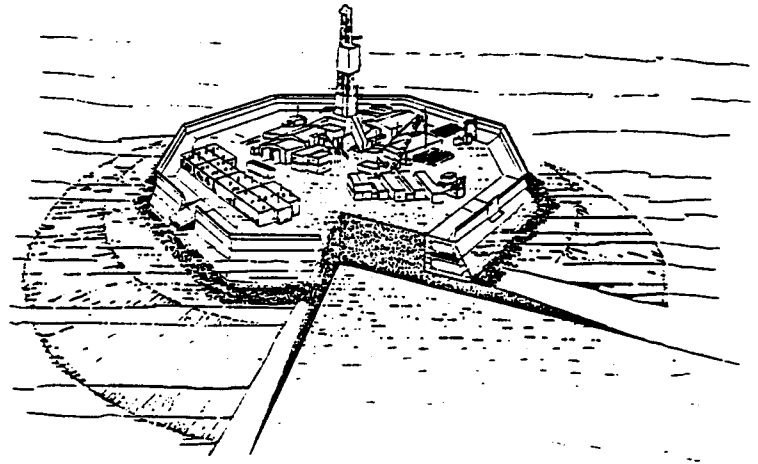
(b)
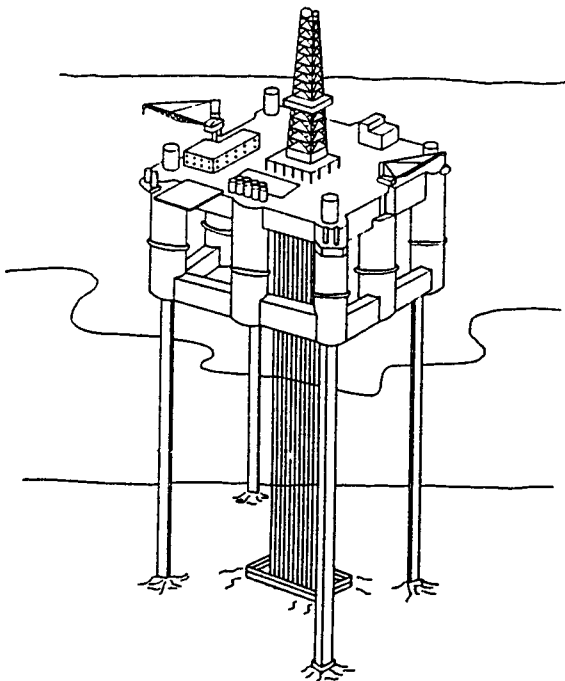
(c)
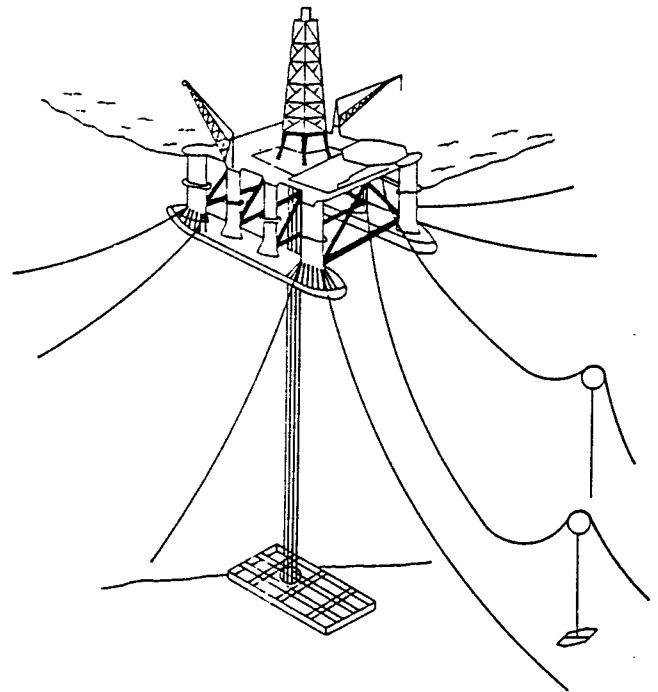
(d)

Figure 1.    Selected offshore structures. (a) gravity platform, (b) artificial island, (c) tension leg platform, (d) semi-submersible rig.
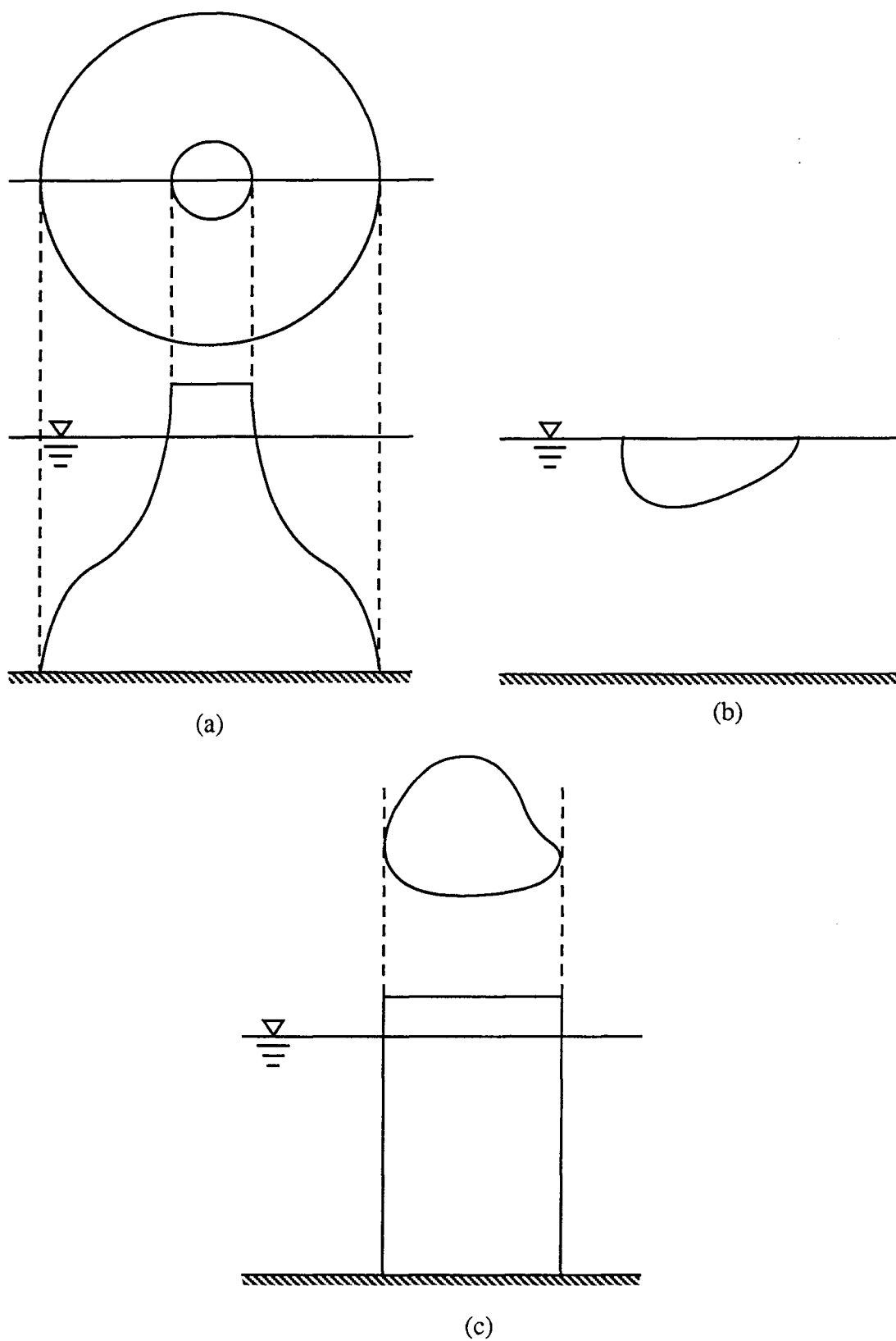
Figure 2.    Restricted configurations for which simplified numerical treatments are possible. (a) vertical axisymmetric bodies, (b) horizontal cylinders of arbitrary section, (c) vertical cylinders of arbitrary section.

123
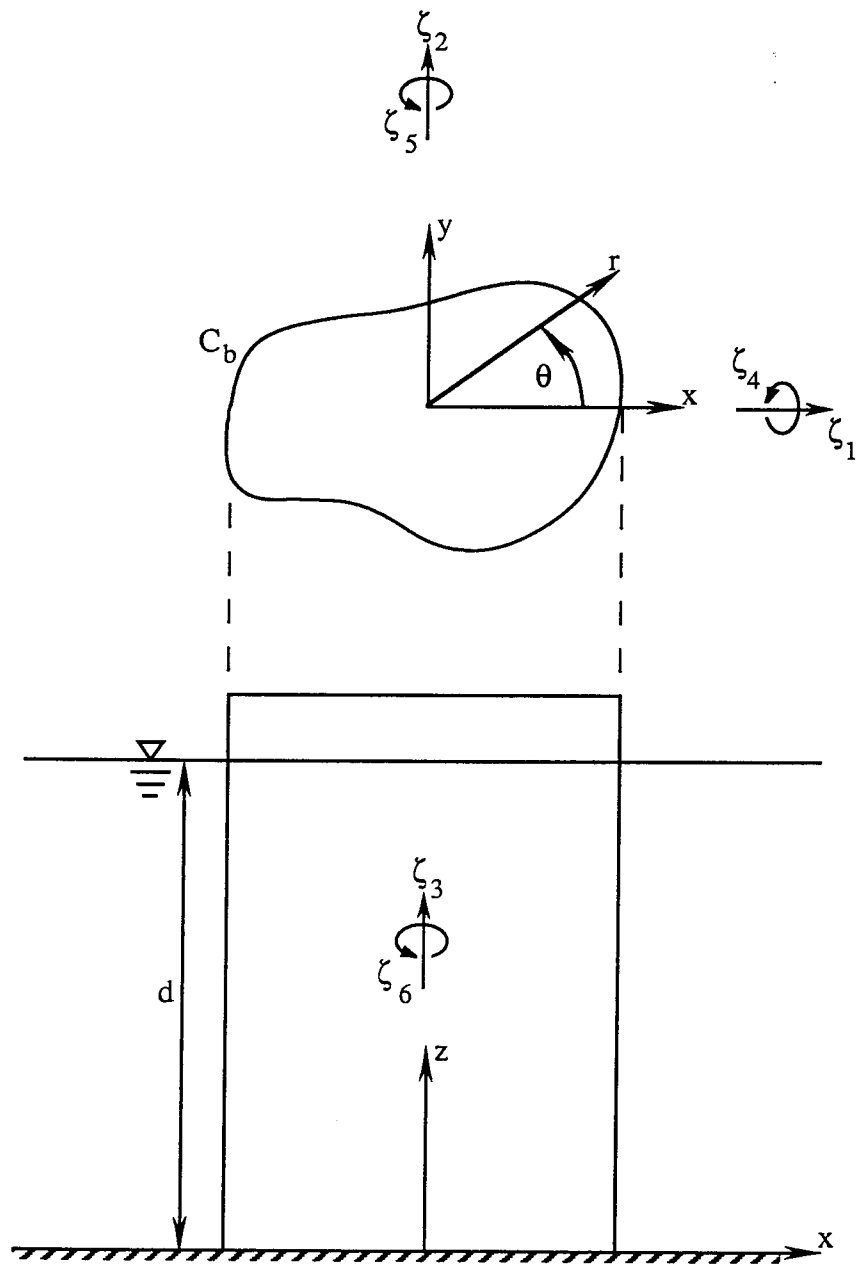
Figure 3.   Definition sketch.
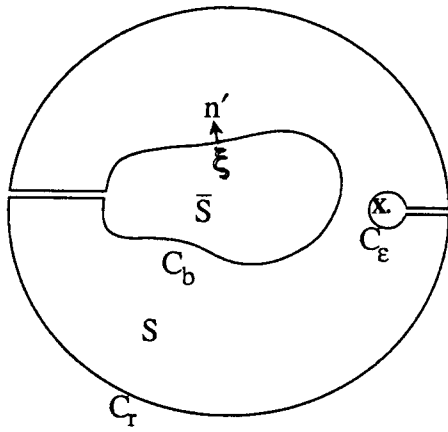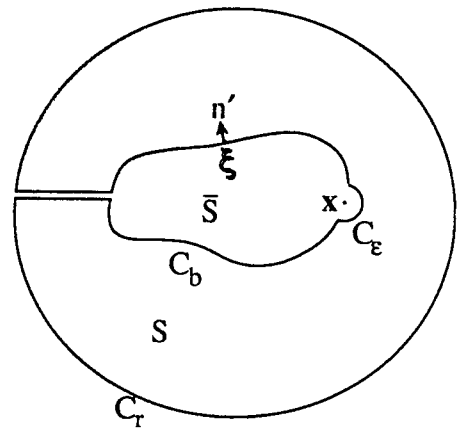
Figure 4. Contour of integration for Green's second identity. (a) field point outside the body surface contour, (b) field point on the body surface contour.
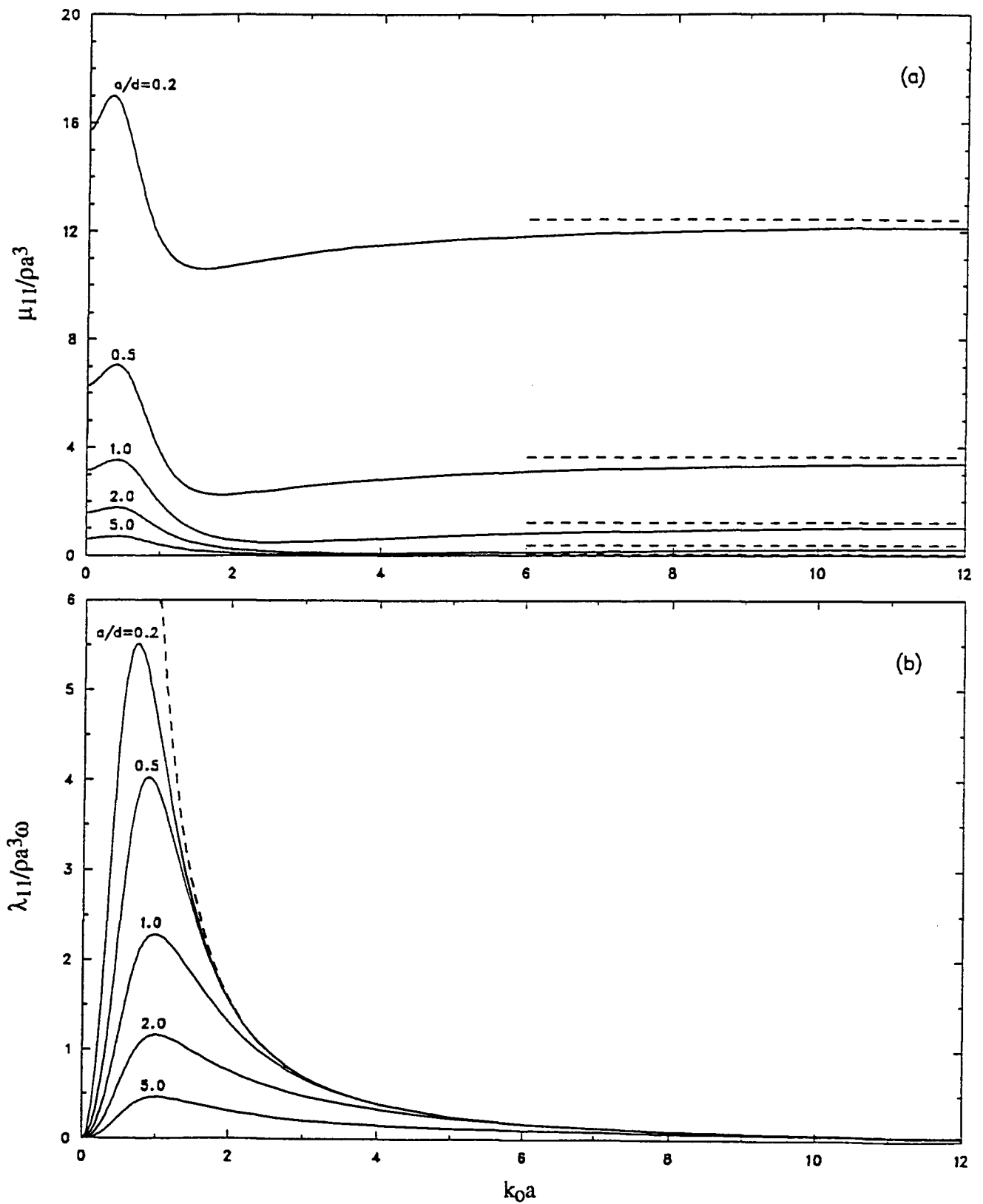
Figure 5. Analytical results for surge hydrodynamic coefficients of a circular cylinder as a function of $k_0a$ for various values of $a/d$. (a) added mass, (b) damping coefficient. ————, complete solution; — — — —, high frequency approximation.
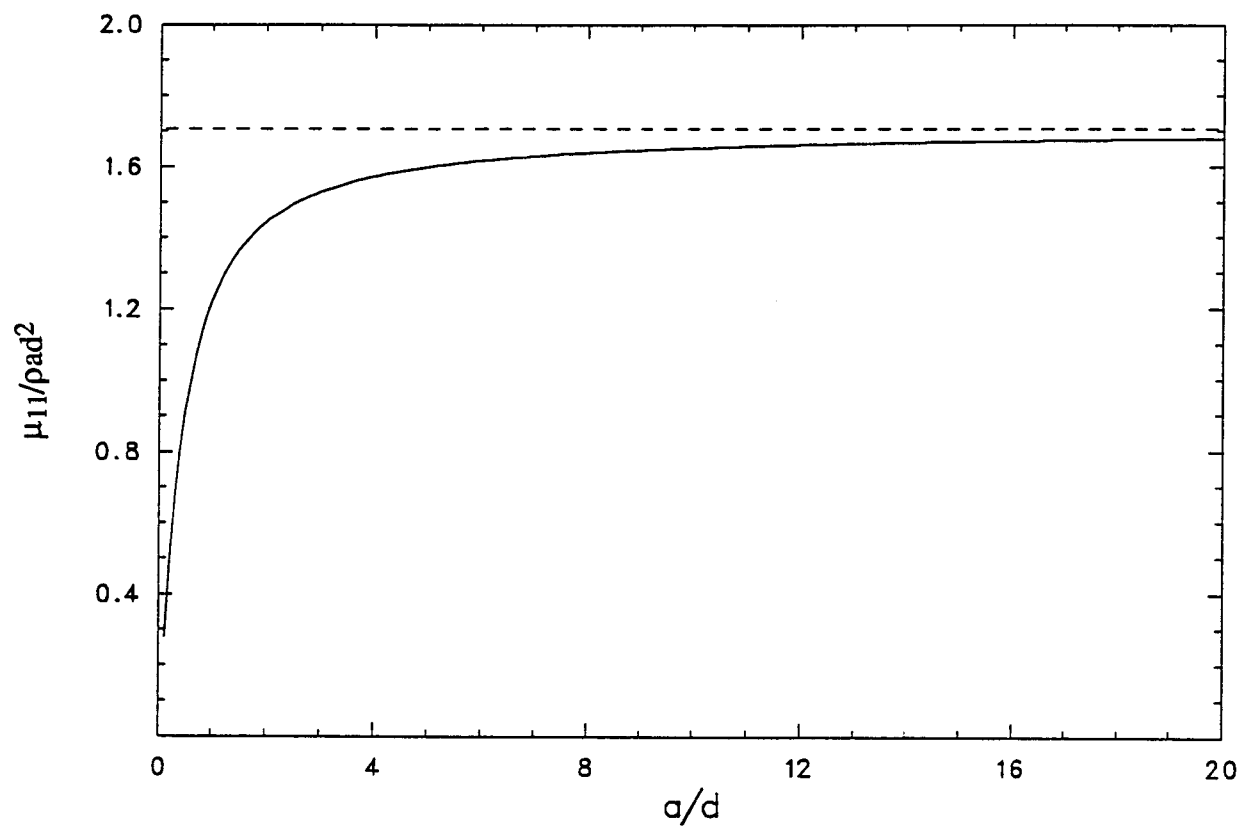
Figure 6.   High frequency approximations for the surge added mass of a circular cylinder as a function of a/d. ————, (3.33);  — — — —,  (3.38).
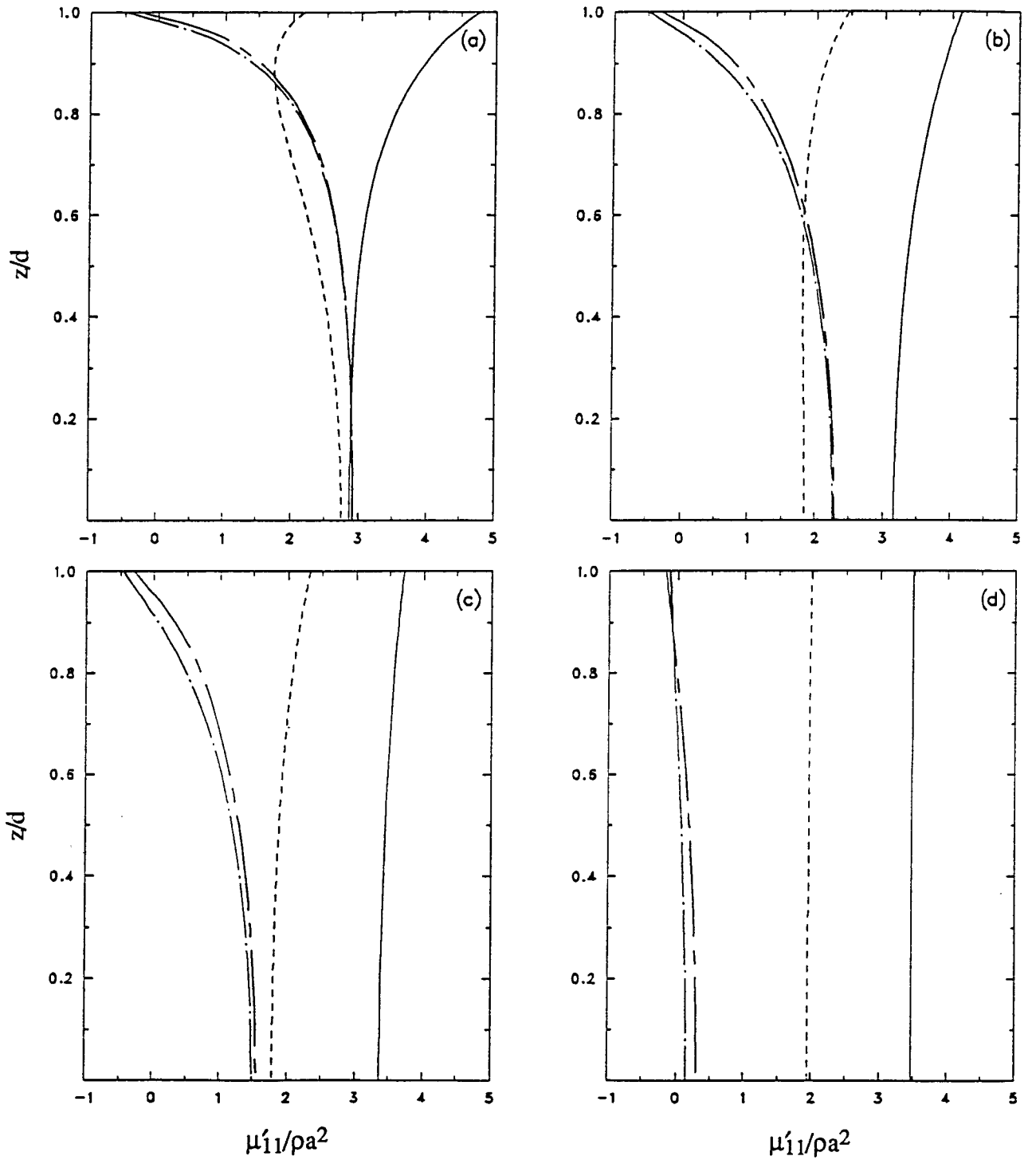
Figure 7. Analytical results for sectional surge added mass of a circular cylinder as a function of z/d for various values of $k_0a$. (a) a/d = 0.2, (b) a/d = 0.5, (c) a/d = 1, (d) a/d = 5. ————, $k_0a = 0.5$; — — — —, $k_0a = 1$; — · — · —, $k_0a = 10$; — · — · —, $k_0a = 20$.

128
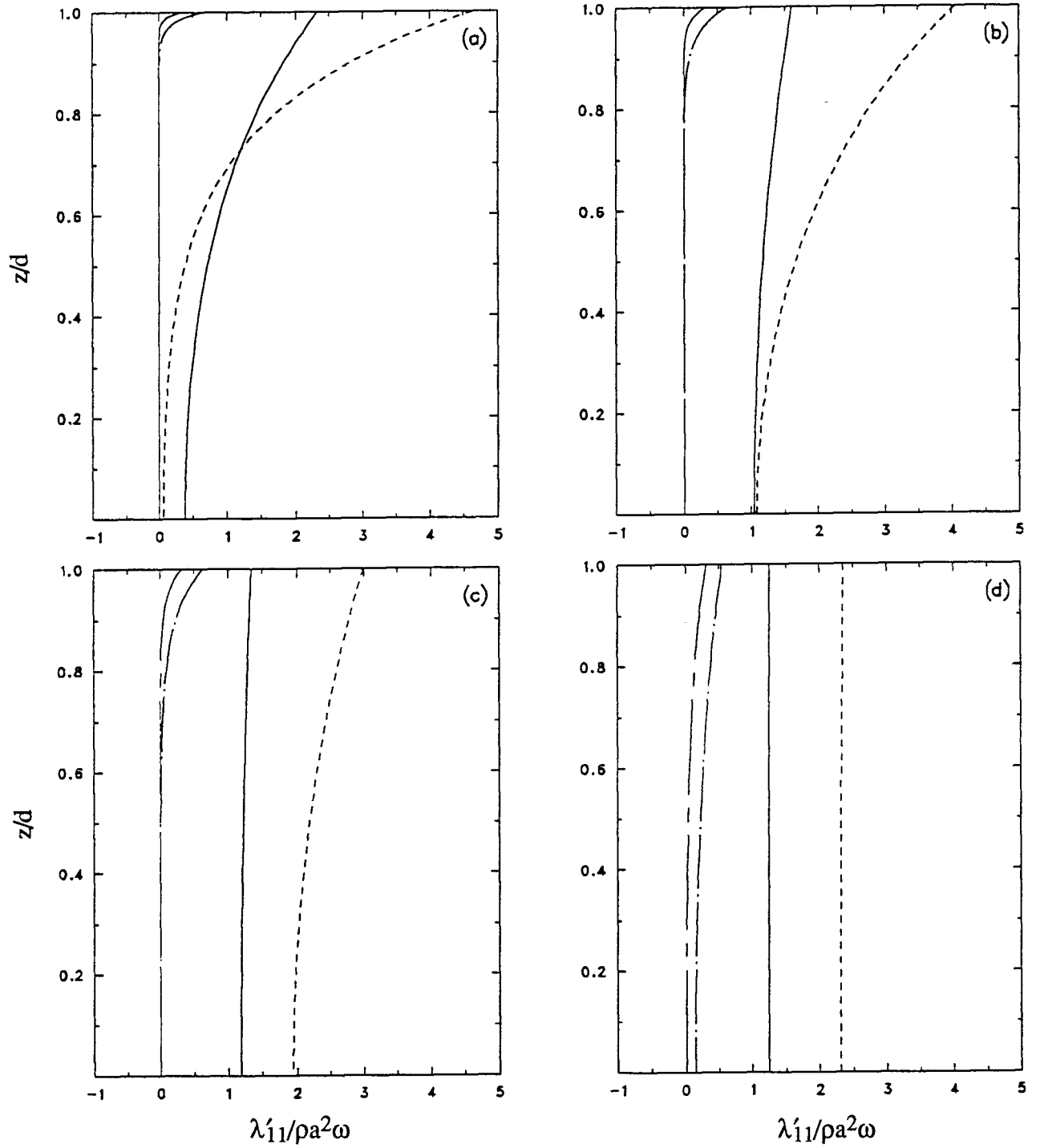
Figure 8. Analytical results for sectional surge damping coefficient of a circular cylinder as a function of $z/d$ for various values of $k_0a$. (a) $a/d = 0.2$, (b) $a/d = 0.5$, (c) $a/d = 1$, (d) $a/d = 5$. ————, $k_0a = 0.5$; — — — —, $k_0a = 1$; — · — · —, $k_0a = 10$; — · — · · —, $k_0a = 20$.
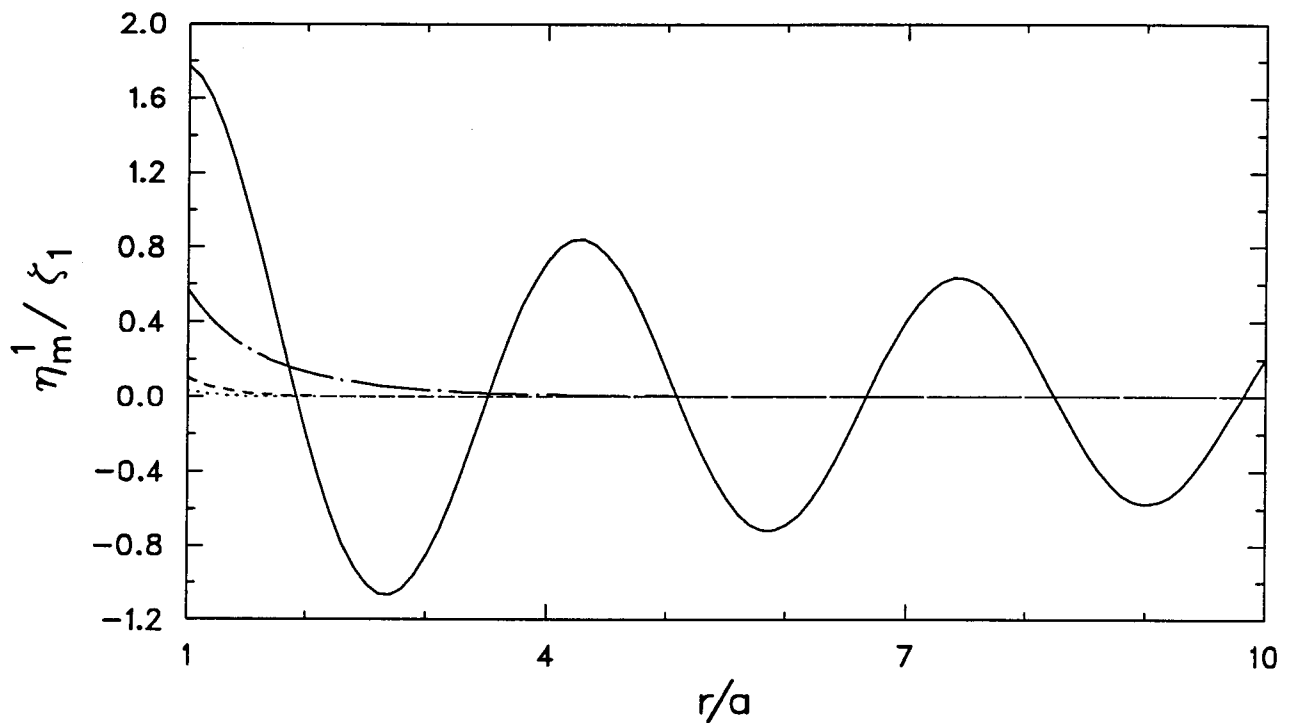
Figure 9.   Instantaneous water surface elevation due to the m-th mode wave caused by surge motion of a circular cylinder with a/d = 0.5 and $k_0a$ = 2. —————, m = 0;  — · — · —, m = 1;  — — — —, m = 2;  ············, m = 3.
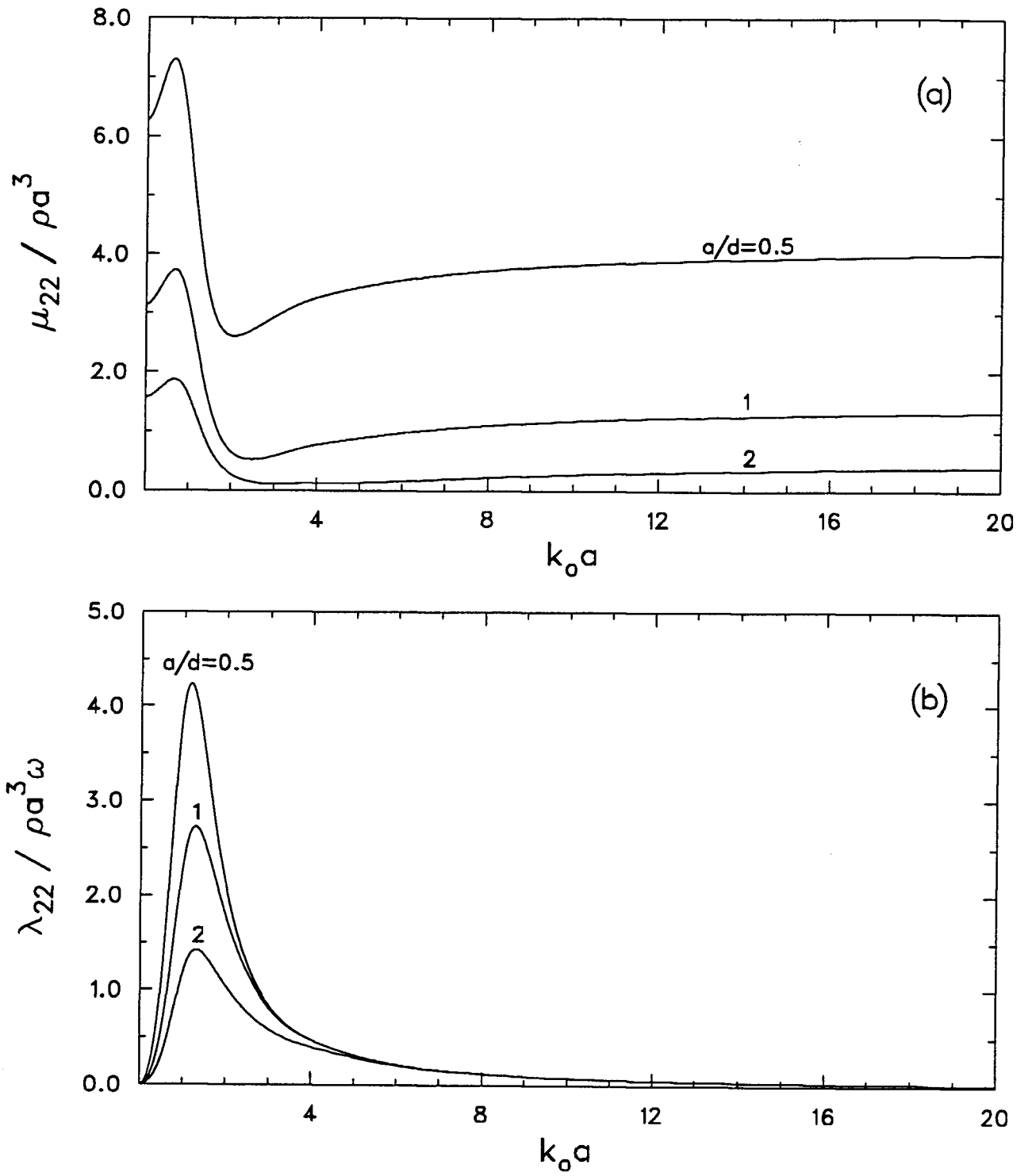
Figure 10. Analytical results for sway hydrodynamic coefficients of an elliptic cylinder with b/a = 0.2 as a function of $k_0a$ for various values of a/d. (a) added mass, (b) damping coefficient.
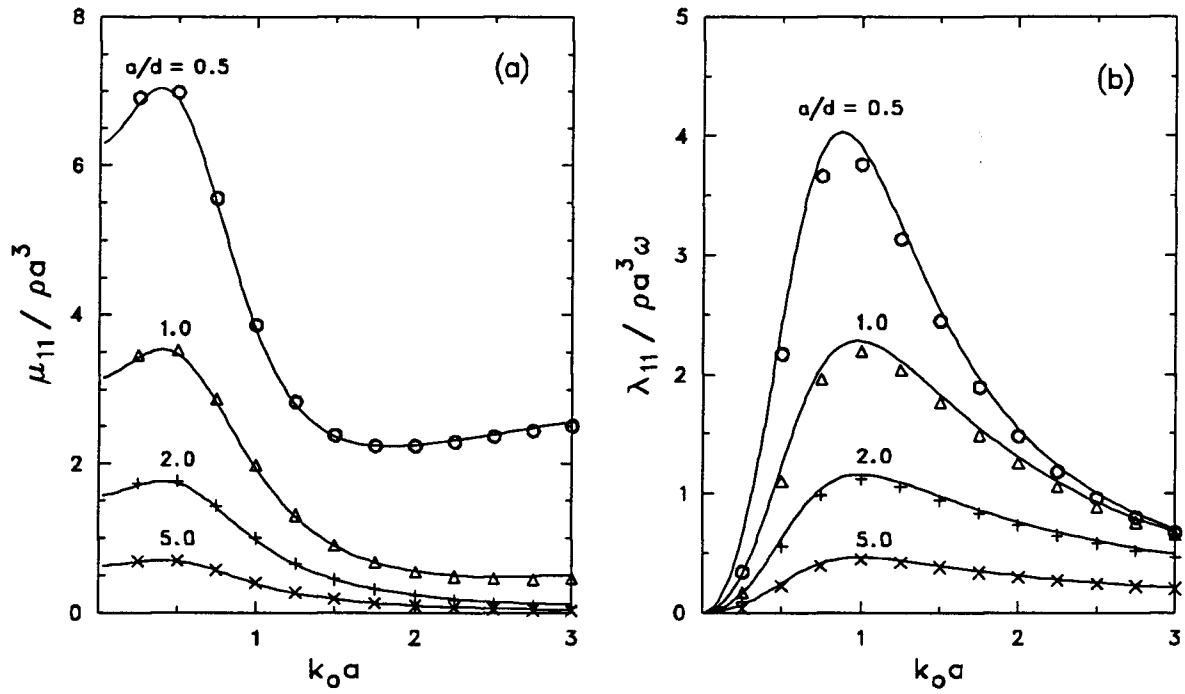
Figure 11. Surge hydrodynamic coefficients of a circular cylinder as a function of $k_0a$ for various values of a/d. (a) added mass, (b) damping coefficient. Numerical solution:  o, a/d = 0.5; $\Delta$, a/d = 1;  +, a/d = 2;  ×, a/d = 5.  Analytical solution: —————, a/d = 0.5, 1, 2, 5.
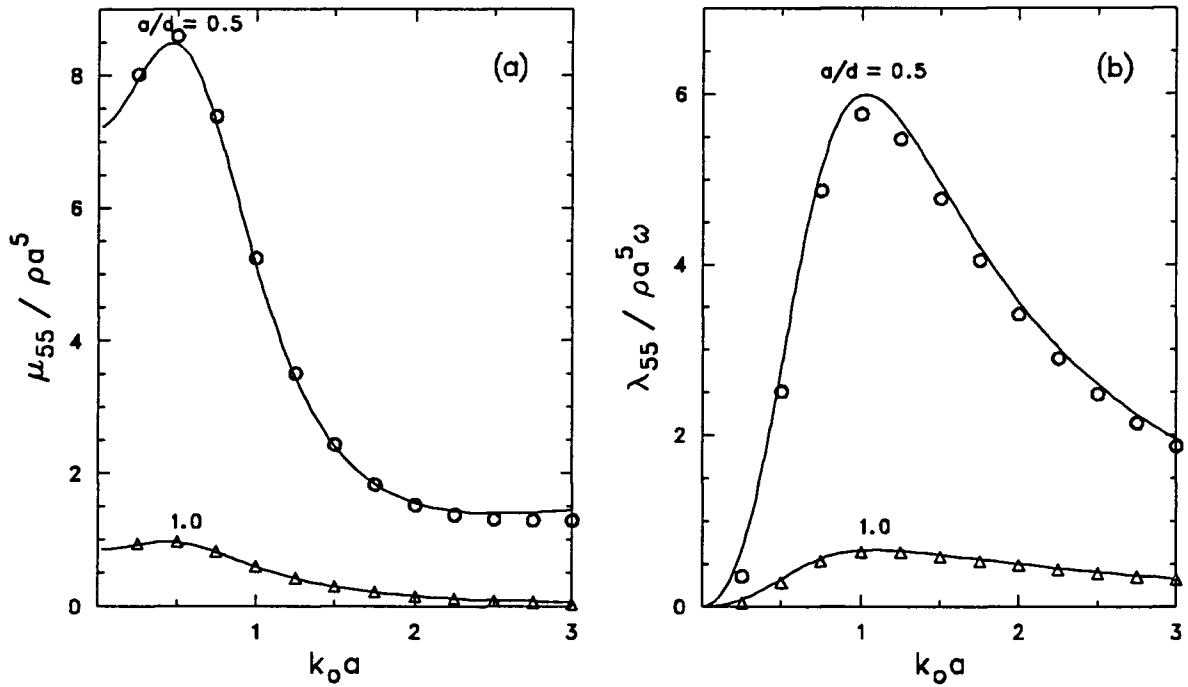


Figure 12. Pitch hydrodynamic coefficients of a circular cylinder as a function of $k_0a$ for various values of a/d. (a) added mass, (b) damping coefficient. Numerical solution:  o, a/d = 0.5; $\Delta$, a/d = 1.  Analytical solution: —————, a/d = 0.5, 1.

132
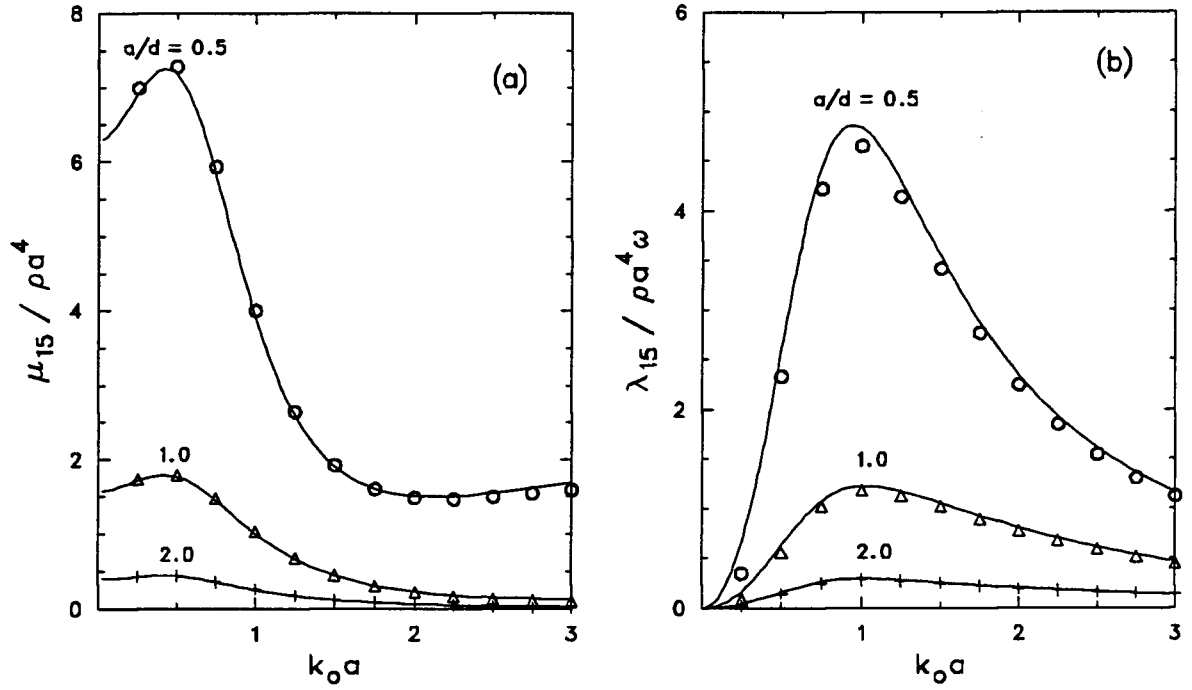
Figure 13. Surge-pitch coupling hydrodynamic coefficients of a circular cylinder as a function of $k_0a$ for various values of a/d. (a) added mass, (b) damping coefficient. Numerical solution: o, a/d = 0.5; Δ, a/d = 1; +, a/d = 2. Analytical solution: ————, a/d = 0.5, 1, 2.
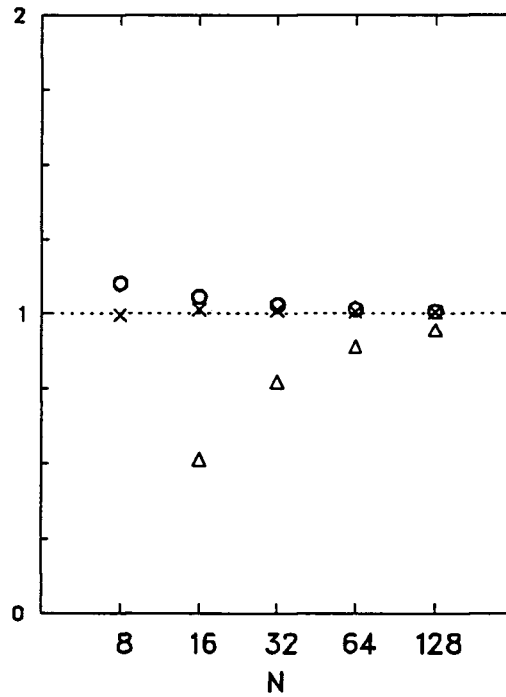


Figure 14. Ratio of the hydrodynamic coefficients of a circular cylinder computed using various numbers of segments N to the corresponding analytical results for $k_0a = 0.5$ and a/d = 0.5. o, $\mu_{11}$; Δ, $\lambda_{11}$; ×, $\lambda_{11}$ from exciting force.

133
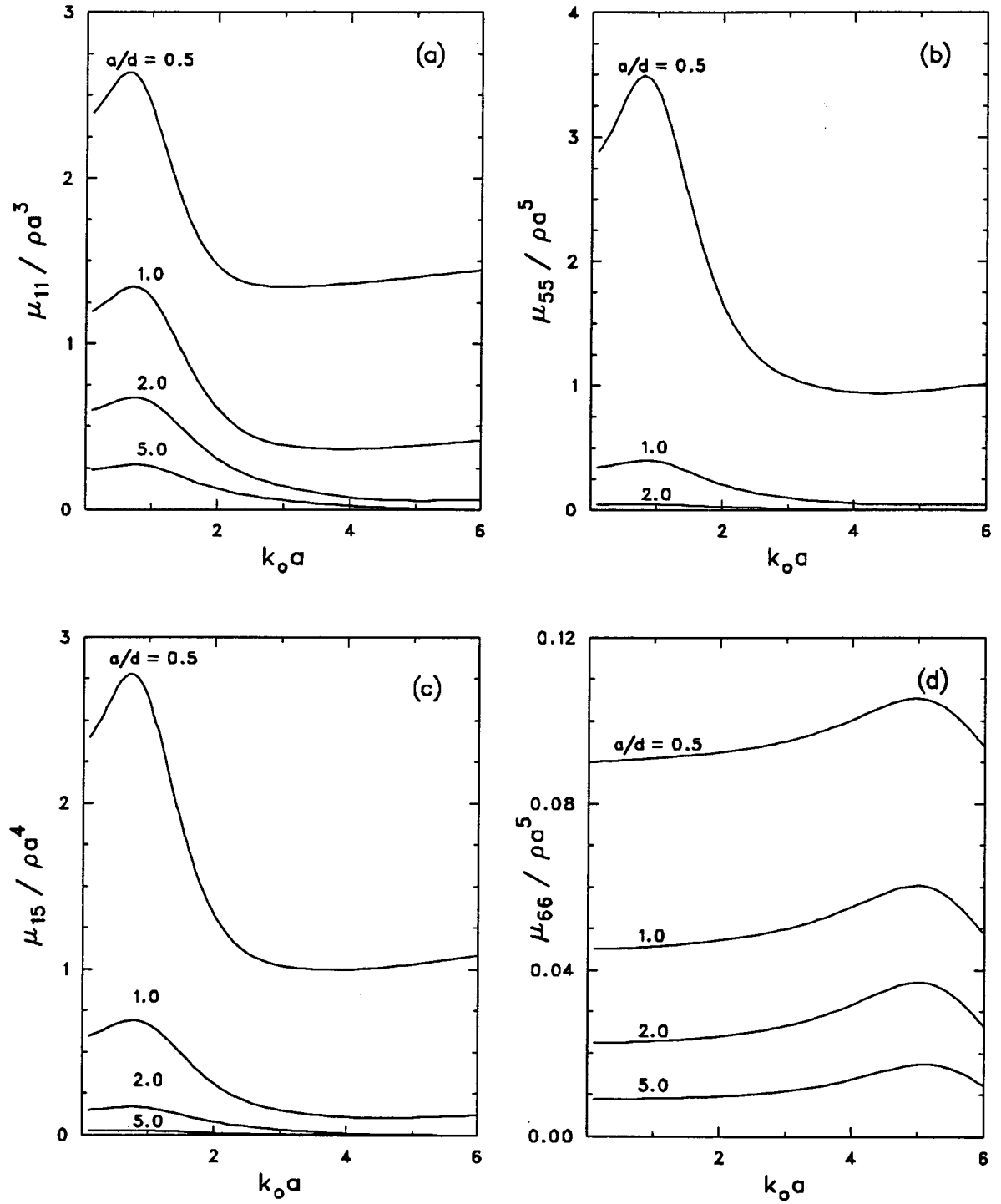
Figure 15. Added masses of a square cylinder as a function of $k_0 a$ for various values of a/d. $\beta = 0°$ or $45°$. (a) sway, (b) roll, (c) sway-roll, (d) yaw.

134
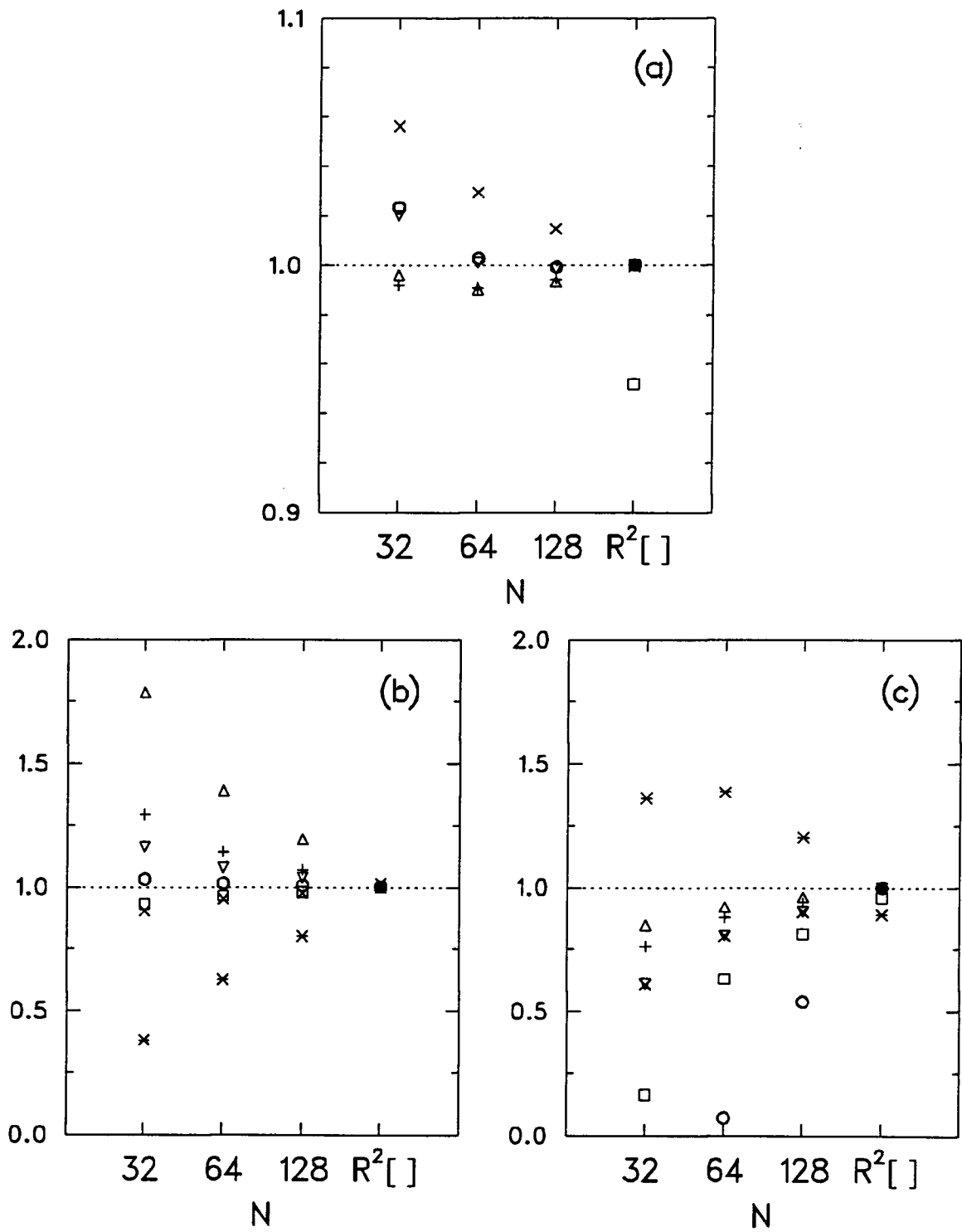
Figure 16. Ratio of sway hydrodynamic coefficients of an elliptic cylinder computed using various numbers of segments N to the corresponding analytical results for the case $b/a = 0.2$ and $a/d = 2$. (a) exciting force, (b) added mass, (c) damping coefficient. o, $k_0a = 0.5$; $\nabla$, $k_0a = 1$; $\triangle$, $k_0a = 2$; +, $k_0a = 5$; ×, $k_0a = 10$; ✳, $k_0a = 16$; □, $k_0a = 20$.

135
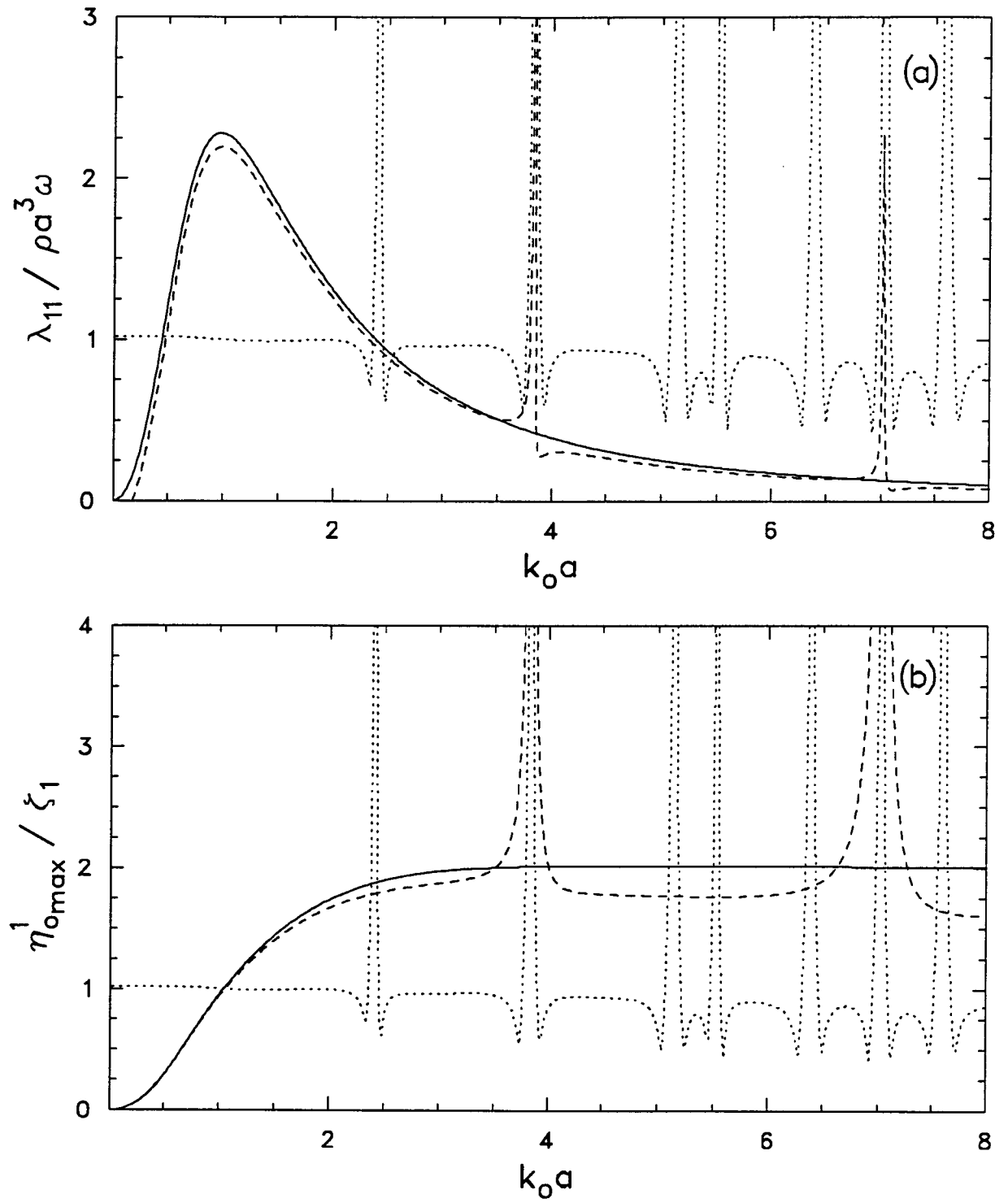
Figure 17. Surge damping coefficient and runup due to propagating mode potential at $(r,\theta) = (a,\pi)$ as a function of $k_0 a$ for the particular case of a circular cylinder with $a/d = 1$. (a) damping coefficient, (b) runup. ————, analytical result; — — — —, numerical result; ··············, condition number.

136
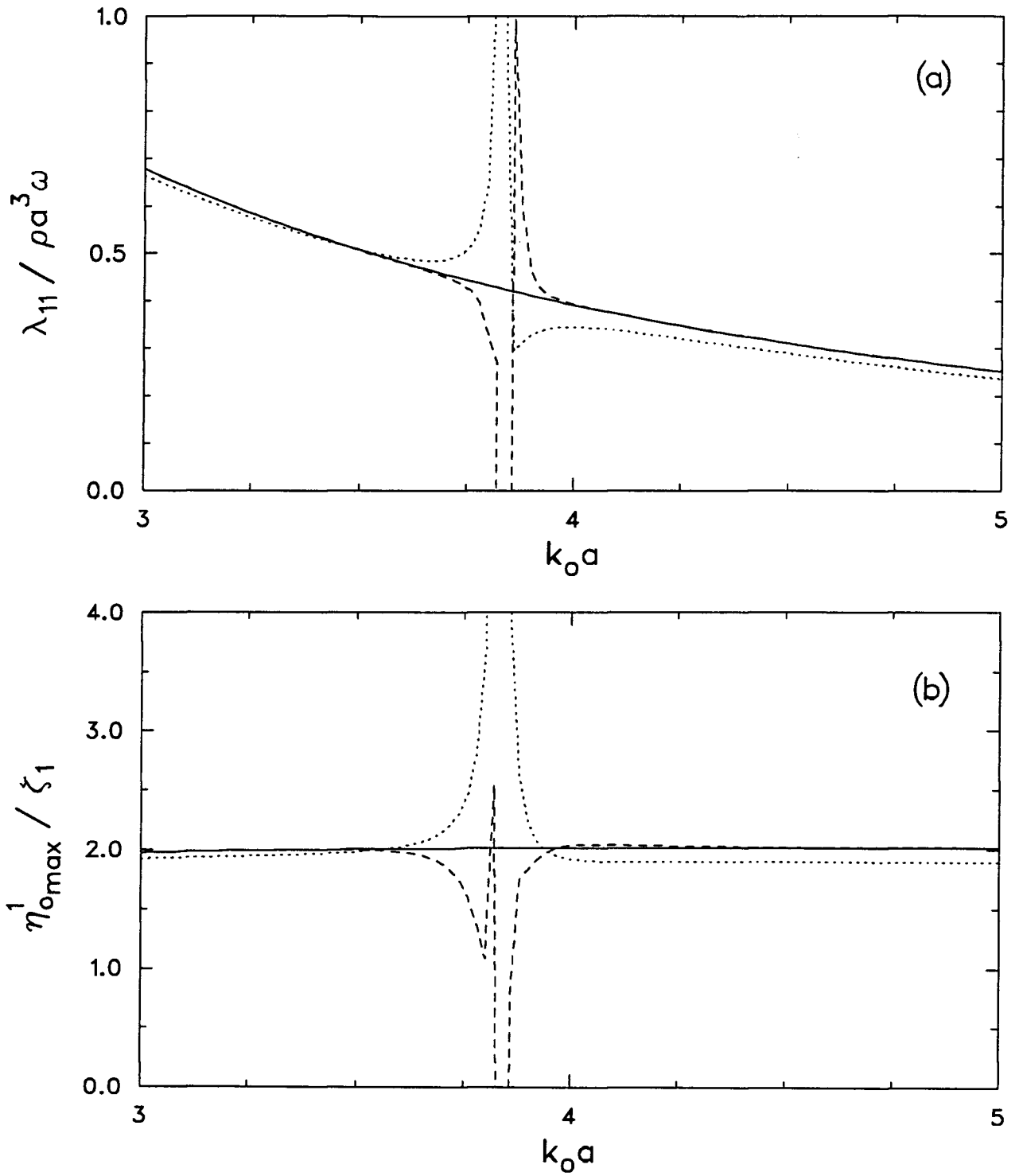
Figure 18. Surge damping coefficient and runup in the neighbourhood of an irregular frequency. (a) damping coefficient, (b) runup. ————, analytical result; ⋯⋯⋯⋯, numerical result with 128 segments; — — — —, numerical result with Richardson extrapolation.
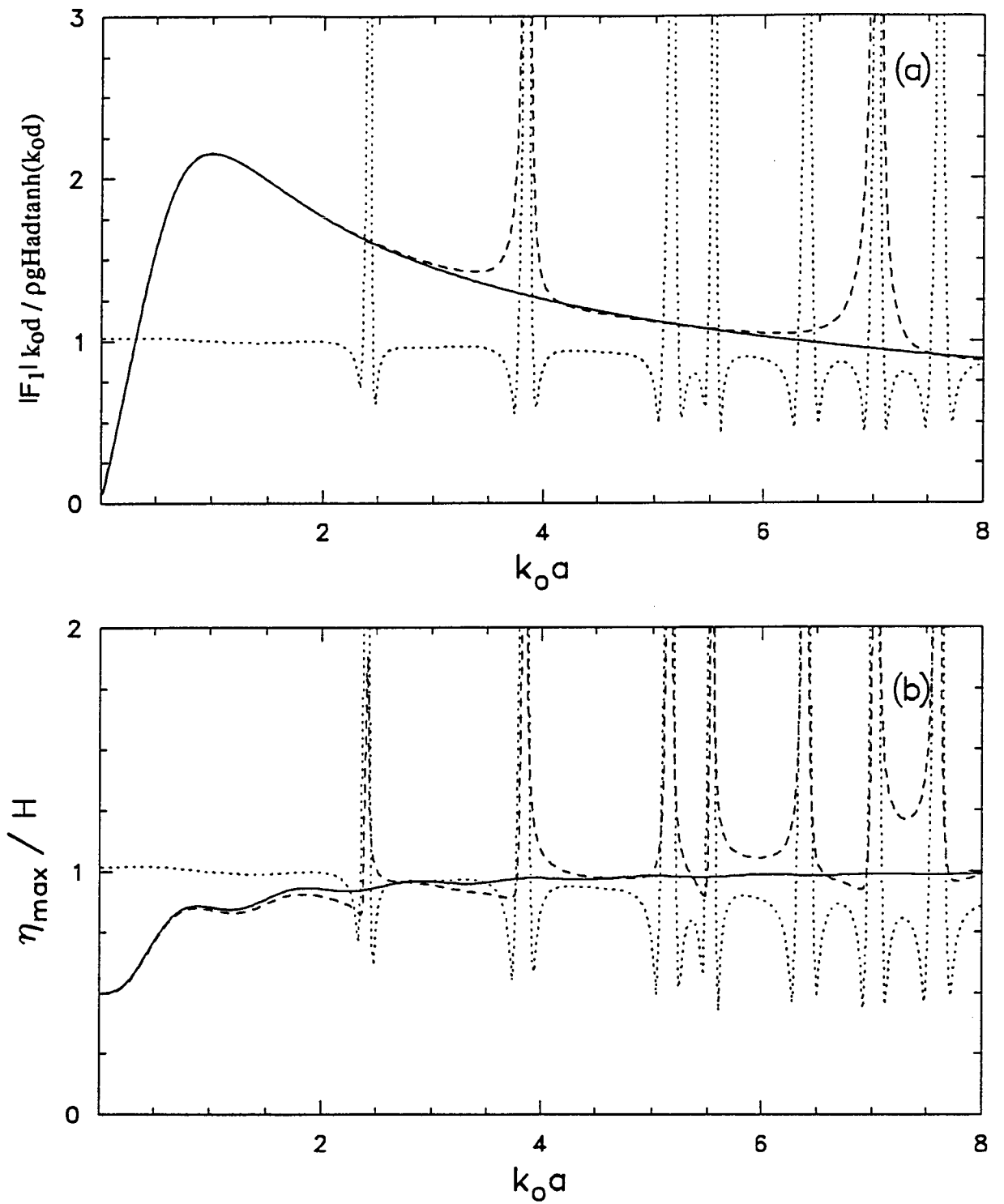
Figure 19. Surge exciting force and runup at $(r,\theta) = (a,\pi)$ for a circular cylinder as a function of $k_0 a$. (a) force, (b) runup. —————, analytical result; – – – –, numerical result; ············, condition number.
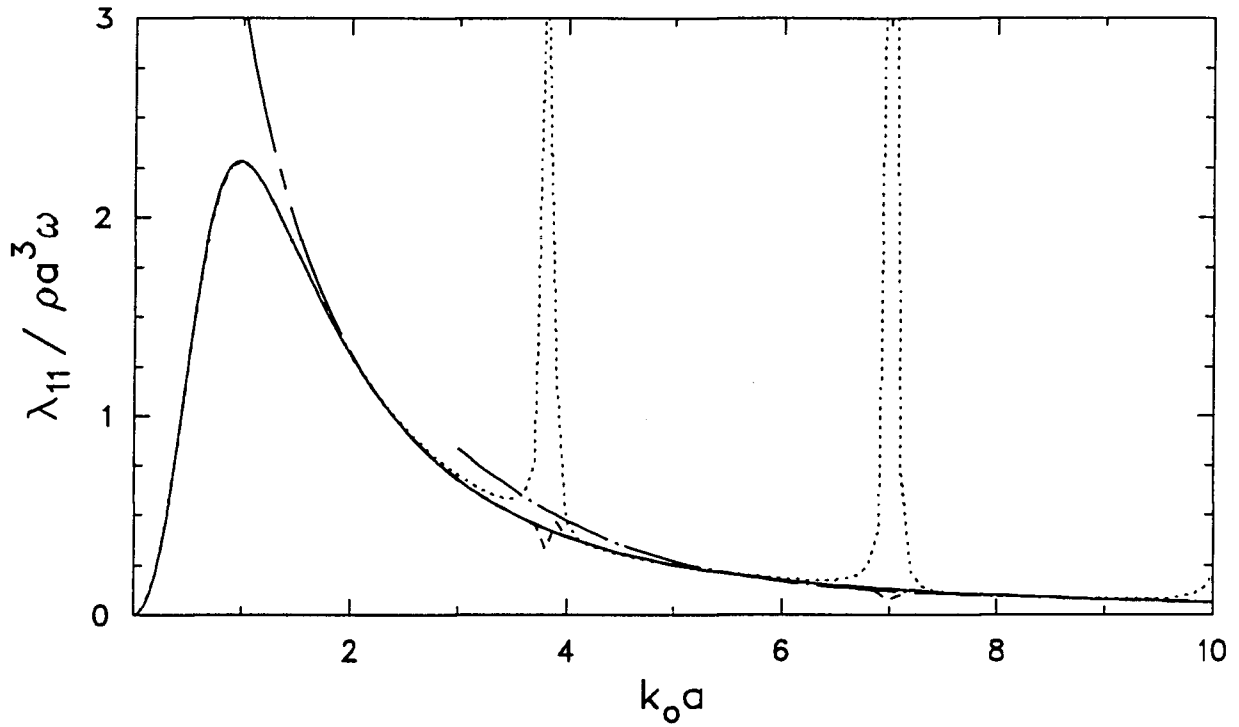
Figure 20. Surge damping coefficient of a circular cylinder as a function of $k_0a$ for $a/d = 1$. ————, analytical solution; — — — —, integral equation method; ············, Haskind relations, with $F_1$ obtained by integral equation method; — · — · —, Haskind relations, with $F_1$ obtained by geometrical optics approximation; — · — · —, Ursell's short-wave solution.
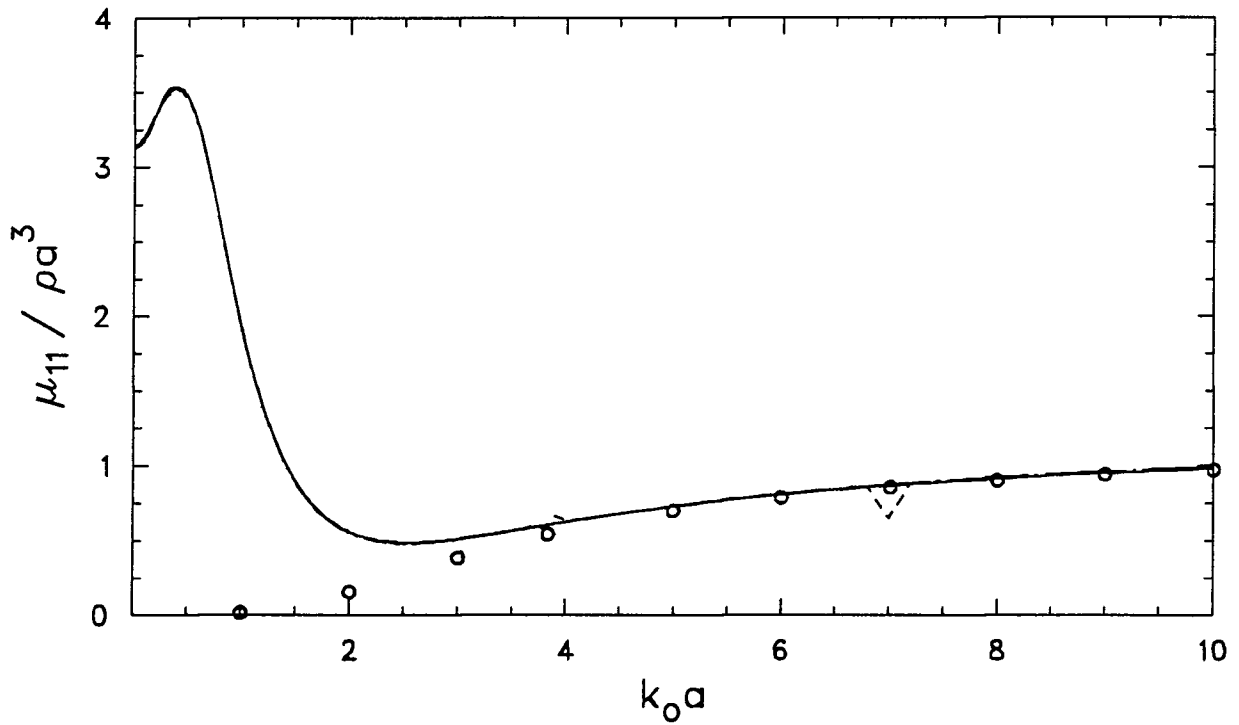


Figure 21. Surge added mass of a circular cylinder as a function of $k_0a$ for $a/d = 1$. ————, analytical solution; — — — —, integral equation method; — · — · —, Kramers-Kronig relation, with analytical values of $\lambda$; ············, Kramers-Kronig relation, with numerical values of $\lambda$; o, evanescent modes alone.
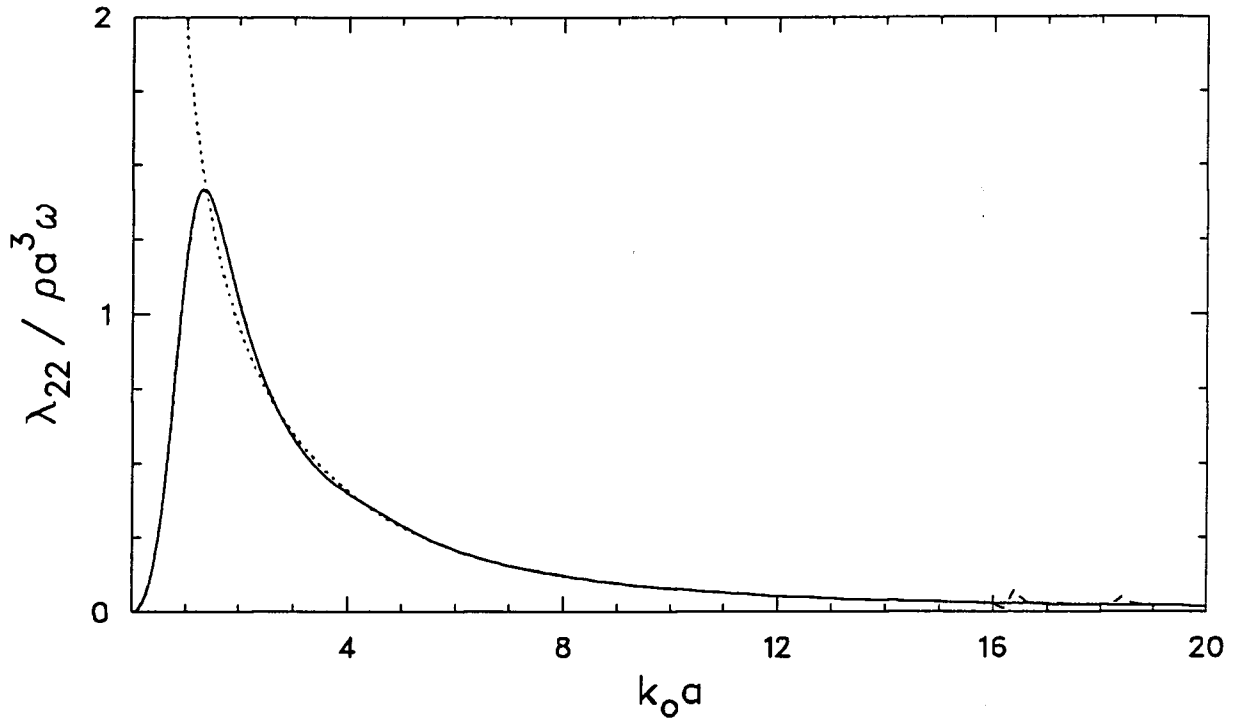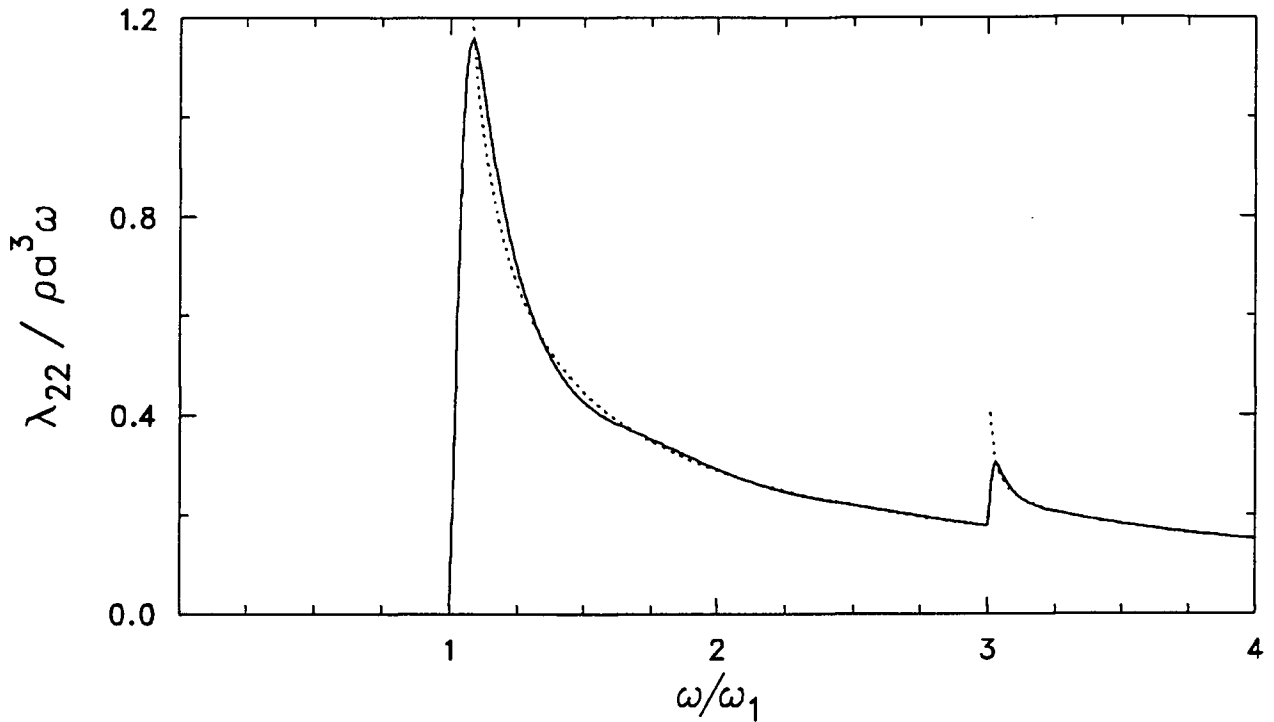
Figure 22. Sway damping coefficient of an elliptic cylinder as a function of $k_0 a$ for $b/a = 0.2$ and $a/d = 2.0$. ————, analytical solution; — — — —, integral equation method; ············, Ursell's short-wave solution.
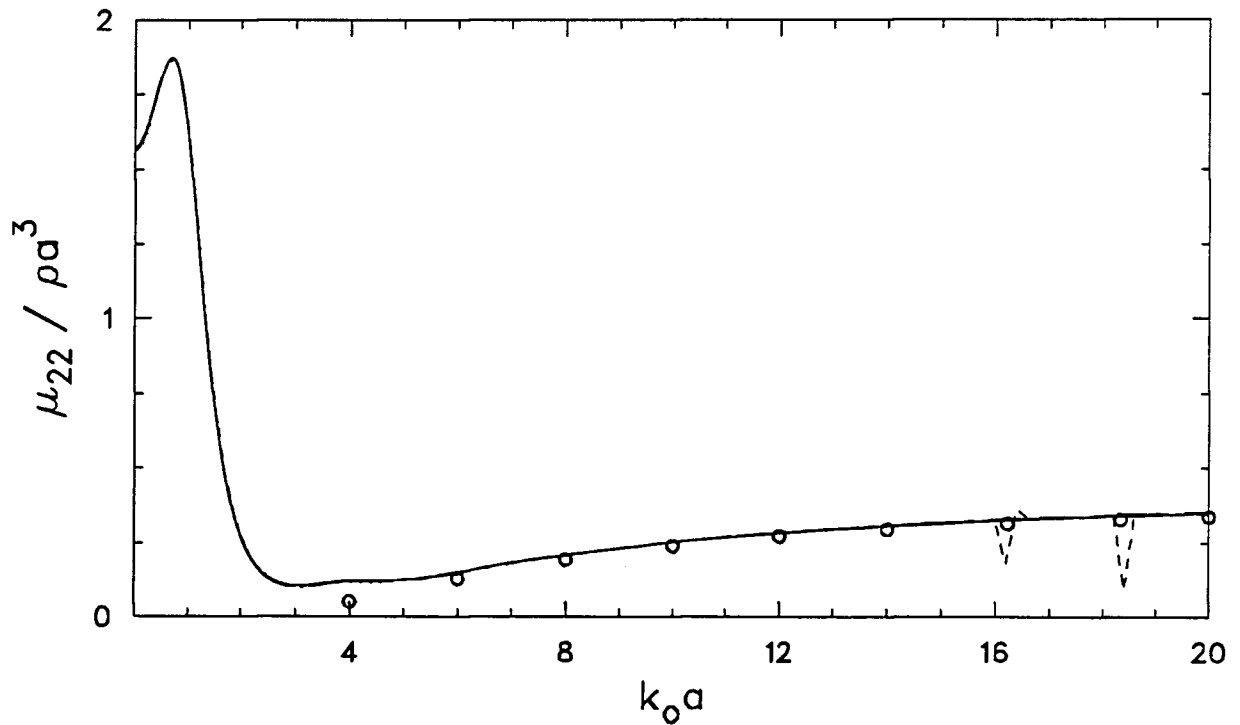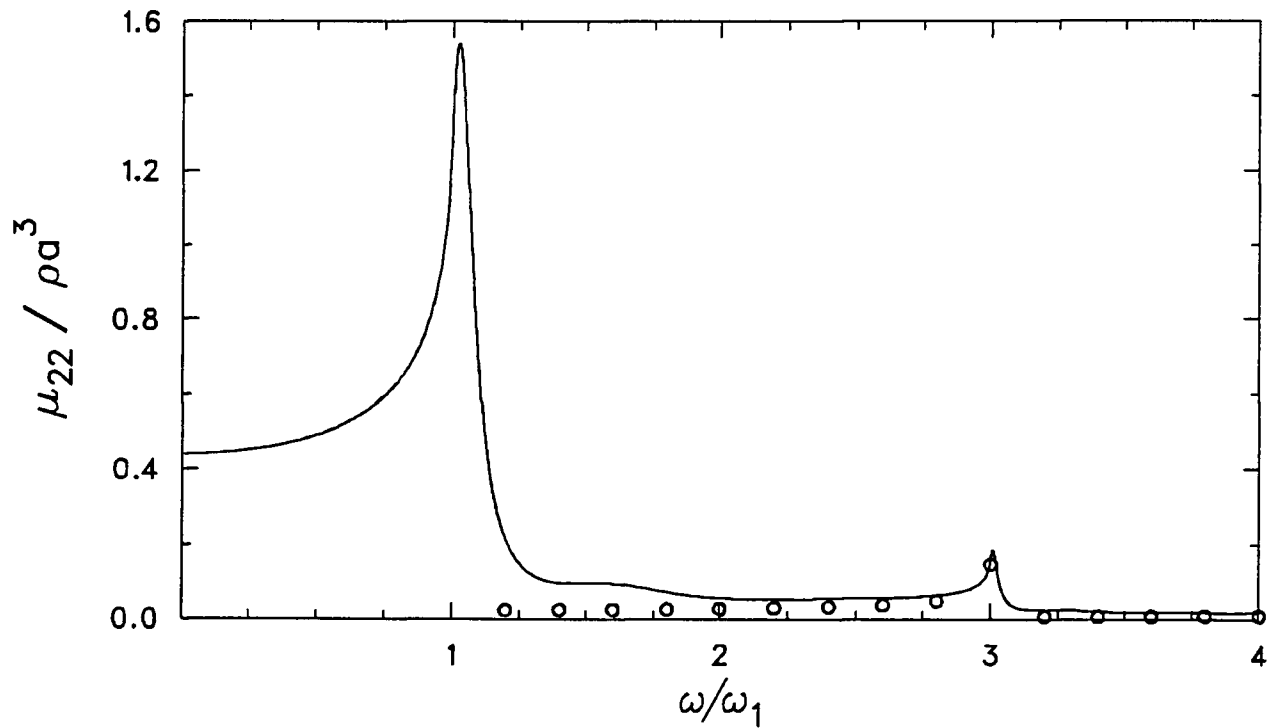


Figure 23. Sway added mass of an elliptic cylinder as a function of $k_0 a$ for $b/a = 0.2$ and $a/d = 2.0$. ————, analytical solution; — — — —, integral equation method; — · — · —, Kramers-Kronig relation, with analytical values of $\lambda$; ············, Kramers-Kronig relation, with numerical values of $\lambda$; o, evanescent modes alone.
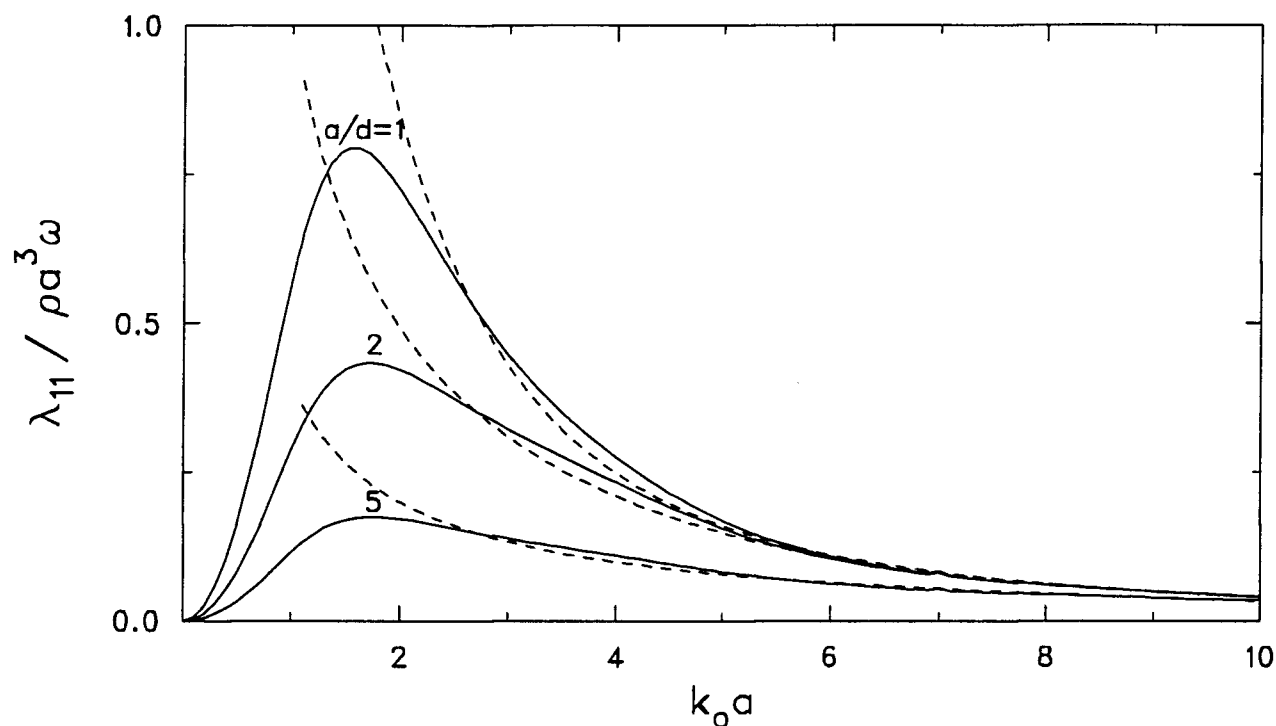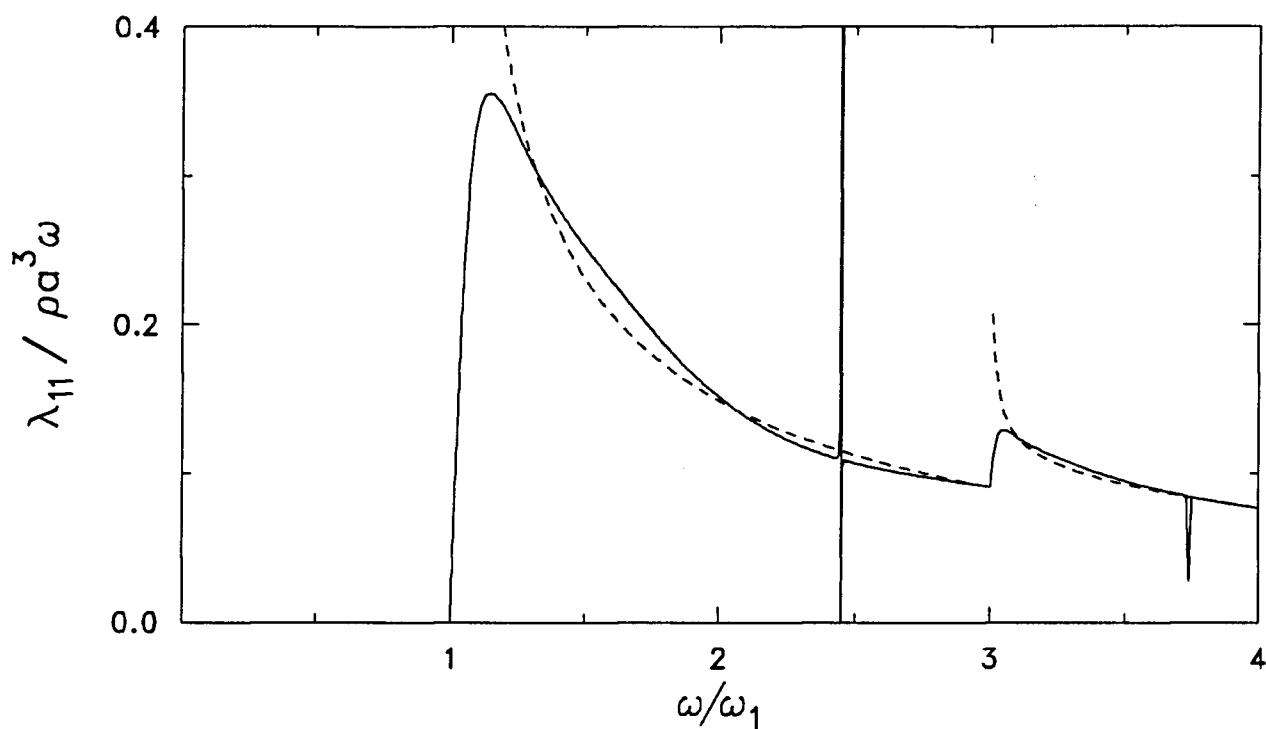
Figure 24. Surge damping coefficient of a square cylinder oscillating parallel to a pair of sides as a function of $k_0 a$ for various values of a/d. —————, integral equation method; — — — —, Ursell's short-wave solution.
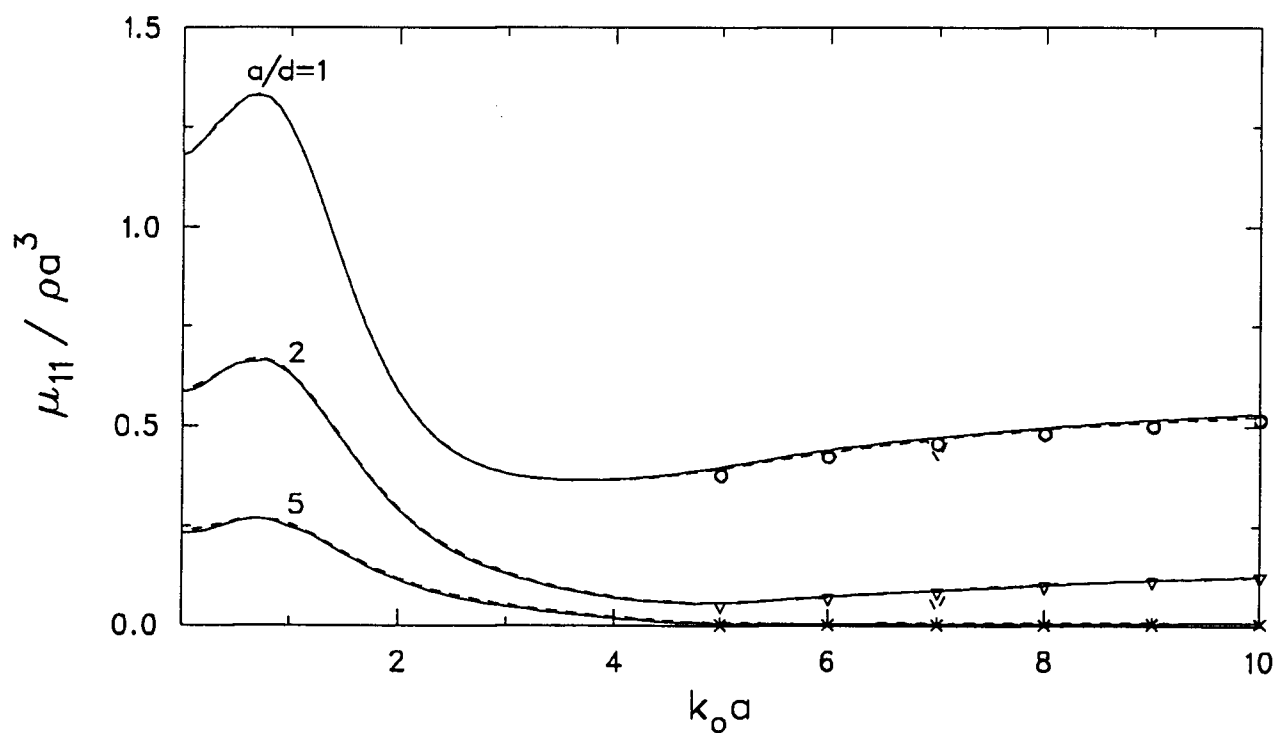


Figure 25. Surge added mass of a square cylinder oscillating parallel to a pair of sides as a function of $k_0 a$ for various values of a/d. —————, Kramers-Kronig relation; — — — —, integral equation method; o, ∇, × evanescent modes alone.
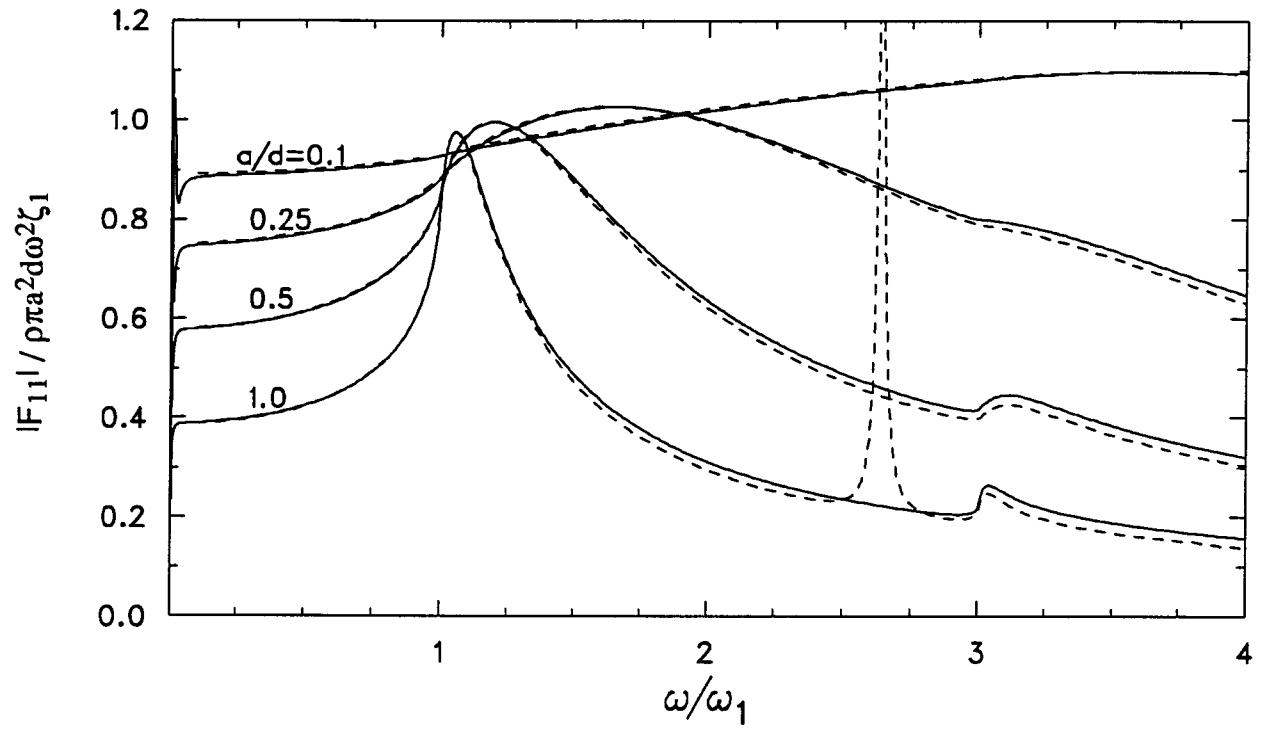
Figure 26. Force on a circular cylinder oscillating in surge in a compressible fluid as a function of $\omega/\omega_1$ for various values of a/d. ————, analytical solution; – – – –, integral equation method.
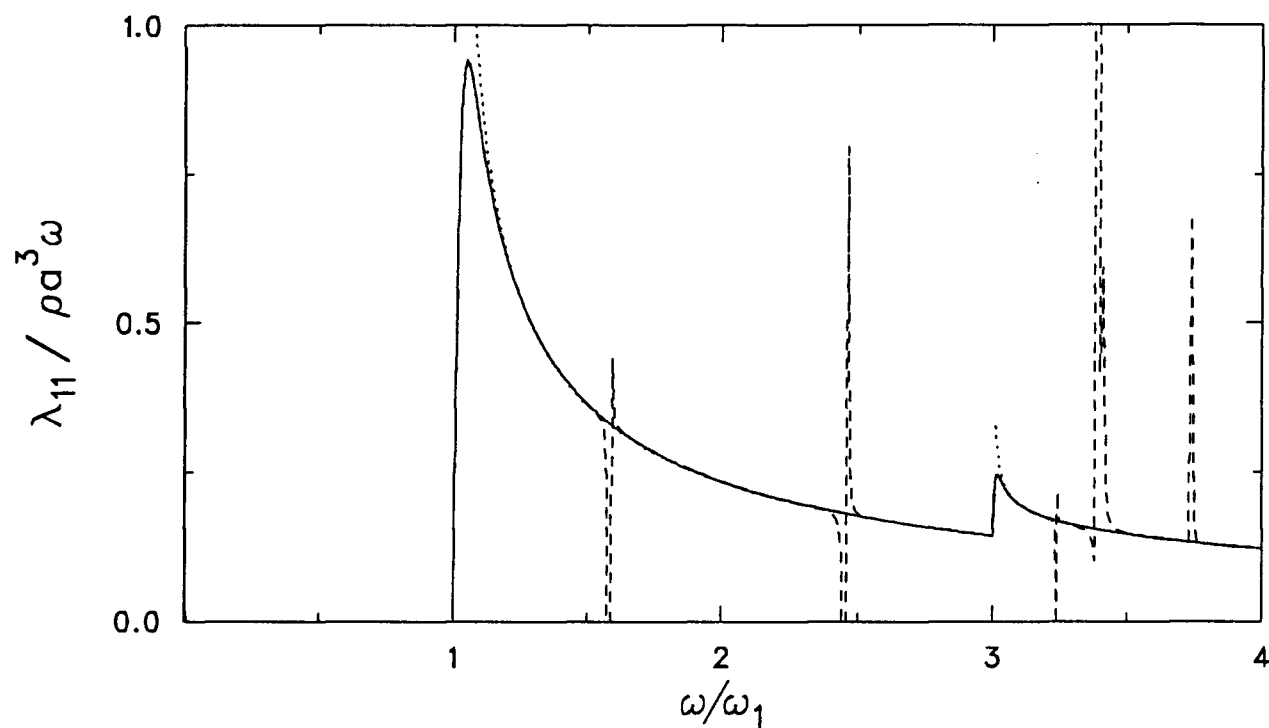
Figure 27. Surge damping coefficient of a circular cylinder in a compressible fluid as a function of $\omega/\omega_1$ for a/d = 2. ————, analytical solution; — — — —, integral equation method; ··········, Ursell's short-wave solution.
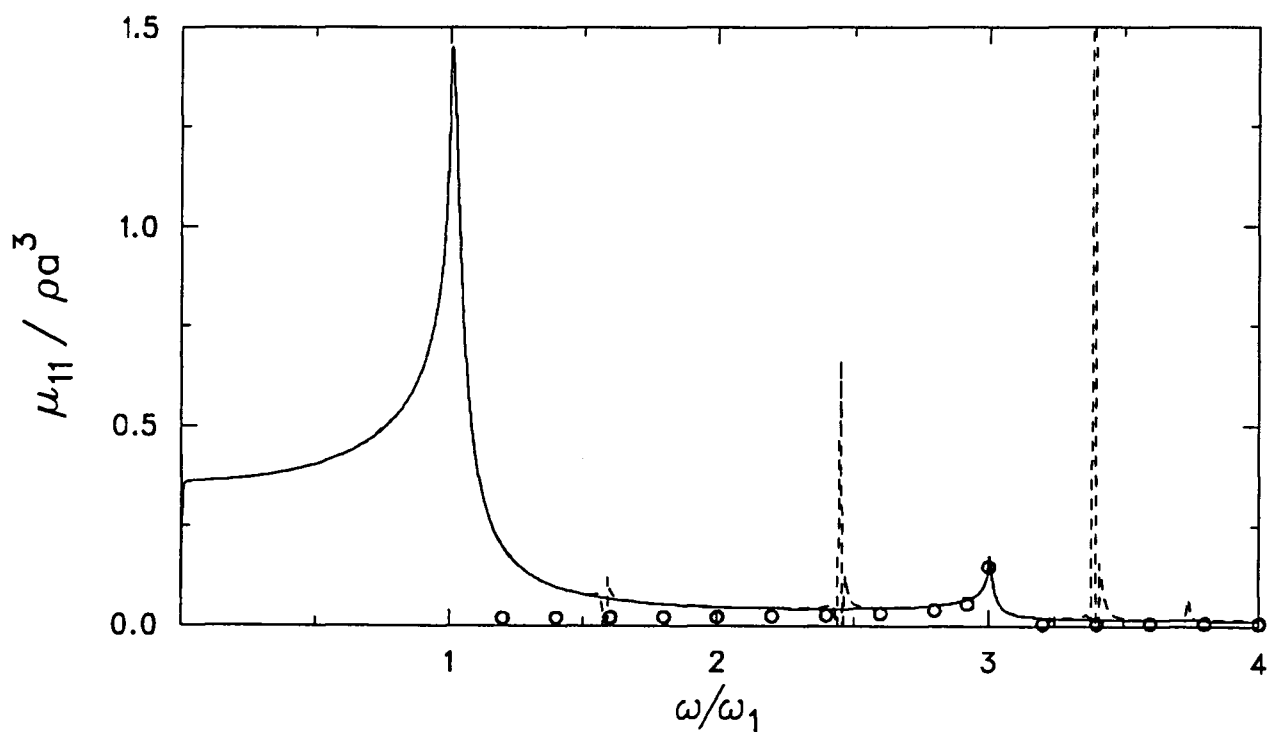


Figure 28. Surge added mass of a circular cylinder in a compressible fluid as a function of $\omega/\omega_1$ for a/d = 2. ————, analytical solution; — — — —, integral equation method; o, evanescent modes alone.

Figure 29. Sway damping coefficient of an elliptic cylinder in a compressible fluid as a function of $\omega/\omega_1$ for b/a = 0.2 and a/d = 2.0. ————————, analytical solution; — — — —, integral equation method; ············, Ursell's short-wave solution.



Figure 30. Sway added mass of an elliptic cylinder in a compressible fluid as a function of $\omega/\omega_1$ for b/a = 0.2 and a/d = 2.0. ————————, analytical solution; — — — —, integral equation method; o, evanescent modes alone.

Figure 31. Surge damping coefficient of a square cylinder oscillating parallel to a pair of sides in a compressible fluid as a function of $\omega/\omega_1$ for a/d = 2. ——————, integral equation method; — — — —, Ursell's short-wave solution.
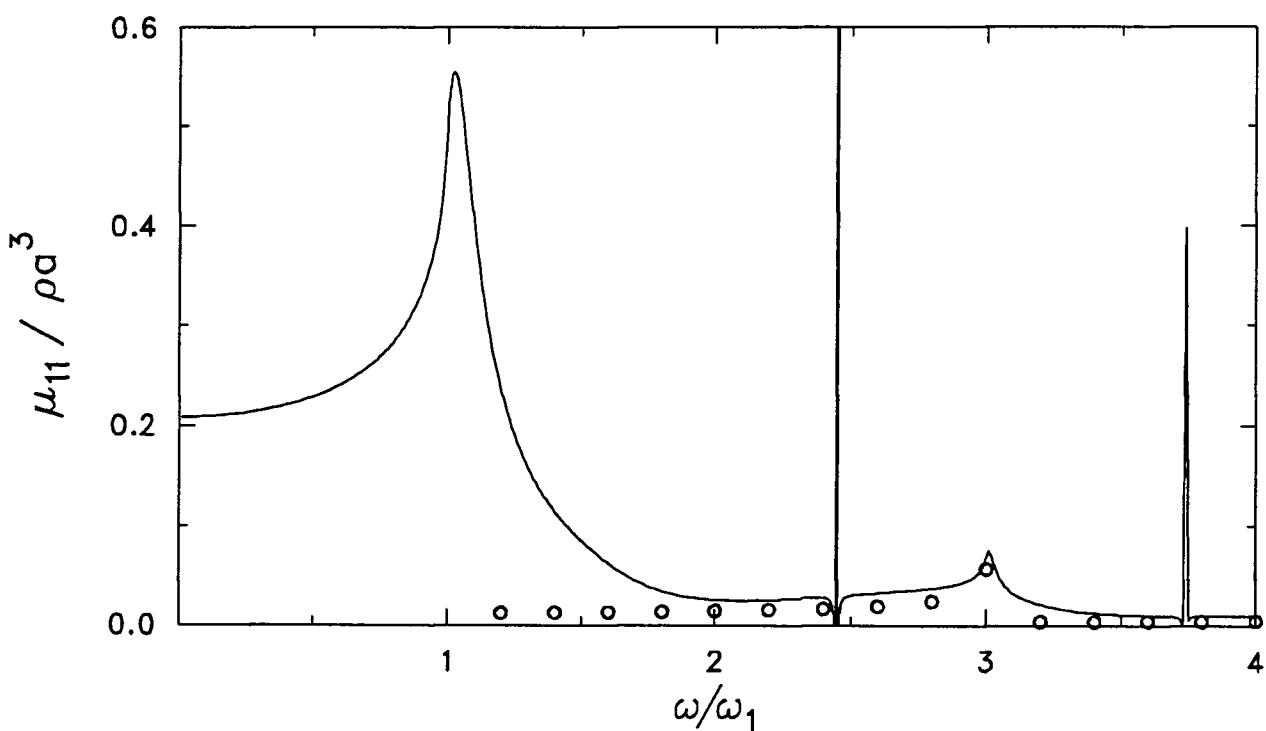


Figure 32. Surge added mass of a square cylinder oscillating parallel to a pair of sides in a compressible fluid as a function of $\omega/\omega_1$ for a/d = 2. ——————, integral equation method; o, evanescent modes alone.

145
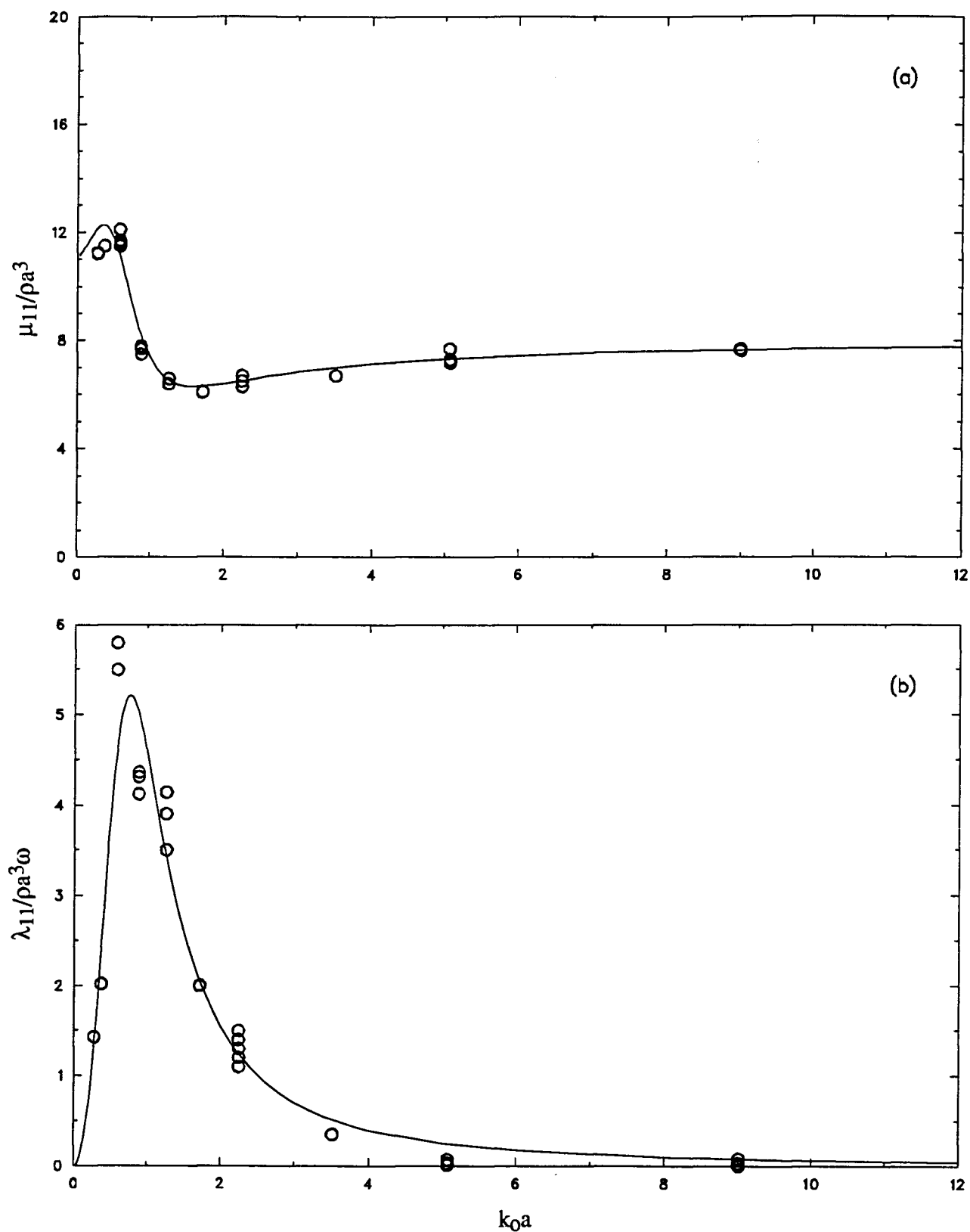
Figure 33. Comparison of theoretical results with the experimental results of Pegg (1983) for surge oscillations of a circular cylinder with a/d = 0.28. (a) added mass, (b) damping coefficient. ————, analytical result;  o, experimental result.
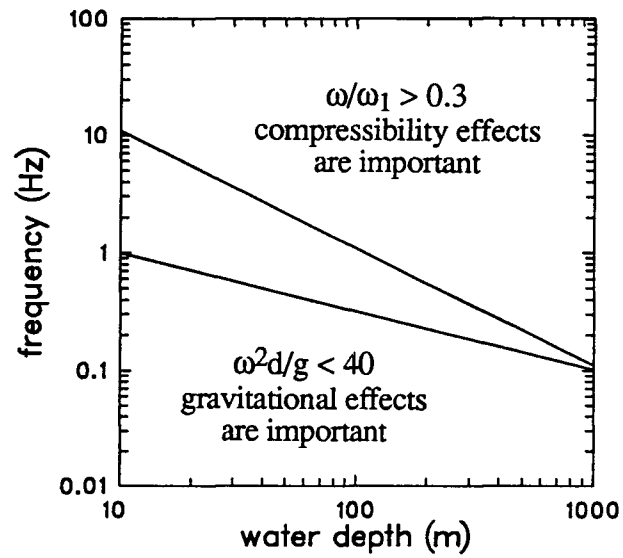
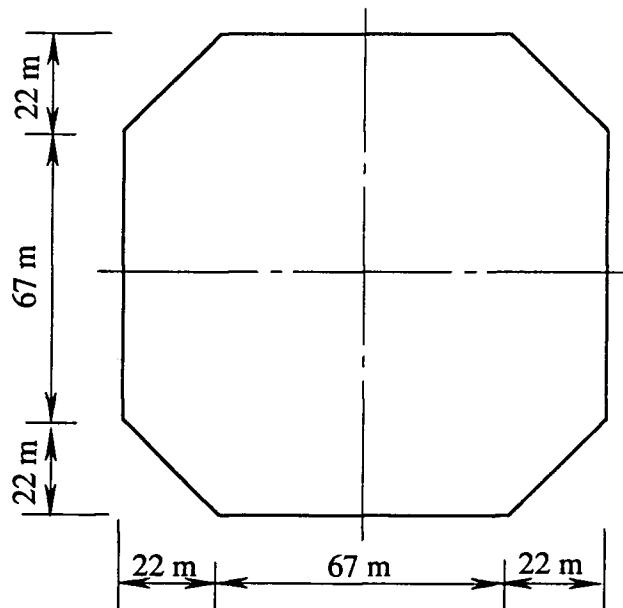Figure 34. Relative importance of gravitational and compressibility effects.



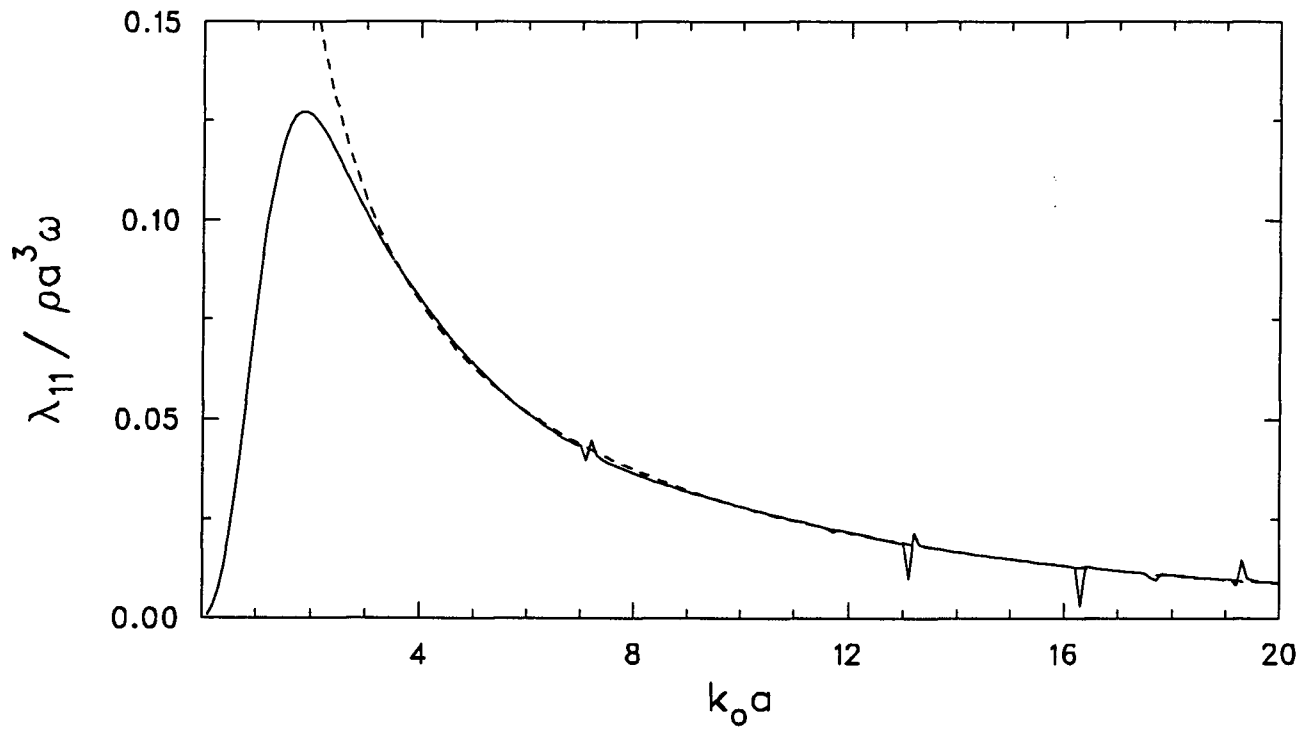Figure 35. Typical cross-section of the Molikpaq structure.

Figure 36. Surge damping coefficient of octagonal cylinder oscillating parallel to a pair of long sides as a function of $k_0a$ for $a/d = 5.6$. —————, integral equation method; — — — —, Ursell's short-wave solution.
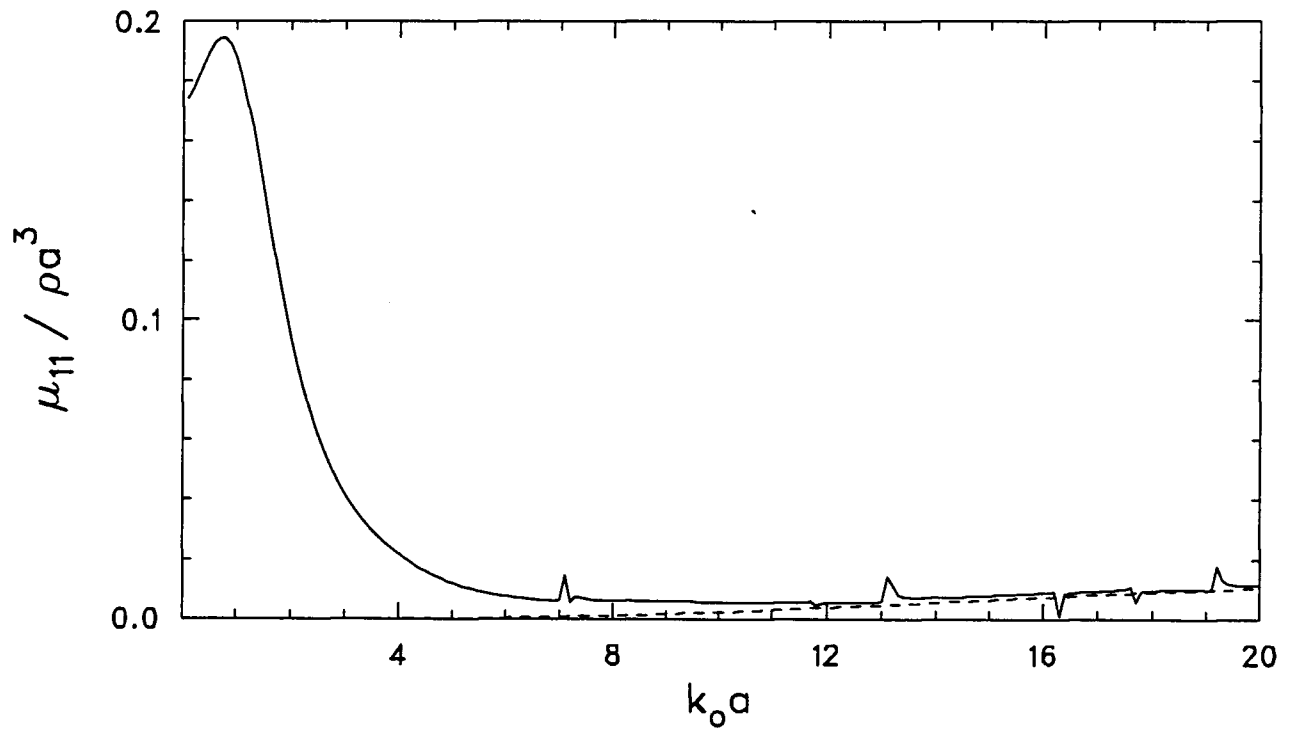


Figure 37. Surge added mass of octagonal cylinder oscillating parallel to a pair of long sides as a function of $k_0a$ for $a/d = 5.6$. —————, integral equation method; — — — —, evanescent modes alone.
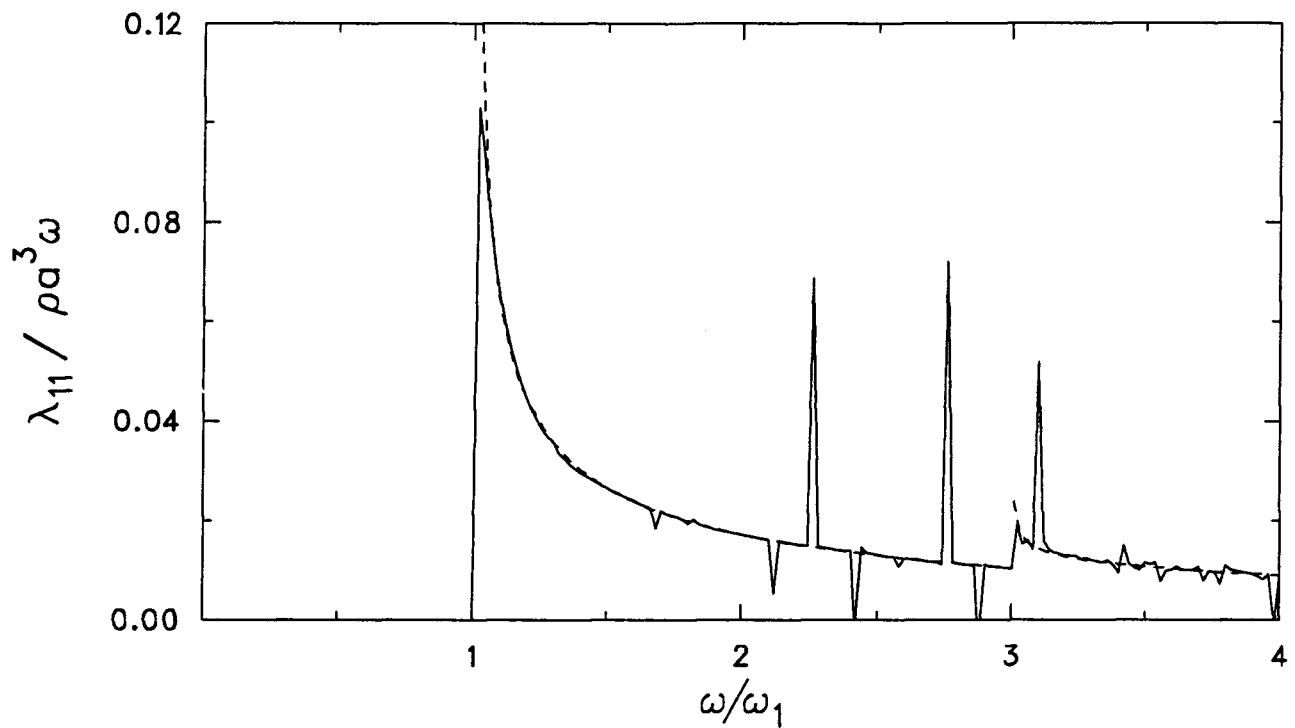
148

Figure 38. Surge damping coefficient of octagonal cylinder oscillating parallel to a pair of long sides in a compressible fluid as a function of $\omega/\omega_1$ for a/d = 5.6. —————, integral equation method; — — — —, Ursell's short-wave solution.
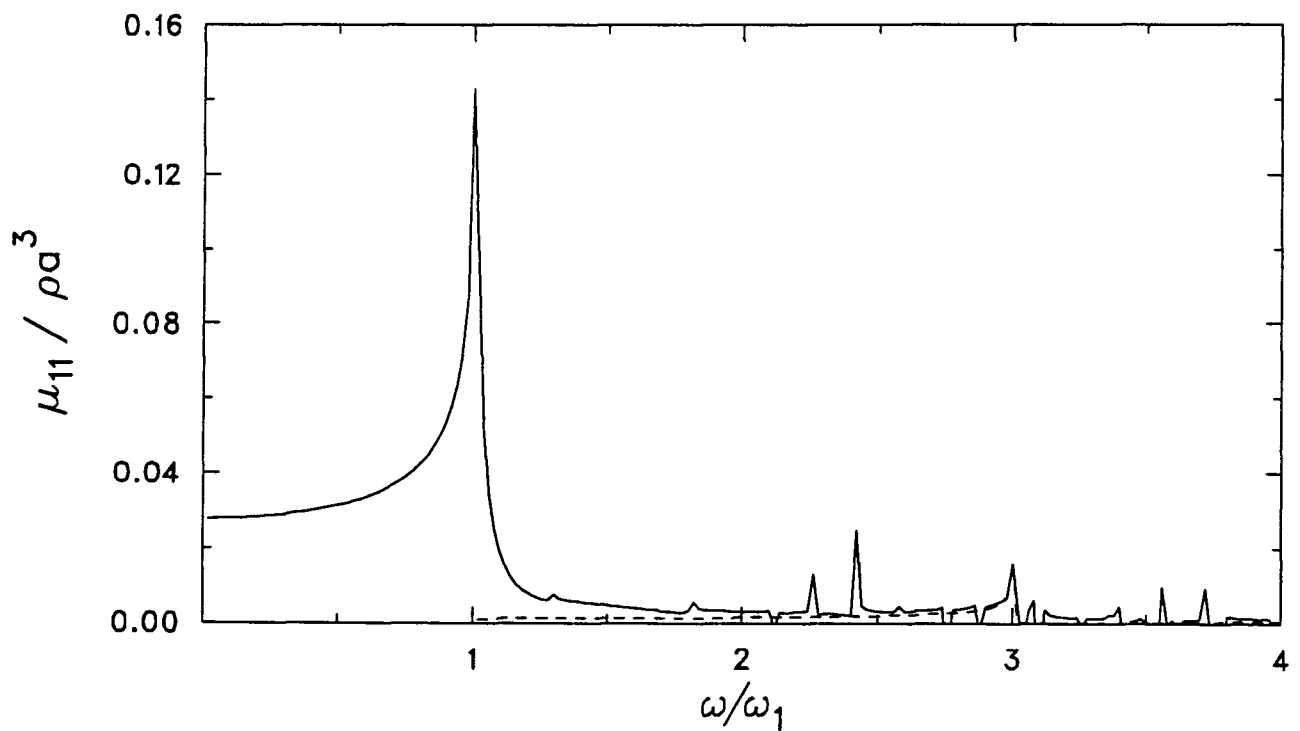


Figure 39. Surge added mass of octagonal cylinder oscillating parallel to a pair of long sides in a compressible fluid as a function of $\omega/\omega_1$ for a/d = 5.6. —————, integral equation method; — — — —, evanescent modes alone.

149